CHEMICAL ENGINEERING SCIENCE
GENIE CHIMIQUE

VOL. 10 1959 No. 4

Liquid flow in ring packed beds

The distribution of liquid flow between the interior and exterior of random packed Raschig ring packings

D. GREENAWAY
University College, London

(*Received* 30 *April* 1958)

Abstract—Investigations on water flow in Raschig ring packings were carried out employing columns constructed of wire gauze to minimize wall effects. A study of the mean flow through the ring interiors revealed that this decreased from 29 to 12 per cent of the total flow as the packing size increased from ½ in. to 1¼ in. Examination of cross-sections cut through a model of a ring packed bed suggested a cause of the observed variation.

Résumé—Pour étudier l'écoulement de l'eau dans des garnissages en anneaux Raschig l'auteur utilise une colonne en toile métallique afin de réduire les effets de paroi. L'étude de l'écoulement moyen à travers l'intérieur des anneaux montre que cet écoulement décroit de 29 à 12% de l'écoulement total quand la dimension du garnissage augmente de ½ in. à 1¼ in. L'examen de la section perpendiculaire d'un modèle de lit de garnissage en anneaux a suggéré une cause de la variation observée.

Zusammenfassung—Die Wasserströmung in Packungen aus Raschigringen wurde untersucht, wobei zur Verminderung des Wandeffektes eine Kolonne aus Maschendraht verwendet wurde. Die Untersuchung der mittleren Strömung durch das Innere der Ringe ergab, dass diese von 29 auf 12% der Gesamtströmung abfiel, wenn der Ringdurchmesser von 12 auf 32 mm erhöht wurde. Eine Nach prüfung von Querschnitten durch ein Modell einer Ringpackung deutete auf die Ursache der beobachteten Veränderung.

INTRODUCTION

IN the past, several attempts have been made to determine the extent of surface wetting occurring when liquid flows over Raschig ring packings. The methods used fall into two distinct categories, namely direct and indirect. Of the direct methods, MAYO and others [1] used paper rings with dye solution as the wetting fluid, while SHULMAN and others [2] employed specially fabricated naphthalene rings, measuring the concentration of naphthalene in the issuing gas stream for wetted and for dry rings. The indirect methods basically consist in comparing mass transfer data for the system in question with data for a similar system, in which it was known that the whole of the ring surfaces was utilized. For example, SHERWOOD and PIGFORD [3] and WEISMAN and BONILLA [4] used the data of TAECKER and HOUGEN [5], obtained for the evaporation of water from rings with a porous surface which ensured complete utilization. This was compared, by the use of CHILTON and COLBURN's j_D mass transfer factor [6], to the mass transfer data of several workers, and the effective area thereby determined. SHULMAN [2, 7] calculated the j_D factor for the sublimation of naphthalene from dry rings and compared this with the mass transfer data of FELLINGER [8].

The results of these investigations are somewhat contradictory. Thus, MAYO found that the wetted area varied with liquid rate but was independent of gas rate, whereas WEISMAN and BONILLA found substantially the reverse. Making this one exception, however, most workers are in agreement

with MAYO's conclusion. Similarly, JESSER and ELGIN [9], investigating the related phenomenon of liquid hold-up, were able to show that this also was independent of gas flow. Considerable disagreement is, nevertheless, apparent in regard to the effect of such factors as ring size and liquid rate. In such a complex system as an irrigated, packed bed many causes can be suggested for such disagreement. For instance, BOND [10] showed that the absorption of a small quantity of ammonia was sufficient to rupture a hitherto stable water film. Furthermore, BAKER *et al.* [11] showed that unless the ratio of column diameter to packing diameter exceeded eight, a high percentage of the liquid would flow adjacent to the wall. Many of the wetted area determinations were carried out under conditions not in accordance with this ratio.

In view of the complexity of these systems, it was considered that it might be profitable to attempt to resolve them into two distinct and perhaps thereby less complex systems. Liquids flowing through a ring packed bed must, at any one point, be flowing over the exteriors or through the interiors of the rings. In flowing over the exteriors there is no constraint on the direction taken by the liquid, beyond that its resultant should be vertically downwards. Through the ring interiors, however, the flow is constrained to a stream running parallel to the ring axis. No previous work having been reported along these lines, an investigation was made into what proportion of the liquid flows through the ring interiors.

APPARATUS AND EXPERIMENTAL

The four ring sizes used in the work were of $\frac{1}{2}$ in., $\frac{3}{4}$ in., 1 in. and $1\frac{1}{4}$ in. diameter. Two columns were employed, each of length 3 ft, one having a diameter of 3 in., for use with the $\frac{3}{4}$ and 1 in. rings, and one of 4 in. for use with the 1 and $1\frac{1}{4}$ in. rings. Since Baker's limitation of 8 : 1 tower to packing diameter was not observed with these sizes, it was decided to minimize wall effects by minimizing wall area. In accordance with this, both columns were constructed of $\frac{1}{2}$ in. copper mesh. Initially it was feared that this mode of construction would result in liquid spurting out of the sides of the column. In the event, this fear proved to be groundless, an occasional drop of liquid only being ejected by this means.

The distributors consisted of cylindrical shells, arranged to be push-fits into the tops of the columns. At right angles to the axes of the cylinders, distributor plates were fitted, drilled with concentric circles of $\frac{1}{8}$ in. holes to secure an even distribution. To keep the impingement velocity of the liquid passing into the column to a minimum, small domes were mounted just above the plates, so that the liquid, leaving the circulatory system nozzle (q.v.), struck the dome and was projected horizontally against the vertical shell wall, where its kinetic energy was substantially destroyed.

The columns were suspended above a reservoir which collected the liquid leaving the column base. A small pump took suction from the base of this reservoir and discharged, via an orifice plate, through a nozzle which projected the liquid vertically down onto the distributor dome.

To determine the liquid flow through the interiors of individual rings, four large apertures, $1\frac{1}{2}$ in. square, were cut at varying levels in the column sides. The ring coinciding with the column centre line and the centre of one of the apertures was then removed from the column after removing those rings immediately beneath it, care being taken not to disturb the surrounding rings. A specially tapped ring of the same size was then inserted in the place of the originally selected ring and the other rings replaced. The tapping consisted of a toy balloon, cut across the diameter parallel to the mouthpiece, and stretched over one of the mouths of the ring. The mouthpiece led, via a length of rubber tube, to a measuring cylinder. A plate was provided around the tube to prevent liquid from reaching the cylinder via the tube exterior. The only limitation in replacing this tapped ring was that the tapped mouth should be lower than the free mouth. Fig. 1 illustrates the tapped ring in position in the column.

Interior flows were determined (by means of the measuring cylinder and a stop-clock), for varying values of the overall flow rate for a series of individual rings at each ring size. The number

VOL. 10 1959

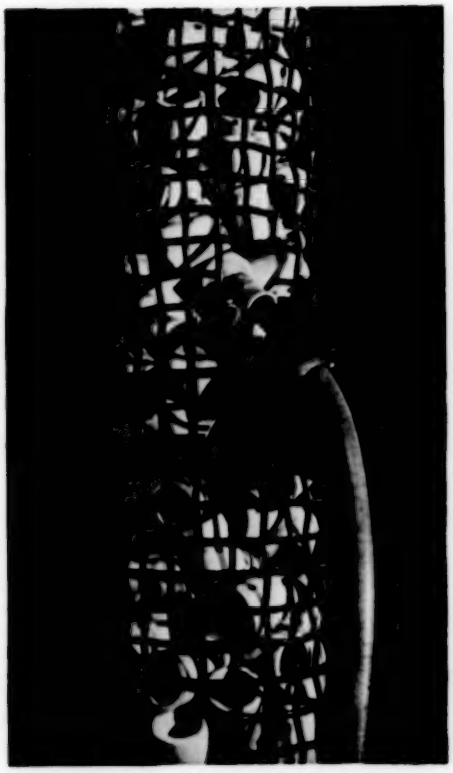

FIG. 1. Tapped ring assembly in position.

of rings in each series investigated in this manner ranged from twenty to forty. During the individual determinations, it was noticed that normally the flow through the ring interiors was smooth and uniform, becoming rather more erratic at very low interior flows. This was not considered to be of any great importance, since its effect on the average value would be negligible.

Water was used as the circulating fluid throughout.

Results

The interior flows at overall flows of 0·5, 1·0, 1·5, 2·0 and 2·5 ml/sec/cm² of bed cross-section were obtained for each ring size by interpolating between the experimental values of overall flow. These interpolated values were averaged to obtain mean interior flows in ml/sec. The results are summarized in Table 1.

The forty individual determinations for the ¾ in. rings were analysed statistically but no significant difference could be detected between the results of each of the four apertures. Were any wall effects present, a falling off in the interior flow would be expected from the central rings as the liquid descended. It was therefore concluded that the method of column construction adopted fulfilled its purpose of minimizing wall effects.

In order to compare interior flow with overall flow, it is first necessary to convert the former from ml/sec into ml/cm² sec units. For this purpose the packed bed can be considered as a series of layers of rings, the rings having a definite average cross-section of this layer per ring. From the geometrical similarity of Raschig rings of all sizes it can be shown that the ring diameter should be inversely proportional to the cube root of the number of rings per unit volume. This was verified for the rings used in the present work, the constant of proportionality being such that the average volume of bed taken up by a ring was equivalent to a cube of side 6·9 per cent in excess of ring diameter. The average area of cross-section taken up by a ring would be the square of this side. This square was therefore divided into the results of Table 1 to obtain mean interior flows in ml/cm² sec, these being plotted in Fig. 2.

Cross-sections Through Packed Beds

Figure 2 indicates the variation of interior flow with ring size and overall flow. To obtain

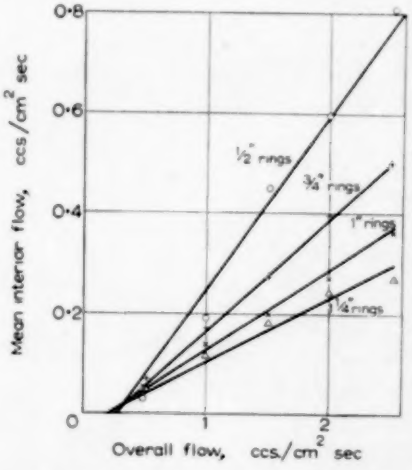

Fig. 2. Variation of interior flow with overall flow.

Table 1. *Mean interior flow*

Overall flow (ml/cm² sec):	0·5	1·0	1·5	2·0	2·5
Ring size (in.)	*Mean interior ring flow* (ml/sec)				
½	0·048	0·338	0·734	1·101	1·488
¾	0·290	0·719	1·126	1·593	2·068
1	0·360	1·029	1·471	1·971	2·686
1¼	0·782	1·333	2·069	2·851	3·048

further insight into this variation, a model of a packed bed was constructed with the object of ascertaining the appearance of plane cross-sections through these beds. Solid $\frac{3}{4}$ in. cylinders were cut from $\frac{3}{4}$ in. thick slabs of black plasticine by means of a cork borer. These cylinders were packed at random into an open topped tin-plate box, 12 in. high with a six inch square base. Molten paraffin wax was poured into the box which had just previously been heated in an oven to a temperature slightly in excess of the wax melting point in order to preclude any premature wax solidification. After thorough cooling, the tinplate was stripped off and the block thus obtained sliced in planes parallel to its base by means of a guided wire. The resultant cross-sections were then traced, a typical tracing being reproduced in Fig. 3.

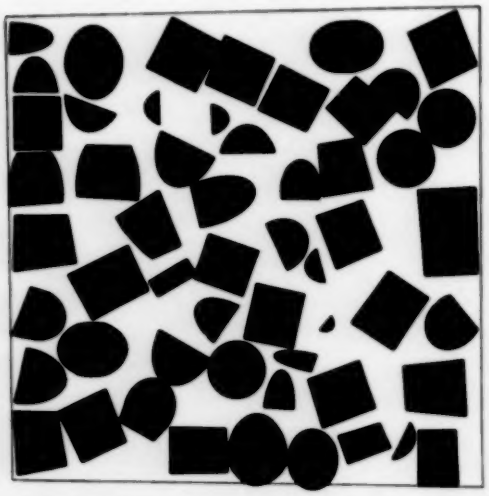

FIG. 3. Typical packed bed cross-section.

Examination of these cross-sections reveals, as would be expected, that all the profiles appear as conic sections of various types. Straight lines must represent sections thorough the ring mouths or sections through the cylindrical surfaces of rings whose axes are parallel to the plane of cross-section. If liquid is considered to be flowing through one of these cross-sections it is apparent that the interior flowing liquid must be moving perpendicularly to the mouth; in half of the cases leaving the ring, while in the remaining half, entering. It was postulated that the total length of the ring mouth profiles, when halved, corrected for wall thickness and divided by the total cross-sectional area, represented a measure of a bed's capacity to accept liquid into the ring interiors. This measure was accordingly denoted as the "inlet availability" of the bed, and on being computed for the mode sections ($\frac{3}{4}$ in. rings) was found to have a value of 0·101 cm/cm². From the geometrical similarity of Raschig rings, it follows that inlet availability is inversely proportional to ring size and hence can be calculated for all the ring sizes used in the present work.

At given values of the overall flow rate the interior flow rate is directly proportional to the inlet availability, values of the proportionality constant being plotted against overall flow in Fig. 4. This plot is linear; its failure to pass

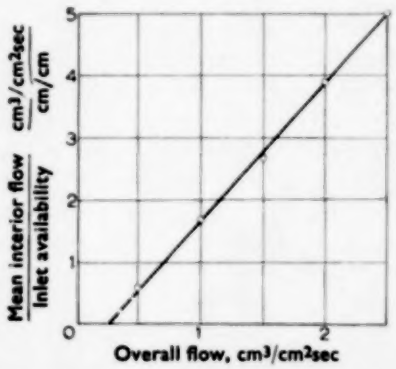

FIG. 4. Variation of the ratio of interior flow to inlet availability with overall flow.

through the origin possibly indicating that a threshold value of overall flow must be reached before interior flow commences. With the aid of this plot, and a knowledge of the inlet availability, interior flows can be estimated.

CONCLUSIONS

The interior flow in ring packed beds has been shown to vary linearly with overall flow through the bed. Figure 2 demonstrates that as ring size increases there is a definite falling off in interior flow. (This constitutes about 29 per cent of the total flow through the bed for $\frac{1}{2}$ in. rings, 19 per

cent for $\frac{3}{4}$ in., 14 per cent for 1 in. and 12 per cent for $1\frac{1}{2}$ in. rings). With ring sizes in excess of $1\frac{1}{4}$ in it can be anticipated that this proportion will be 10 per cent or less and that, as a consequence, the interior surface can contribute little to the mass transfer in the bed. A model of a packed bed has been used to explain the observed variations and to derived a method of predicting the interior flow.

Further work demonstrates how a knowledge of the interior flow can be used to resolve liquid hold-up into interior and exterior components, thereby obtaining better insight into the flow through ring packed beds.

Acknowledgements—This work constitutes part of a Ph.D. Thesis submitted in the University of London [12] Thanks are due to Professor M. B. DONALD of the Ramsay Laboratory of Chemical Engineering for constant advice and interest, and to the Esso Petroleum Company Limited whose provision of a maintenance grant enabled this research to be pursued.

REFERENCES

[1] MAYO F., HUNTER T. G. and NASH A. W. *J. Soc. Chem. Ind.* 1935 **44** 375.

[2] SHULMAN H. L., ULLRICH C. F., PROULX A. Z. and ZIMMERMAN J. O. *Amer. Inst. Chem. Engrs. J.* 1955 **1** 253.

[3] SHERWOOD T. K. and PIGFORD R. L. *Absorption and Extraction* (2nd Ed.) McGraw-Hill, New York 1952.

[4] WEISMAN I. and BONILLA C. F. *Industr. Engng. Chem.* 1950 **42** 1099.

[5] TAECKER R. G. and HOUGEN O. A. *Chem. Engng. Progr.* 1949 **45** 188.

[6] CHILTON T. H. and COLBURN A. P. *Industr. Engng. Chem.* 1934 **26** 1183.

[7] SHULMAN H. L. and DEGOUFF J. J. *Industr. Engng. Chem.* 1952 **44** 1915.

[8] FELLINGER I. Sc.D. Thesis, Mass. Inst. Tech. 1941.

[9] JESSER B. W. and ELGIN J. C. *Trans. Amer. Inst. Chem. Engrs.* 1943 **39** 277.

[10] BOND J. Ph.D. Thesis, London 1955 ; BOND J. and DONALD M. B. *Chem. Engng. Sci.* 1957 **6** 237.

[11] BAKER T. H., CHILTON T. H. and VERNON H. C. *Trans. Amer. Inst. Chem. Engrs.* 1935 **31** 296.

[12] GREENAWAY D. Ph.D. Thesis, London 1958.

Chemical Engineering Science, 1959, Vol. 10, pp. 202 to 211. Pergamon Press Ltd. London. Printed in Great Britain

Chemical reactions catalysed on a tube wall

S. KATZ

American Cyanamid Company, New York City, New York, U.S.A.

(*Received* 10 *July* 1958)

Abstract—The progress of a reaction catalysed on a tube wall is analysed for an assigned radial pattern of axial velocity. A procedure is given for mathematically transforming an observed axial profile of cross-section average reactant concentrations into a plot of the instantaneous reaction rate vs. the wall concentration at which the reaction is proceeding. It is also shown how to calculate the average conversion at any contact time for an arbitrary reaction rate function.

Résumé—L'évolution d'une réaction catalysée sur la paroi d'un tube est étudiée pour une distribution radiale fixe de la vitesse longitudinale. Un moyen est donné pour transformer mathématiquement un profil observé longitudinal de concentration moyenne de réactants pour une section déterminée, en fonction de la concentration de paroi à laquelle la réaction se développe. L'auteur montre aussi comment calculer la conversion moyenne pour un temps de contact quelconque pour toute fonction arbitraire de la vitesse réactionnelle.

Zusammenfassung—Das Fortschreiten einer Reaktion, die an einer Rohrwand katalysiert ist, wird für eine angenommene radiale Verteilung der Axialgeschwindigkeit untersucht. Ein Verfahren wird angegeben zur mathematischen Tranformation eines beobachteten axialen Profils der über den Querschnitt gemittelten Konzentrationen der Reaktanten in eine Beziehung zwischen der momentanen Reaktionsgeschwindigkeit und der Wandkonzentration, bei der die Reaktion fortschreitet. Es wird auch gezeigt, wie man die mittlere Umsetzung bei irgend einer Kontaktzeit berechnen kann für eine beliebige Funktion der Reaktionsgeschwindigkeit.

1. INTRODUCTION

A GAS, rich in some reactive material, flows down the inside of a tube. At the tube wall, the reactive molecules are converted into a new substance at a rate which is some function of their concentration at the wall. The reactive molecules diffuse out to the tube wall just rapidly enough to balance this reaction rate.

Two questions suggest themselves. The first is a question of kinetic analysis: without making any prior assumption about the form of the rate function, what accessible measurements can one transform mathematically into a knowledge of the instantaneous reaction rates and of the corresponding wall concentrations of the reactive subtance. The second is a design question: knowing the rate function and the other physical parameters of the system, how can one calculate the contact time, say, needed to achieve a desired conversion. The present study is aimed at kinetic analyses, although certain new forms of answer to design questions will appear as a by-product.

The design question has been considered in a variety of contexts. For example, TOWNSEND [1] studied a gas flow with a parabolic velocity profile, and solved an ion-diffusion problem with an absorbing tube wall. This corresponds chemically to the case of infinitely fast reaction. TAYLOR [13, 14] studied a similar flow, and gave an approximate solution to a diffusion problem with a reflecting tube wall. This corresponds chemically to the case of infinitely slow reaction. DAMKÖHLER [2] and BARON and his co-workers [3] solved corresponding problems with first order reactions of finite speed taking place at the tube wall, but with a flat velocity profile (plug flow) in the tube.

CHAMBRÉ [15] formulated this class of problems in a general way that accounted for the hydrodynamics of the boundary layer which develops at the

wall, as well as for the reaction catalysed on the wall. He gave, for certain classes of flows, integral equations expressing surface reaction rate as an integral operator on surface reactant concentration. Also, he and ACRIVOS [4] gave an exact (in terms of boundary layer theory) analytical solution of their enlarged design problem for a limited class of rate functions. Further, by approximating the gas velocity profile near the catalytic surface, they arrived at integral equations of the same kind for the general boundary layer situation, expressing surface reaction rate as an integral operator on wall reactant concentration. These integral equations furnished in principle a method of carrying out kinetic analyses, in that if a reactant concentration profile were measured at the catalytic surface, it could be transformed into a surface reaction rate by applying a suitable integral operator.

The present study sets itself the more limited objective of accounting for a reaction catalysed on the wall of a cylindrical tube, where the process gas undergoes an axial flow with a preassigned radial gradient. In this limited context, it is able to indicate a much easier experimental way to make kinetic analyses, by permitting the experimenter to work with cross-section average concentrations, rather than forcing him to measure concentrations right at the wall. A solution to the design problem is given, in terms of an integral equation in the wall concentration of the reactant. The integral equation gives the wall reactant concentration as an integral operator on the surface reaction rate. This inversion of the integral equations of [4] and [15] permits the direct calculation of reactant concentration at the wall from a knowledge of the instantaneous surface reaction rate. It is shown further that if the cross-section average reactant concentration be known as a function of contact time, a suitably scaled differentiation with respect to contact time will give a profile of instantaneous reaction rates. Thus, without making any prior assumption about the form of the rate function, one can obtain reaction rate as a function of wall concentration by making suitable measurements of the cross-section average concentrations alone.

The numerical procedures involved in setting up the integral equations needed to handle either the design problem or the kinetic analysis problem are quite formidable. They can, however, be scaled so as to depend only on the shape of the velocity profile, and not at all on the actual speed of the gas, the diameter of the tube, the size of the diffusion coefficient, the inlet condition of the gas, or the form of the rate function. These preliminary set-up calculations can thus be performed once and for all for any physical situation involving, say, a parabolic velocity profile. The calculations that then have to be made in any particular case of design or data analysis are, in comparison, quite modest in size.

For our present purposes, it seems to be necessary to evaluate the kernel in our integral equation anew, despite the wealth of mathematically very similar problems already treated in the literature (see, for example, [17]). Perhaps the closest to our needs is the numerical solution to the Graetz problem for a parabolic velocity profile given by SELLARS and his co-workers [16]. Their solution, however, is given as an expansion in eigenfunctions vanishing at the tube wall, and so, because of Gibbs' phenomenon difficulties (see, for example, [5]) cannot, as we require, be readily evaluated at the wall. It has, as a result, limited utility for our kinetic analyses, although it can be used as a kernel in the integral equations of [15] for design calculations.

The present mathematical analysis holds for quite general velocity profiles. Since, however, axial diffusion is neglected compared to the main convective effect of the gas stream, the range of application will likely be for Poiseuille flow (parabolic profile) and a correspondingly small molecular (laminar) diffusivity. It should be noted also that the mathematical analysis is all for a steady state, isothermal situation. An experimental study that meets these conditions is in progress, and will be reported in the near future, along with the explicit numerical schemes for analysing the data.

Section 2 below formulates the mathematical problem corresponding to the physical system in question, and Section 3 carries out the reduction to an integral equation. Section 4 sketches the use of the integral equation in kinetic analyses,

and Section 5 its use in the design problem. Section 6 is essentially a mathematical appendix on the development in a suitable eigenfunction expansion of the kernel of the integral equation given in Section 3.

2. THE DIFFERENTIAL EQUATIONS

In a cylindrical tube, establish a co-ordinate system:

z = axial co-ordinate (measured in the direction of gas flow from $z = 0$ at inlet), ft

r = radial co-ordinate (measured from $r = 0$ at tube centre to $r = R$ at tube wall), ft

Gas flows down the tube at a steady velocity

U = average axial velocity (in the direction of increasing axial co-ordinate z), ft/sec

and with a velocity profile $p(r)$, so that

$Up(r)$ = axial velocity at radial co-ordinate r, ft/sec

The velocity profile p must then be taken to be normalized on the cross-section area of the tube

$$\frac{1}{\pi R^2}\int_0^R p(r)\, 2\pi r\, dr = 1. \qquad (1)$$

A general power law class of profiles p vanishing at the tube wall is

$$p(r) = \frac{\nu+1}{\nu}\left\{1 - \left(\frac{r}{R}\right)^{2\nu}\right\};\ \nu > 0 \qquad (2)$$

where $\nu = 1$ corresponds to the Poiseuille parabolic flow, $\nu = 2$ to the turbulent fourth power profile, and infinite ν to plug flow. The flow is taken to be at constant temperature.

In the process stream, let the concentration of the reactive molecules be

$c(r, z)$ = reactant concentration, mols/ft^3

with the uniform value at the tube inlet

c_0 = inlet reactant concentration, mols/ft^3

Let the reactive molecules have diffusivity

D = radial diffusivity of reactant, ft^2/sec

(axial diffusivity is neglected), and let them be consumed at the tube wall at the rate

$k(c)$ = surface reaction rate, mols/ft^2 sec

It is this function k whose form will be left unspecified in what follows. The assumption of constant temperature permits us to take k to depend only on the reactant concentration c.

A differential material balance on the reactive molecules at any point in the tube then gives

$$D\left(\frac{\partial^2 c}{\partial r^2} + \frac{1}{r}\frac{\partial c}{\partial r}\right) - Up(r)\frac{\partial c}{\partial z} = 0;$$
$$0 < r < R,\quad z > 0 \qquad (3)$$

At the tube inlet, the reactant concentration is specified

$$c = c_0;\quad 0 < r < R,\quad z = 0 \qquad (4)$$

At the tube wall, a differential material balance gives

$$-D\frac{\partial c}{\partial r} = k(c);\quad r = R,\quad z > 0 \qquad (5)$$

Finally, for mathematical completeness, a regularity condition at the tube centre is imposed

$$c \text{ bounded};\quad r = 0,\quad z > 0 \qquad (6)$$

Equations (3)–(6) represent the mathematical specification of the concentration function $c(r, z)$.

Of particular interest in what follows will be the cross-section average reactant concentration weighted by the local gas velocity,

$$\bar{c}(z) = \frac{1}{\pi R^2}\int_0^R c(r, z)\, p(r)\, 2\pi r\, dr \qquad (7)$$

This is a true average, in view of the normalization (1) of p. The definition (7) of $\bar{c}$ imagines a measurement as made by collecting the total flow past a cross-section of the tube for a given time, and assaying the material so collected for reactant. It is adopted as conforming most closely to the experimental work mentioned in the preceding section, but it is by no means the only reasonable definition. For example, if one viewed a measurement as made by focussing attention on a differential slice of the tube and instantaneously assaying the material in that slice for reactant, the simple area average

$$\bar{c}(z) = \frac{1}{\pi R^2}\int_0^R c(r, z)\, 2\pi r\, dr$$

would be the more appropriate.

VOL. 10 1959

It will be more convenient to carry out the subsequent analysis in terms of certain dimensionless variables. Introduce the dimensionless co-ordinates

$$\left.\begin{aligned} x &= \frac{r}{R} \\ &= \text{dimensionless radial co-ordinate} \\ \theta &= \frac{z/U}{R^2/2D} \\ &= \text{dimensionless axial co-ordinate} \end{aligned}\right\} \quad (8)$$

It will be noted that θ is a contact time, normalized on a diffusion time. Define in terms of the velocity profile p the weighting function

$$\rho(x) = 2\,x\,p(R\,x)$$

with, from (1),

$$\int_0^1 \rho(x)\,dx = 1 \quad (9)$$

The power law form of $\rho(x)$ corresponding to (2) is

$$\rho(x) = \frac{2(\nu+1)}{\nu}\,x\,(1-x^{2\nu}); \quad \nu > 0 \quad (10)$$

where, as before, $\nu = 1$ corresponds to parabolic flow, etc. Finally, define a dimensionless concentration function

$$v(x,\theta) = \frac{1}{c_0}\,c\left(Rx, \frac{R^2U\,\theta}{2D}\right) \quad (11)$$

= dimensionless reactant concentration

and a dimensionless rate function

$$h(v) = \frac{R}{c_0 D}\,k(c_0 v) \quad (12)$$

= dimensionless surface reaction rate

In terms of these new quantities, the boundary value problem in equations (3)-(6) becomes

$$\left.\begin{aligned} &\frac{\partial}{\partial x}\left(x\frac{\partial v}{\partial x}\right) = \rho(x)\frac{\partial v}{\partial \theta};\ 0<x<1,\ \theta>0 \\ &v = 1 \qquad ;\ 0<x<1,\ \theta=0 \\ &v \text{ bounded} \qquad ;\ x=0,\ \theta>0 \\ &\frac{\partial v}{\partial x} + h(v) = 0 \qquad ;\ x=1,\ \theta>0 \end{aligned}\right\} \quad (13)$$

The equations (13) represent the mathematical specification of the dimensionless concentration function $v(x,\theta)$. The parameters R, c_0, D, U have been scaled out, and all that remains is the velocity profile shape $\rho(x)$, and the dimensionless rate function $h(v)$. Define finally an average v,

$$\bar{v}(\theta) = \int_0^1 v(x,\theta)\,\rho(x)\,dx \quad (14)$$

By virtue of the normalization (9) of ρ, this is a true average. Also,

$$\bar{v}(\theta) = \frac{1}{c_0}\,\bar{c}\left(\frac{R^2U\,\theta}{2D}\right) \quad (15)$$

by (7) and (11).

The following section will discuss the reduction of (13) to an integral equation.

3. Reduction to an Integral Equation

The reduction of (13) to an integral equation begins by replacing the assigned function of concentration $h(v)$ by an assigned function of "time" $f(\theta)$. The non-linear boundary value problem (13) is thus replaced by the linear problem

$$\left.\begin{aligned} &\frac{\partial}{\partial x}\left(x\frac{\partial w}{\partial x}\right) = \rho(x)\frac{\partial w}{\partial \theta};\ 0<x<1,\ \theta>0 \\ &w = 1 \qquad ;\ 0<x<1,\ \theta=0 \\ &w \text{ bounded} \qquad ;\ x=0,\ \theta>0 \\ &\frac{\partial w}{\partial x} + f(\theta) = 0 \qquad ;\ x=1,\ \theta>0 \end{aligned}\right\} \quad (16)$$

in the new function $w(x,\theta)$. There is a certain arbitrariness in the choice of the problem (16). One could, for example, replace the assignment of $\partial w/\partial x$ at $x=1$ by an assignment of w. This would lead however in Section 6 to an eigenvalue problem (28) with $\phi = 0$ at $x = 1$, and the series expansions made in these eigenfunctions would be subject to Gibbs' phenomenon difficulties (see, for example, [5]) at the wall $x = 1$.

Introducing Laplace transforms (see, for example, [6]) suggests the form of the solution of (16). Setting

$$\left.\begin{aligned} w^*(x,\sigma) &= \int_0^\infty e^{-\sigma\theta}\, w(x,\theta)\,d\theta \\ f^*(\sigma) &= \int_0^\infty e^{-\sigma\theta} f(\theta)\,d\theta \end{aligned}\right\}$$

the equations (16) give

$$\left.\begin{aligned} &\frac{\partial}{\partial x}\left(x\frac{\partial w^*}{\partial x}\right) = \rho(x)\{\sigma w^* - 1\}; && 0<x<1 \\ &w^* \text{ bounded} && ; \ x=0 \\ &\frac{\partial w^*}{\partial x} + f^*(\sigma) = 0 && ; \ x=1 \end{aligned}\right\} \quad (17)$$

The equations (17) can be solved in the form

$$w^*(x,\sigma) = \frac{1}{\sigma} - I^*(x,\sigma) f^*(\sigma) \qquad (18)$$

where I^* has the nature of a transfer function connecting f with w and must itself satisfy the equations

$$\left.\begin{aligned} &\frac{\partial}{\partial x}\left(x\frac{\partial I^*}{\partial x}\right) = \rho(x)\,\sigma I^* ; && 0<x<1 \\ &I^* \text{ bounded} && ; \ x=0 \\ &\frac{\partial I^*}{\partial x} = 1 && ; \ x=1 \end{aligned}\right\} \quad (19)$$

Now $I(x,\theta)$, the inverse Laplace transform of $I^*(x,\sigma)$,

$$I^*(x,\sigma) = \int_0^\infty e^{-\sigma\theta} I(x,\theta)\,d\theta$$

is essentially the response of w to a unit impulse f, since (18) can be translated back into the time domain to give the solution of (16) in terms of I as

$$w(x,\theta) = 1 - \int_0^\theta I(x,\theta-\tau) f(\tau)\,d\tau \qquad (20)$$

Taking the Laplace transform inverse of (19) gives a boundary value problem for I

$$\left.\begin{aligned} &\frac{\partial}{\partial x}\left(x\frac{\partial I}{\partial x}\right) = \rho(x)\frac{\partial I}{\partial \theta}; && 0<x<1, \ \theta>0 \\ &I = 0 && ; \ 0<x<1, \ \theta=0 \\ &I \text{ bounded} && ; \ x=0, \ \theta>0 \\ &\frac{\partial I}{\partial x} = \delta(\theta) && ; \ x=1, \ \theta>0 \end{aligned}\right\} \quad (21)$$

In (21), $\delta(\theta)$ is a Dirac delta function (see, for example, [7]), strictly, a right-sided delta function with

$$\int_0^\theta \delta(\tau)\,\psi(\tau)\,d\tau = \begin{cases} 0; & \theta = 0 \\ \psi(0); & \theta > 0 \end{cases}$$

for suitable testing functions ψ.

The question of solving (21) will be taken up in the concluding section of this study. It should be noted now, however, that I depends only on on the velocity profile shape ρ, and not at all on any other specific physical or geometrical characteristic of the physical system. Proceeding then as though I were known, recall from (13) and (16) that w reduces to the dimensionless concentration v if $f(\theta)$ is replaced by $h\{v(1,\theta)\}$. Making this identification in (20) gives

$$v(x,\theta) = 1 - \int_0^\theta I(x,\theta-\tau)\, h\{v(1,\tau)\}\,d\tau \quad (22)$$

Taking $x = 1$ in (22) gives the desired integral equation in the tube wall concentration $v(1,\theta)$

$$v(1,\theta) = 1 - \int_0^\theta M(\theta-\tau)\, h\{v(1,\tau)\}\,d\tau \quad (23)$$

where

$$M(\theta) = I(1,\theta) \qquad (24)$$

Equation (23) contains the root of the solution of the boundary value problem (13). In kinetic analyses, it will be used to translate a knowledge of the reaction rate $h\{v(1,\theta)\}$ to a knowledge of the corresponding wall concentration $v(1,\theta)$. In making designs, (23) will be solved for $v(1,\theta)$, and correspondingly $h\{v(1,\theta)\}$, and the solution substituted into (22) to give the detailed performance of the reactor. These matters will be discussed in the two sections following.

4. Application to Kinetics Studies

Preliminary to the application of the integral relation (23) to rate data lies the determination of these rate data from cross-section average concentrations.

To see how this determination is to be made, integrate the first equation of (13) with respect to x. Recalling (14) gives

$$\frac{d\,\bar{v}(\theta)}{d\,\theta} = \int_0^1 \rho(x)\,\frac{\partial v(x,\theta)}{\partial\,\theta}\,dx$$

$$= \int_0^1 \frac{\partial}{\partial x}\left\{x\,\frac{\partial v(x,\theta)}{\partial\,x}\right\}dx$$

$$= x\,\frac{\partial v(x,\theta)}{\partial\,x}\Bigg|_{x=0}^{x=1}$$

which, on applying the boundary conditions in (13), becomes

$$h\{v(1,\theta)\} = -\frac{d\,\bar{v}(\theta)}{d\,\theta} \qquad (25)$$

A kinetics experiment might then proceed along the following lines. A suitably fine grained profile of cross-section average reactant concentration $\bar{c}(z)$, as defined in (7), would be measured. (More realistically, measurements of $\bar{c}$ might be made on a single apparatus for a single value of z over a suitably fine grained range of the average gas velocity U). The measured $\bar{c}$ would then be scaled, as in (8), (15), to a profile of dimensionless average concentrations $\bar{v}(\theta)$. Differentiating $\bar{v}(\theta)$ numerically according to (25) would give the corresponding profile of dimensionless reaction rate $h\{v(1,\theta)\}$, and carrying out the integration in (23) numerically with a precalculated $M(\theta)$ would give the corresponding profile of dimensionless wall concentrations $v(1,\theta)$. These dimensionless wall concentrations and reaction rates could then be scaled back to the physical quantities $c(R,z)$ and $k\{c(R,z)\}$ according to (8), (11), (12). This scaling back and forth would, of course, require a knowledge of the gross physical parameters of the system: the inlet reactant concentration c_0, the reactant diffusivity D, the mean gas velocity U, the tube radius R.

The end product of the analysis would be a table (plot) of the instantaneous reaction rate $k(c)$ against the reactant concentration c for whatever range of wall concentrations $c(R,z)$ happened to be implicit in the experimental set-up. Such information could then serve to test assumptions about the reaction mechanism, exactly as if it had been obtained from, say, suitable measurements made right at the catalytic surface of a differential reactor.

The same sort of analysis could of course be made for homogeneous reactions, but there, as is clear (and well known), measurement of average concentration will in general give knowledge only of average reaction rates. It is just the specific character of the surface catalysed reaction that permits measurements of average concentration to lead to knowledge of the reaction rates at specific places where the working concentrations can be deduced as well.

5. Application to Reactor Design

Suppose that here the surface rate function $k(c)$ and the velocity profile $Up(r)$ have been specified, as well as the other parameters of the physical system: the inlet reactant concentration c_0, the reactant diffusivity D and the tube radius R. Suppose further that the dimensional scaling in (8), (11), (12) has been carried out, leaving only the dimensionless reactant concentration $v(x,\theta)$, the dimensionless rate function $h(v)$, the velocity profile shape $\rho(x)$, and of course the precalculated integral kernels, $I(x,\theta)$ and $M(\theta)$.

The first step in the design would be to solve the integral equation (23). This would give the wall reactant concentration $v(1,\theta)$, and concurrently the instantaneous surface reaction rate $h\{v(1,\theta)\}$. Then, if one wanted to predict the detailed performance of the reactor, one could enter (22) with $h\{v(1,\theta)\}$ as a known function of θ, and calculate $v(x,\theta)$ for any desired x and θ. If, however, it were sufficient to know the average conversion at any cross-section, one would proceed differently. Averaging the initial condition of (13) according to (14) gives

$$\bar{v}(0) = 1$$

and with this, (25) can be integrated to give

$$v(\theta) = 1 - \int_0^\theta h\{v(1, \tau)\}\, d\tau \qquad (26)$$

In (26), the integrand can be regarded as a known function of θ, following the solution of (23), and one running integration would give a plot of v against θ from which any desired conversion could be picked off.

It remains to discuss the solution of the integral equation (23). This is a non-linear integral equation of Volterra type, and can be solved, formally at least, by the iterative scheme

$$v_{n+1}(1, \theta) = 1 \quad \int_0^\theta M(\theta - \tau)\, h\{v_n(1, \tau)\}\, d\tau\,; \quad n = 0, 1, 2, \ldots \qquad (27)$$

starting from any first guess at v, say,

$$v_0(1, \theta) = 1$$

Convergence of this scheme is discussed for linear integral equations in, for example, [8]. The linear case, where $h(v)$ is proportional to v, corresponds physically to the case of a first order reaction. Convergence is proved in the linear case under certain regularity conditions on the kernel M, encompassing the weak singularity to be expected in M (see the example in Section 6) because of the wall condition in (21). The extension of the proof to the non-linear case at hand is straightforward, and requires only certain mild regularity conditions on the rate function $h(v)$. For instance, that h, as a function of v, have a continuous second derivative would be enough not only to guarantee the convergence analytically, but to permit an integration by parts in (23) to remove the singularity of M. Such an integration by parts would furnish a means of carrying out the iterative solution (27) by repeated numerical integration, using a precalculated $M(\theta)$ (or rather, its indefinite integral). The final integration in (26) would of course also be carried out numerically

The design method sketched above (perhaps with an improved first guess at $v(1, \theta)$ made along the lines of [18]) assumes that one has precalculated the kernel $M(\theta)$ in the integral equation (23). This, as discussed in Section 6, is itself a very formidable calculation, and would likely be made only in cases where extensive kinetic analyses were to be carried out along the lines of Section 4. If an isolated design calculation had to be made, one would use instead the integral equation of [15], for which, in the case of Poiseuille flow, the kernel has been calculated in [16]. Or possibly, it would be more economical to work directly from the partial differential equations (3)-(6), or their dimensionless form (13). One would, as is commonly done, introduce a network of points in the x-θ plane, replace the differential equations by the appropriate difference equations, and solve these difference equations numerically (see, for example, [11]).

6. Evaluation of the Kernel

This section will present expansions of the integral kernels I and M of Section 3 in series of certain eigenfunctions. The relevant eigenvalue problem arising out of (21) is to find constants λ and functions $\phi(x)$ for which

$$\left.\begin{aligned} &\frac{d}{dx}\left(x\frac{d\phi}{dx}\right) + \lambda\rho(x)\phi = 0;\ 0 < x < 1 \\ &\phi \text{ bounded} \qquad ;\ x = 0 \\ &\frac{d\phi}{dx} = 0 \qquad ;\ x = 1 \end{aligned}\right\} \qquad (28)$$

Problems very similar to this (with ϕ rather than $d\phi/dx$ vanishing at $x = 1$) were solved numerically by Townsend [1] and by Sellars and his coworkers [16] for a parabolic velocity profile, $v = 1$ in the $\rho(x)$ of (10). These workers made their calculations in terms of analytic approximations to the solutions $\phi(x)$. It is possible that more economical computing schemes can be arrived at by introducing, as is commonly done, a chain of points on the x-axis, replacing (28) by the appropriate difference equations, and carrying out the calculation of the eigensolutions by what are essentially algebraic means (see, for example, [12]). We shall, however, reserve for future report the question of numerical solutions of (28), and shall give here only an expansion, in series of these solutions, of the impulse response $I(x, \theta)$ of (21) and its boundary value $M(\theta)$ of (24).

The problem (28) is an example of an eigenvalue problem of Sturm-Liouville type with a

singular endpoint, such as is discussed for example in [9]. The singularity (the vanishing of the coefficient of $d^2\phi/dx^2$ at $x = 0$) is the same as occurs in Bessel's equation, which is indeed the particular case of (28) with $\rho(x) = 2x$, corresponding to infinite ν (plug flow) in (10). There is only a sequence of values of λ for which (28) has solutions $\phi(x)$ not identically 0. In the cases of physical interest where $\rho(x) \geqslant 0$, these eigenvalues λ are all $\geqslant 0$, and may accordingly be arranged in the order

$$0 \leqslant \lambda_0 < \lambda_1 < \lambda_2 < \ldots . \tag{29}$$

To each λ_n corresponds a single eigenfunction

$$\phi = \phi_n(x); \quad n = 0, 1, 2, \ldots . \tag{30}$$

satisfying (28), and quite arbitrary functions $f(x)$ can be expanded in series of the ϕ_n. Further, the eigenfunctions $\phi_n(x)$ are orthogonal with the weight $\rho(x)$

$$\int_0^1 \phi_m(x)\,\phi_n(x)\,\rho(x)\,dx = 0; \quad m \neq n \tag{31}$$

and can clearly be normalized to make

$$\int_0^1 \phi_n^2(x)\,\rho(x)\,dx = 1 \tag{32}$$

Thus a Fourier expansion

$$f(x) = \sum_{n=0}^{\infty} f_n\,\phi_n(x); \quad 0 < x < 1 \tag{33}$$

has the coefficients

$$f_n = \int_0^1 f(x)\,\phi_n(x)\,\rho(x)\,dx \tag{34}$$

Note finally that the leading eigen solution (29), (30) is

$$\lambda_0 = 0, \quad \phi_0(x) = 1 \tag{35}$$

as may be seen by inspecting (28).

In solving (21) for the impulse response I, it turns out to be convenient to work through the step response

$$s(x, \theta) = \int_0^\theta I(x, \tau)\,d\tau$$

Inserting the Laplace transform of s into (19) and inverting the result shows how to integrate (21) to obtain a boundary value problem for s

$$\left.\begin{aligned}
&\frac{\partial}{\partial x}\left(x\frac{\partial s}{\partial x}\right) = \rho(x)\frac{\partial s}{\partial \theta}; && 0 < x < 1, \ \theta > 0\\
&s = 0 && ; \ 0 < x < 1, \ \theta = 0\\
&s \text{ bounded} && ; \ x = 0, \quad \theta > 0\\
&\frac{\partial s}{\partial x} = 1 && ; \ x = 1, \quad \theta > 0
\end{aligned}\right\} \tag{36}$$

from which I may be recovered as

$$I(x, \theta) = \frac{\partial s(x, \theta)}{\partial \theta} \tag{37}$$

We rewrite the boundary value problem (36) by setting

$$s(x, \theta) = \frac{x^2}{2} + s_1(x, \theta) + s_2(x, \theta) \tag{38}$$

with

$$\left.\begin{aligned}
&\frac{\partial}{\partial x}\left(x\frac{\partial s_1}{\partial x}\right) = \rho(x)\frac{\partial s_1}{\partial \theta}; && 0 < x < 1, \ \theta > 0\\
&s_1 = -\frac{x^2}{2} && ; \ 0 < x < 1, \ \theta = 0\\
&s_1 \text{ bounded} && ; \ x = 0, \ \theta > 0\\
&\frac{\partial s_1}{\partial x} = 0 && ; \ x = 1, \ \theta > 0
\end{aligned}\right\} \tag{39}$$

and

$$\left.\begin{aligned}
&\frac{\partial}{\partial x}\left(x\frac{\partial s_2}{\partial x}\right) = \rho(x)\frac{\partial s_2}{\partial \theta} - 2x && ; \ 0 < x < 1, \ \theta > 0\\
&s_2 = 0 && ; \ 0 < x < 1, \ \theta = 0\\
&s_2 \text{ bounded} && ; \ x = 0, \quad \theta > 0\\
&\frac{\partial s_2}{\partial x} = 0 && ; \ x = 1, \quad \theta > 0
\end{aligned}\right\} \tag{40}$$

The term $x^2/2$ in (38) is taken to cancel the inhomogeneous boundary condition in (36). It is taken as $x^2/2$ rather than as, for example, x, in order to preserve the expected flatness of the solution at $x = 0$.

The boundary value problem (39) may be solved in terms of the eigen solutions (29), (30) by direct separation of variables. Let

$$a_n = \int_0^1 \frac{x^2}{2} \phi_n(x) \rho(x)\, dx; \quad n = 0, 1, 2, \ldots. \quad (41)$$

so that, recalling (33), (34), we have

$$\frac{x^2}{2} = \sum_{n=0}^{\infty} a_n \phi_n(x); \quad 0 < x < 1$$

Then

$$s_1(x, \theta) = -\sum_{n=0}^{\infty} a_n \phi_n(x) e^{-\lambda_n \theta}$$

which, taking specific note of the leading eigensolution (35), may be written

$$s_1(x, \theta) = -a_0 - \sum_{n=1}^{\infty} a_n \phi_n(x) e^{-\lambda_n \theta}$$

The problem (40) is solved somewhat less directly. Let

$$b_n = \int_0^1 2x \phi_n(x)\, dx; \quad n = 0, 1, 2, \ldots. \quad (43)$$

so that, by (33) and (34),

$$2x = \rho(x) \sum_{n=0}^{\infty} b_n \phi_n(x); \quad 0 < x < 1$$

and note that, by (35),

$$b_0 = 1$$

Then assuming a solution for s_2 in the form

$$s_2(x, \theta) = \sum_{n=0}^{\infty} \phi_n(x) \psi_n(\theta) \quad (44)$$

leads to the following ordinary differential equations in the ψ_n

$$\left.\begin{aligned} \frac{d\psi_n}{d\theta} + \lambda_n \psi_n &= b_n; \quad \theta > 0 \\ \psi_n &= 0 \qquad\quad ; \quad \theta = 0 \end{aligned}\right\} \quad n = 0, 1, 2, \ldots.$$

which have the solution

$$\left.\begin{aligned} \psi_0 &= \theta \\ \psi_n &= b_n \frac{1 - e^{-\lambda_n \theta}}{\lambda_n}; \quad n = 1, 2, \ldots. \end{aligned}\right\} \quad (45)$$

Substituting (45) into (44) and recalling (35) gives

$$s_2(x, \theta) = \theta + \sum_{n=1}^{\infty} b_n \phi_n(x) \frac{1 - e^{-\lambda_n \theta}}{\lambda_n} \quad (46)$$

Substituting (42) and (46) back into (38) and applying (37) gives the solution of (21) as

$$I(x, \theta) = 1 + \sum_{n=1}^{\infty} (\lambda_n a_n + b_n) \phi_n(x) e^{-\lambda_n \theta} \quad (47)$$

and its boundary value M of (24) as

$$M(\theta) = 1 + \sum_{n=1}^{\infty} (\lambda_n a_n + b_n) \phi_n(1) e^{-\lambda_n \theta} \quad (48)$$

where a_n and b_n are given by (41), (43).

The analytical behaviour to be expected of (47), (48) can be seen by considering the special case of the problem corresponding to plug flow

$$\rho(x) = 2x$$

obtained by taking infinite ν in (10). The eigenvalue problem (28) then has the Bessel function solutions

$$\left.\begin{aligned} \phi_0(x) &= 1 \\ \phi_n(x) &= \frac{J_0(\alpha_n x)}{J_0(\alpha_n)}; \quad n = 1, 2, \ldots \end{aligned}\right\}$$

ortho-normalized as in (31) and (32), with the eigenvalues

$$\left.\begin{aligned} \lambda_0 &= 0 \\ \lambda_n &= \tfrac{1}{2} \alpha_n^2; \quad n = 1, 2, \ldots. \end{aligned}\right\}$$

where the α_n are the positive zeros of J_1

$$\left.\begin{aligned} J_1(\alpha_n) &= 0; \quad n = 1, 2, \ldots \\ 0 < \alpha_1 &< \alpha_2 < \ldots \end{aligned}\right\}$$

as tabulated, for example, in [10]. The kernels I and M turn out to have the simple forms

$$\left.\begin{aligned} I(x, \theta) &= 1 + \sum_{n=1}^{\infty} \frac{J_0(\alpha_n x)}{J_0(\alpha_n)} e^{-\alpha_n^2 \theta/2} \\ M(\theta) &= 1 + \sum_{n=1}^{\infty} e^{-\alpha_n^2 \theta/2} \end{aligned}\right\}$$

Acknowledgements—The author is indebted to J. HOROWITZ, H. M. HULBURT and J. E. LONGFIELD, American Cyanamid Company, for many stimulating discussions on various aspects of this problem.

VOL. 10 1959

References

[1] Townsend J. S. *Phil. Trans. Roy. Soc.* 1899 **A193** 129.

[2] Damköhler G. *Z. Electrochem.* 1936 **42** 846.

[3] Baron T., Manning W. R. and Johnstone H. F. *Chem. Engng. Progr.* 1952 **48** 125.

[4] Chambré P. L. and Acrivos A. *J. Appl. Phys.* 1956 **27** 1322.

[5] Courant R. and Hilbert D. *Methods of Mathematical Physics*, Vol. 1, Chap. 2 Interscience, New York 1953.

[6] Churchill R. V. *Modern Operational Mathematics in Engineering*. McGraw Hill, New York 1944.

[7] Friedman B. *Principles and Techniques of Applied Mathematics* Chap. 3. Wiley, New York 1956.

[8] Mikhlin S. G. *Integral Equations and their Applications to Certain Problems in Mechanics, Mathematical Physics and Technology.*

[9] Titchmarsh E. C. *Eigenfunction Expansions associated with Second-Order Differential Equations*, Chap. 2. Oxford 1946.

[10] Jahnke E. and Emde F. *Tables of Functions with Formulae and Curves*, Chap. 8. Dover, New York 1945.

[11] Collatz L. *Numerische Behandlung von Differentialgleichungen*, Kap. 4. Springer, Berlin 1955.

[12] Fox L. *The Numerical Solution of Two-Point Boundary Problems in Ordinary Differential Equations*, Chap. 7. Oxford 1957.

[13] Taylor G. *Proc. Roy. Soc.* 1953 **A219** 186.

[14] Taylor G. *Proc. Roy. Soc.* 1954 **A225** 473.

[15] Chambré P. L. *Appl. Sci. Res.* 1956 **A6** 97.

[16] Sellars J. R., Tribus M. and Klein J. S. *Trans. Amer. Soc. Mech. Engrs.* 1956 **78** 441.

[17] Tribus M. and Klein J. *Symposium on Heat Transfer University of Michigan* 1952, p. 211. University of Michigan 1953.

[18] Huber A. *Monatsh. Math. Phys.* 1939 **47** 240.

Chemical Engineering Science, 1959, Vol. 10, pp. 212 to 224. Pergamon Press Ltd. London. Printed in Great Britain

The shrinkage forces developed in porous substances by capillary effects

K. W. Pearce and M. B. Donald
University College, London

(*Received* 12 *September* 1958)

Abstract—Shrinkage forces in porous solids are of importance in filtration, drying and granulation. The geometrical method of calculated shrinkage forces is limited to regularly packed beds of spheres with small amounts of moisture, whereas the study of energy changes has provided an approach capable of dealing with porous beds of widely differing configurations and moisture contents.

Résumé—Les forces de contraction dans les solides poreux sont importantes en filtration, séchage et granulation. La méthode géométrique pour le calcul de ces forces est limitée aux lits réguliers de garnissage avec sphères et faibles humidités. L'étude des variations énergétiques a permis d'obtenir une méthode de calcul des lits poreux de configurations et teneur en eau très différentes.

Zusammenfassung—Schrumpfungskräfte in porösen Feststoffen sind bei der Filtration, beim Trocknen und bei der Granulation von Bedeutung. Die geometrische Methode zur Berechnung von Schrumpfungskräften ist auf regelmässig geschüttete Kugelbetten mit kleinen Feuchtigkeiten begrenzt, während die Untersuchung der Energieänderungen auch für poröse Betten von sehr verschiedenen Formen und Feuchtigkeitsgehalten anwendbar ist.

1. Introduction

When a wet porous substance is dried the drying process creates within that substance forces which tend to make it shrink. The amount of shrinkage exhibited on drying depends on the magnitude of the shrinkage forces and the compressibility of the substance. Shrinkage forces arise from the surface tension effects associated with the numerous, highly curved liquid-gas interfaces in the pores. Another more studied manifestation of these surface tension effects is the suction developed by a wetted porous substance and it is the purpose of this paper to examine the relationship between the suction and the shrinkage forces.

2. The Pull Between Two Plates Due to the Presence of a Water Droplet Between Them

Before proceeding with a discussion of the previous work done on shrinkage forces it is instructive to examine the pull developed between two plates due to the presence of a water droplet. The magnitude of the pull, P, is given by the following equation [1].

$$P = A.T.\left(\frac{1}{r_f} - \frac{1}{R_f}\right) + B.T.\sin\alpha \qquad (1)$$

where A is the wetted area of each plate
B is the wetted perimeter
T is the surface tension of the water
α is the angle of contact of the liquid
r_f is the smaller radius of curvature of the film and
R_f is the bigger radius of curvature.

Thus the expression for P consists of two terms. The first, $A.T.\left(\frac{1}{r_f} - \frac{1}{R_f}\right)$ describes the pull due to suction in the water and will be called the "suction" term. The second, $B.T.\sin\alpha$, describes the pull due to the tension in the water surface and will be called the "surface tension" term. In the special case of flat parallel plates the "surface tension" term will disappear when the angle of contact is zero. If the plates are curved then this term will reappear, but the angle involved will depend on the geometry of the plates as well as the angle of contact. As the meniscus is stationary the components of forces due to suction and surface tension, acting parallel

to the direction of movement of the meniscus, will be equal in magnitude and opposite in direction. Therefore when the equilibrium of the meniscus is being considered the two terms must be equated and when the pull between the two plates is required they must be added. The principle illustrated in this simple case is an important one and should be kept in mind when we come to discuss the work of HAINES [2, 3, 4] and FISHER [5, 6].

Consider the two straight parallel plates illustrated in Fig. 1 (a). If the water is withdrawn through a small hole in the centre of the right-hand plate then the suction will remain constant and the pull, P, will fall, due to the decline in the wetted area, A. Suction vs. moisture and pull vs. moisture graphs may be constructed for this system and these are given in Fig. 1 (b). The system may be elaborated a little and the plates be bent near their centres (see Fig. 1 (c)) so as to reduce the local distance between them; the suction vs. moisture relation will then correspond closely to the drainage curve for beds of uniform particles.

Figure 1 (d) shows the suction vs. moisture and pull vs. moisture graphs for the pair of curved plates.

Such simple models cannot be used too freely

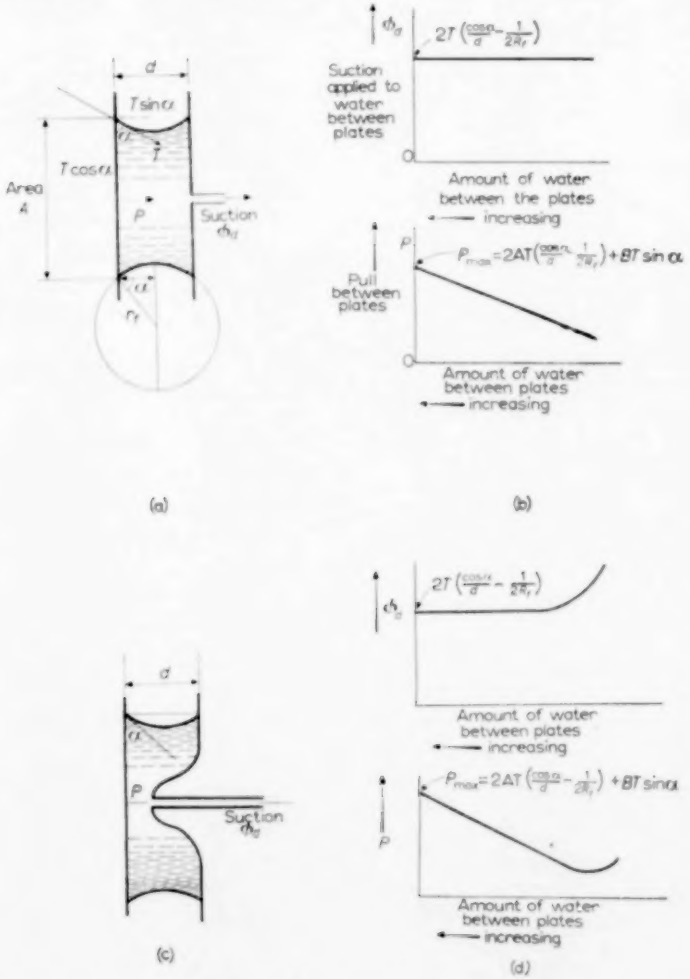

FIG. 1. The pull between two wetted plates.

when discussing capillary effects in porous beds, but, as the mathematical procedures used by HAINES and FISHER are essentially the same as those just used, these two workers might have saved themselves much argument if they had returned to such fundamental cases. FISHER would certainly have quickly discovered that his basic ideas were untenable.

3. PREVIOUS WORK

HAINES [2] calculated the pull between two spheres caused by a water droplet between them. This pull was then related to the corresponding face area on the outside of a bed of regularly packed spheres and so the pull per unit area of bed exterior, or cohesion, was evaluated. The method used by HAINES when calculating the pull was essentially the same as that discussed above and illustrated in Fig. 1, but the calculations were more complicated because the plates were not flat but parts of the surfaces of two spheres. He neglected the "surface tension" term in his calculations and assumed that the angle of contact of the water was zero.

HAINES was able to estimate the cohesion only when the water was present as discrete droplets at the points of contact of the spheres (the pendular state) and when the water completely filled the pores (saturation). He had also to assume that the bed consisted of uniform spheres in regular rhombohedral or cubical packing. His results are given in Fig. 2 together with an experimental curve of cohesion vs. moisture content for a bed of ignited silt particles. The device used to estimate cohesion was devised by ATTERBERG [7] and measures the force required to split a block of test material by driving a wedge into it. HAINES concluded from his investigations that the cohesion would rise continuously with an increase of moisture and reach a maximum at saturation. In his first paper [2] HAINES considered that this maximum value would equal the entry suction. The entry suction is defined as the suction that must be applied to a bed of particles in order to cause air to begin to enter the pore spaces in the bed.

FISHER [5] added precision to HAINES' approximate calculations by including the "surface tension" term omitted by him, but considered that the cohesion would fall with increasing moisture to reach zero at saturation. The following equation was produced [6] in an attempt to disprove HAINES' results, it is applicable only to uniform spheres.

$$c = \left(\phi d + \frac{2T}{r}\right)(A_s - a_i) \qquad (2)$$

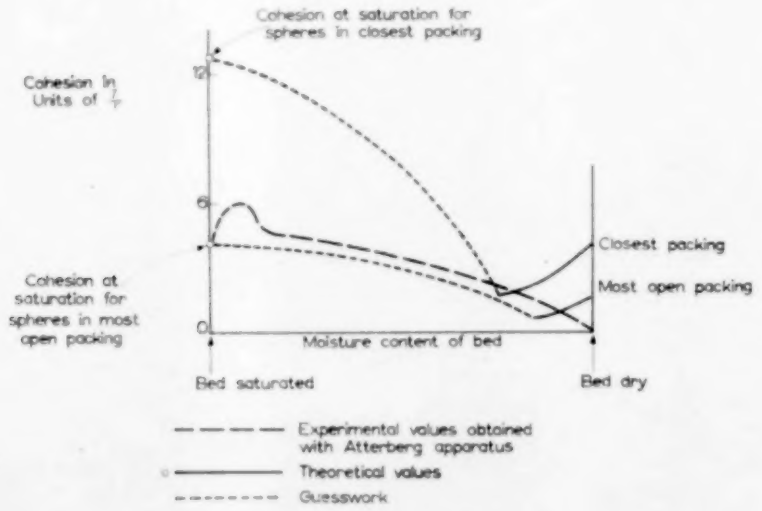

FIG. 2. Haines' results on cohesion (2).

Where c is the cohesion, or shrinkage force per unit area of bed exterior,

ϕ_d is the suction in the water films,

r is the radius of the spheres composing the bed,

A_e is the projection of the drained areas on the outside of the bed per unit area of bed exterior and

a_i is the projection of the drained areas on the inside of the outermost layer of spheres, per unit area of bed exterior.

FISHER proceeded to argue that the suction, ϕ_d, must increase continually with decreasing moisture for a series of stable states (this had been shown experimentally by HAINES) and therefore to obtain a rise in cohesion with the addition of water ($A_e - a_i$) must increase quickly with the addition of water, which he considered to be unlikely.

HAINES [3] interpreted the theorem in a different manner; he discussed the case of saturation in a bed of spheres in closest or rhombohedral packing with air just about to enter the top layer of pores. The bed was then subject to its entry suction of 12·9 T/r and a_i was zero. HAINES estimated A_e to be 0·75 (he did not indicate how he obtained his figure) and on substituting for the various quantities in equation (2) the cohesion became $10T/r$. The acceptance of this value by HAINES showed that he had abandoned his original concept of the equality between cohesion and applied suction at saturation.

FISHER also refuted the experimental results of HAINES by asserting that the Atterberg apparatus measured the work required to break the test sample rather than the cohesion and he showed that this work increased with increasing moisture over the pendular range.

The results of the controversy between HAINES and FISHER was to cast doubt upon the ability of the Atterberg apparatus to measure cohesion and to persuade HAINES to abandon his original idea of the equality between cohesion and applied suction at saturation. Although HAINES upheld the concept of falling cohesion with falling moisture, a method of calculating the cohesion had still to be found for the wide range of moisture contents between the pendular state and saturation.

4. A RE-EXAMINATION OF FISHER'S EQUATION WHEN APPLIED TO THE SATURATION CASE

It will be useful to restate the equation

$$c = \left(\phi_d + \frac{2T}{r}\right)(A_e - a_i) \qquad (2)$$

where A_e is the projection of the drained areas of the outside of the bed per unit area of bed exterior, and

a_i is the projection of the drained areas on the inside of the outermost layer of spheres per unit area of bed exterior.

Consider the top view of a bed surface as depicted in Fig. 3 (a). The arbitrary boundary encloses an area of unity and a drained area of A_e. As the bed is saturated a_i must be zero. Within the boundary the projected water surface

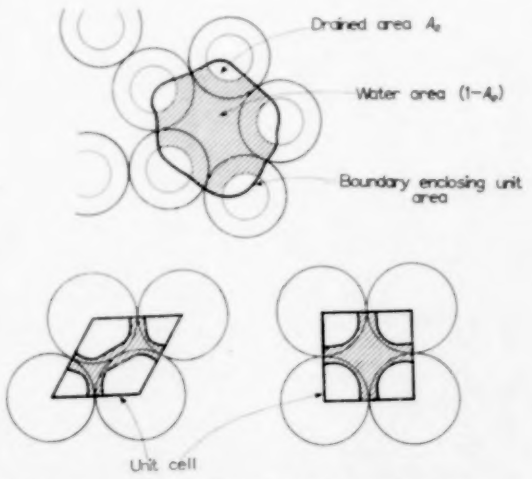

FIG. 3. Air–water interfaces in beds of uniform spheres at saturation.

3 (a) Uniform spheres in random packing.

3 (b) Uniform spheres in rhombohedral packing, projected area of spheres per unit cell area = 0·91 (A_e on air entry = 0·86).

3 (c) Uniform spheres in cubical packing, projected area of spheres per unit cell area = 0·77 (A_e on air entry = 0·71).

area is $(1 - A_e)$ and the "surface tension" force acting normal to the bed surface, according to FISHER's argument [6], is $(2 \cdot T \cdot A_e/r)$. This force also acts upon the air–water interface within the boundary and, since a state of equilibrium is assumed, it must be balanced by the suction in the water acting over the projection of the water surface area, $(1 - A_e)$. The condition for a stationary interface is therefore:—

$$\frac{2T \cdot A_e}{r} = \phi_d (1 - A_e). \qquad (3)$$

At saturation FISHER's equation becomes:

$$c = \phi_d \cdot A_e + \frac{2 \cdot T \cdot A_e}{r} \qquad (4)$$

and so we see that

$$c = \phi_d A_e + \phi_d (1 - A_e) = \phi_d$$

Thus the cohesion is equal to the applied suction at saturation.

It is interesting to examine the case of spheres in closest packing when air is about to enter the bed. The entry suction as given by HAINES [3] is $12{\cdot}9\ T/r$. Substituting this in equation (3) we may obtain A_e.

$$A_e = \frac{\phi_{de}}{\phi_{de} + (2T/r)} = \frac{12{\cdot}9}{14{\cdot}9} = 0{\cdot}86$$

This is higher than the value of 0·75 quoted by HAINES. As HAINES gave no indication of his method of calculating A_e the source of his error is unknown. Figs. 3 (b) and 3 (c) illustrate the cases of air entry for rhombohedral and cubical packing.

5. The Relationship Between Cohesion and Suction Developed by a Porous Bed

FISHER's equation can only be used to estimate cohesion when the configuration of the water films within the bed is accurately known, i.e. with uniform spherical particles in regular packing and with the water present as discrete droplets at the points of contact between the particles. When the bed is composed of particles of varying size and shape and in random arrangement FISHER's equation is inadequate and some other method for calculating cohesion must be found.

Much insight into the nature of the water films within porous beds may be gained by studies of their suction vs. moisture relationships. For example the suction developed by a porous bed immediately gives the curvature of the water films within it, and the work done when extracting a given quantity of water from the bed provides a clue as to the change in surface area of the water films accompanying this withdrawal. Before considering these area changes and their implications in more detail we must discuss the important work of HAINES [4] in connection with the suctions developed by porous beds.

HAINES prepared saturated beds of particles and subjected them to steadily increasing suctions. Some typical relationships between applied suction (called suction potential by HAINES) and moisture content are shown in Fig. 4. The moisture content is denoted by a ratio, M, where

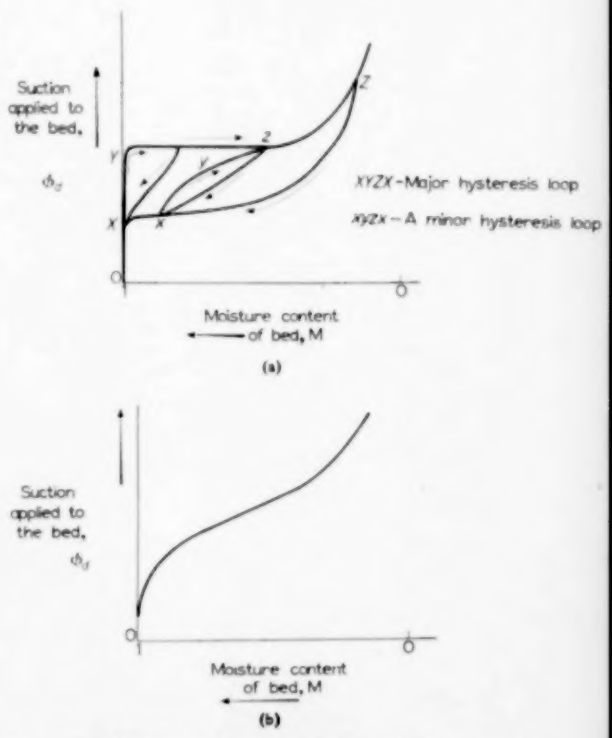

FIG. 4. Typical suction vs. moisture content curves for porous beds.
4 (a) Curve for a bed having uniform pores.
4 (b) Curve for a bed having non-uniform pores.

$$M = \frac{\text{total volume of water in the bed pores}}{\text{total volume of the bed pores}}$$

thus at saturation M is equal to unity. The curve in Fig. 4 (a) is for uniform random packed spheres and it illustrates the phenomenon of hysteresis which is discussed shortly. Fig. 4 (b) refers to sand of non-uniform particle size and shape. Haines was the first to point out that the shape of the suction-moisture curve indicated the pore size distribution of the bed. A flat curve, Fig. 4 (a), shows that there are a large number of pores of similar size and entry suction, whereas a sloping curve, Fig. 4 (b), suggests that there is a wide variation in the size of the pores.

Haines also calculated the suctions developed in some of the water films occurring in beds of regularly packed spheres. Two important values are the entry suctions, ϕ_{de}, for rhombohedral and cubical packing. He estimated these by calculating the size of an air bubble about to force its way between the spheres as illustrated in Fig. 5. The radii of the air bubbles were 0·155 r and 0·43 r for rhombohedral and cubical packing respectively. The entry suctions were thus calculated as 12·9 T/r and 4·6 T/r. For random packed beds of uniform glass spheres, called 'glistening dew,' of diameter 360 μ, HAINES found by experiment that the entry suction was around $6T/r$.

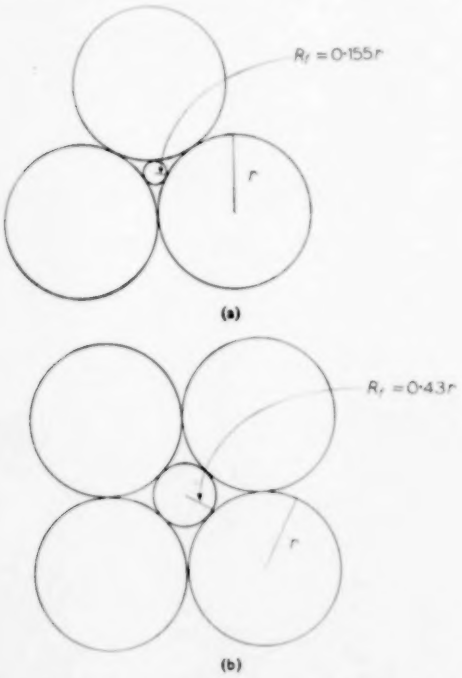

FIG. 5. Air entry for beds of spheres in regular packing.
5 (a) Air bubble about to pass between spheres in rhombohedral packing.
5 (b) Air bubble about to pass between spheres in cubical packing.

Different suctions are possible at the same moisture content depending on whether the water is being drained from the bed or imbibed into it. This phenomenon is known as hysteresis and it is illustrated in Fig. 4 (a). The suction under drainage is always greater than the suction during imbibition for a given moisture content. There are two types of hysteresis loop: the largest or major loop, XYZX, and the minor loops, of which there can be any number, xyzx.

The free energy of the surfaces within a porous bed

The increase in total surface energy of a system accompanying the isothermal creation of unit surface area of that system is

$$Z = T - R\frac{dT}{dR} \qquad (5)$$

where T is the free energy of unit surface area and may be identified with the mechanical work performed,

$R\,dT/dR$ is the heat absorbed from the surrounds to maintain the temperature of the system and

R is the absolute temperature.

All drainage and imbibition processes to be discussed are assumed to take place isothermally, therefore the mechanical work performed on or by the bed will be associated with the term T in equation (5) and $R\,.\,dT/dR$ will be neglected.

There are three types of surface within a porous bed: solid–gas, solid–liquid and liquid–gas, and the free energies of unit area of these surfaces are denoted by the symbols T_{sg}, T_{sL} and T_{Lg} respectively. At saturation the free energy of a porous bed is $S_0'\ T_{sL}$*, where S_0' is the solid

*This neglects the relatively small solid–gas and liquid–gas areas present at saturation.

surface per unit volume of bed. After air entry has taken place suppose that a fraction n' of solid surface is drained and that the water surface is H then the increase in free energy is

$$F = n' S_0' T_{sg} - n' S_0' T_{sL} + H T_{Lg}$$

If the angle of contact of the liquid is zero then

$$T_{sg} = T_{Lg} + T_{sL}$$

and

$$F = T_{Lg}(n' S_0' + H) \qquad (6)$$

At saturation F will be zero and at complete dryness F will have a maximum value of $T_{Lg} S_0'$.

In future the term, F, describing the increase in the free energy of the surfaces within a porous bed accompanying the removal of water will be referred to as the energy of the porous bed. Changes of energy accompanying changes of moisture content may be deduced from the capillary characteristics of the bed.

The areas under the drainage and imbibition lines of a suction vs. moisture content graph are a measure of the work performed during these processes. As pointed out by HAINES [4] the presence of an hysteresis loop indicates that work has been wasted in the drainage cycle and so the energy of the bed must always be less than the drainage work down to a given moisture content. The converse will be true during imbibition. A unique relation between the energy of the bed and the moisture content is wholly consistent with hysteresis but the water films have different suctions and thus different shapes during drainage and imbition and so an energy loop is more likely.

Constructing the energy loop

Fig. 6 (a) shows a graph of suction against moisture content for a bed of random packed uniformly shaped spheres. Fig. 6 (b) shows a graph where units of work or energy are plotted as ordinates and moisture content as abscissae. The energy of the porous bed and hence the work done on it or capable of being done by it will be zero at saturation (M equal to unity).

When the porous bed is drained from saturation to a moisture content M_2 the work done on the bed is equal to the area under the drainage curve

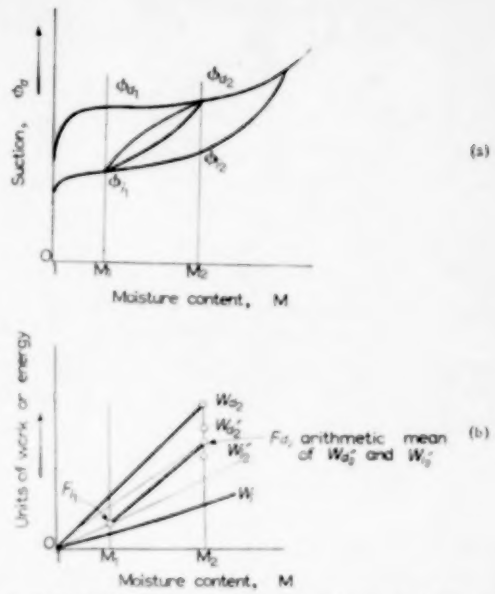

FIG. 6. Calculating the energy changes in wetted porous beds.

6 (a) Suction vs. moisture relation.
6 (b) Energy vs. moisture relation.

of the major hysteresis loop down to the moisture content M_2 and is represented by the point W_{d_2} in Fig. 6 (b). The existence of hysteresis loops indicates that energy is wasted in the drainage cycles and is sufficient reason to assume that the energy of the bed under the suction ϕ_{d_2} is less than the work done up to that suction, W_{d_2}. Now we can also reach the suction ϕ_{d_2} from the suction ϕ_{i_1} via the drainage curve of the minor hysteresis loop between them (see Fig. 6a). Let us assume that the energy of the bed when the bed is imbibing water at a suction ϕ_{i_1} is F_{i_1} which will be below the drainage work vs. moisture content line 0-W_{d_2} (see Fig. 6 b). If the bed is drained from the moisture content M_1 down to the moisture content M_2 the suction will increase to ϕ_{d_2} and the work performed on the bed will be given by the area under the drainage curve of the minor hysteresis loop and will be represented in Fig. 6b by the jump from F_{i_1} to W_{d_2}'. Both W_{d_2} and W_{d_2}' correspond to the same configurations of the water films but W_{d_2}' is the smaller term and comes closer to the actual energy of the bed under the suction ϕ_{d_2}'. If the bed is allowed

VOL. 10 1959

to return to the moisture content M_1 and the suction ϕ_{i_1} it will perform the amount of work given by the area under the imbibition line of the minor hysteresis loop represented in Fig. 6 (b) as the drop from W_{i_2}' to F_{i_1}. Because the minor hysteresis loop is narrow the energy wasted during the cycle from ϕ_{i_1} to ϕ_{d_2} and back again is small compared to the total energy changes, and so it can be assumed, with but little error, that the increase in energy of the bed accompanying a change in moisture conditions represented by the extremities of a minor hysteresis loop is equal to the arithmetic mean of the areas under the drainage and imbibition curves of that same minor hysteresis loop. Energy increments calculated in this way can be put together to construct a complete energy loop and Fig. 7 illustrates the necessary steps.

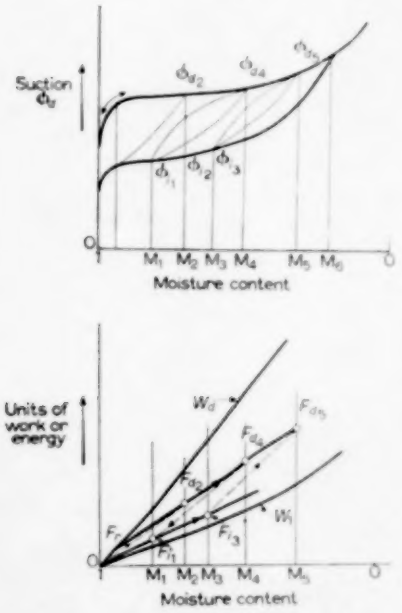

FIG. 7. Constructing the energy loop.

Starting at the origin the first part of the drainage curve is found to be reversible (as indicated by the double arrow) and so the increement in the energy of the bed is given by the drainage work line (W_d) up to F_r. The minor hysteresis loop between 1 and M_2 may now be used to fix the point F_{d_2} as explained in Fig. 6 (b). Having positioned F_{d_2} we may next draw a straight line between F_r and F_{d_2} and assume that it represents the energy vs. moisture relationship for drainage. If it is further assumed that the line $F_r - F_{d_2}$ may be extrapolated then the position of F_{d_4} may be determined. The accuracy of such an extrapolation depends on the distances involved and will be greater the closer are the minor hysteresis loops. By using the minor hysteresis loop between M_4 and M_1, F_{i_1} may be positioned from F_{d_4} and F_{i_3} from F_{i_1} by extrapolating the line $0\text{-}F_{i_1}$. F_{d_5} may be obtained from F_{i_3} from the third minor loop and if we continue in this stepwise manner the complete energy loop can be constructed when sufficient hysteresis data are available. As explained previously when the bed becomes completely dry the energy will have reached a maximum value of $T_{Lg} S_0'$.

A general cohesion vs. moisture relationship

Until now we have used only the moisture content, M, as the abscissae in all the graphs. When discussing energy changes in porous beds we should, to be rigorous, use the volume of water withdrawn from the bed as abscissae and not moisture content, but the two quantities are directly proportional to one another in beds of constant porosity and so the previous arguments are quite valid. However during the following derivation of the cohesion equation we shall have to consider the effects of small changes in bed porosity and so, for the moment, we must replace the moisture content, M, by the volume of water withdrawn, V_w. The two quantities are related by the expression

$$V_w = e\, V_B (1 - M) \qquad (7)$$

where e is the porosity of the bed i.e. the ratio: total volume of pores/total volume of the bed and V_B is the total volume of the bed.

In this paper we are primarily concerned with shrinkage forces and so the cohesion equation will be derived assuming that the bed is under a drainage suction. For mathematical purposes the drainage energy characteristics of a porous bed are conveniently represented as a plot of $(dF_d/dV_w)_e$ as ordinates against V_w as abscissae. (dF_d/dV_w) has the dimension of suction and as it

is closely related to the drainage suction it will be given the symbol ϕ_d'.

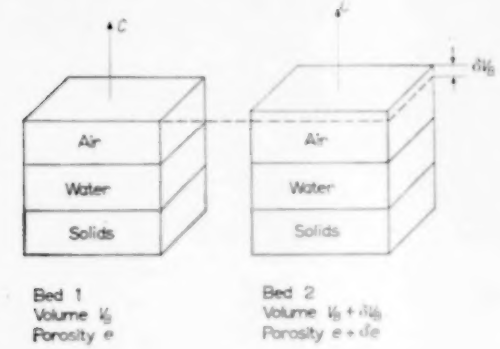

(a)

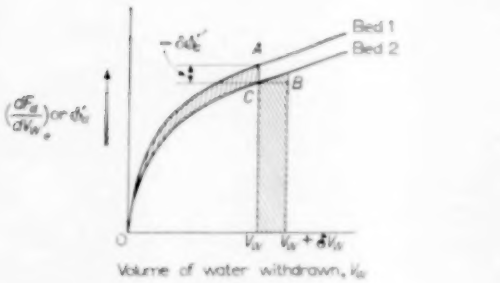

(b)

FIG. 8. Stretching a wetted porous bed.
8 (a) The two porous beds.
8 (b) Energy characteristics of the two porous beds.

Two porous beds in slightly different capillary and energy states are depicted in Fig. 8 (a). They are identical in every respect save porosity. They each contain the same number of particles the same volume of water and the pore configurations are such that bed 1 may be made identical to bed 2 by an elemental increase in volume δv_B. The shrinkage forces acting on the beds may be deduced in the following way. Both beds are saturated with water and then subject to a series of drainage and imbitition cycles which enable graphs of ϕ_d' against V_w to be prepared for each bed (see Fig. 8 (b). The beds are then saturated with water again and drained to the conditions illustrated in Fig. 8 (a) and represented by the abscissae V_w, $V_w + \delta V_w$ in Fig. 8 (b). From the areas under the curves of ϕ_d' against V_w we can deduce the difference in energy between the two beds, δF_d, and this will equal the mechanical work which must be done against the shrinkage forces when bed 1 is given a reversible isothermal stretch so that it becomes identical to bed 2. If the beds are assumed to have unit cross-sectional areas perpendicular to the direction of stretching then the mechanical work done will be $c\,\delta V_B$

From Fig. 8 (b) we see that

$$\delta F_d = \text{area } 0\,CB\,(V_w + \delta V_w) - \text{area } 0\,AV_w \quad (8)$$

As the area $0\,CV_w$ is common to both curves

$$\delta F_d = \text{area } V_w\,CB\,(V_w + \delta V_w) - \text{area } 0\,AC\,0 \quad (9)$$

Both beds have the same volume of water, therefore

$$\delta V_w = \delta V_B$$

and so

$$\text{area } V_w\,.\,C.B.\,(V_w + \delta V_w) \approx \phi_d'\,\delta V_B \quad (10)$$

The area $0\,AC\,0$ is equal to the mean value of $\delta\phi_d'$ over the range 0 to V_w multiplied by V_w. The problem is now to calculate $\delta\phi_d'$ at a constant value of the water withdrawn. Consider the graph in Fig. 9, the two vertical lines represent the same moisture content M in both beds and the left hand line is the position at which we must estimate $\delta\phi_d'$. From Fig. 9 we see that $\delta\phi_d'$ consists of two parts: that caused by an increase

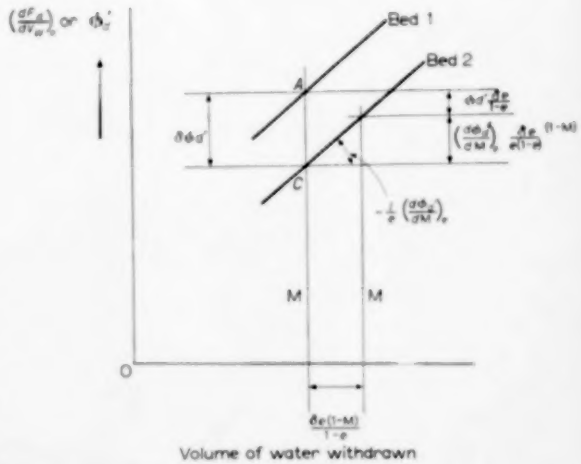

FIG. 9. Estimating $\delta\phi_d'$.

VOL. 10 1959

of porosity δe at constant moisture content and that caused by a reduction in the water withdrawn at a constant porosity $e + \delta e$. Let us first consider the effect of changing the porosity. It will be assumed that when two beds have the same moisture content the shape of the water films in the pore spaces will be similar and that the increase in the radius of curvature of the water films will be similar to the increase in the mean pore radius accompanying the increase in porosity. It has been stated [8] that for a given particle size and shape

$$\phi_d = \text{constant} / \frac{e}{1-e}$$

$$\text{therefore } \left(\frac{d\,\phi_d}{de}\right)_M = -\frac{\text{constant}}{e^2} = \frac{-\phi_d}{e\,(1-e)}$$

Thus an elemental increase in porosity of δe will reduce the suction values by a fraction $\delta e/e\,(1-e)$. It is reasonable to assume that the values of ϕ_d' will be similarly reduced and so

$$\left(\frac{d\,\phi_d'}{de}\right)_M = \frac{-\phi_d'}{e\,(1-e)} \tag{11}$$

and the first part of $\delta\phi_d'$ is $\phi_d'/e\,(1-e)$. The second part is given by the product of the gradient of the lower curve at the abscissa V_w and the separation between the two vertical lines. The gradients of the upper and lower curves are nearly the same and so

$$\left(\frac{d\,\phi_d}{d\,V_w}\right)_{e+\delta e} \approx \left(\frac{d\,\phi_d'}{d\,V_w}\right)_e$$

The separation between the vertical lines is

$$(e + \delta e)\,(1-M)\,(V_B + \delta\,V_B) - e\,(1-M)\,V_B$$

now $\delta\,V_B/V_B$ equals $\delta\,e/(1-e)$ and so the separation is

$$(e + \delta\,e)\,(1-M)\,V_B\left(1 + \frac{\delta e}{1-e}\right) - e\,(1-M)\,V_B$$

which can be simplified to $(\delta e/1-e)\,(1-M)\,V_B$ by neglecting terms of the second degree. Therefore the second part of $\delta\phi_d'$ is $(d\,\phi_d'/d\,V_w)_e \cdot \delta e/(1-e)\,(1-M)\,V_B$ and so

$$\delta\,\phi_d' = \phi_d'\,\frac{\delta e}{e\,(1-e)} + \left(\frac{d\,\phi_d'}{d\,V_w}\right)_e \cdot \frac{\delta e}{1-e}\,(1-M)\,V_B \tag{12}$$

now V_w equals $e\,(1-M)\,V_B$ and so $(d\,\phi_d'/d\,V_w)_e$ can be replaced by $-\,(d\,\phi_d'/dM)_e \,.\, 1/e\,V_B$. Therefore

$$\delta\phi_d' = \phi_d'\,\frac{\delta e}{e\,(1-e)} - \left(\frac{d\,\phi_d'}{dM}\right)_e \frac{\delta e}{e\,(1-e)}\,(1-M) \tag{13}$$

Taking mean values over the moisture content range 1 to M and denoting these by the subscript m we have

$$(\delta\phi_d')_m = (\phi_d')_m\,\frac{\delta e}{e\,(1-e)} - \left[\left(\frac{d\,\phi_d'}{dM}\right)_e (1-M)\right]_m \frac{\delta e}{e\,(1-e)} \tag{14}$$

and the area $0\,AC\,0$ is equal to $(\delta\phi_d')_m$. V_w and since V_w equals $e\,(1-M)\,V_B$ and $\delta\,V_B/V_B$ equals $\delta\,e/1-e$ we have

$$(\delta\phi_d')_m\,V_W = \delta\,V_B\left\{(\phi_d')_m\,(1-M) - \left[\left(\frac{d\,\phi_d'}{dM}\right)_e (1-M)\right]_m (1-M)\right\} \tag{15}$$

From equations (9), (10) and (15) we find that the difference in energy between the two beds is

$$\delta F_d = \phi_d'\,\delta\,V_B - (\phi_d')_m\,(1-M)\,\delta\,V_B + \left[\left(\frac{d\,\phi_d'}{dM}\right)_e (1-M)\right]_m (1-M)\,\delta\,V_B \tag{16}$$

which is identical to the mechanical work performed stretching the bed by a volume $\delta\,V_B$ i.e. $c\,\delta\,V_B$, where c is the cohesion in the porous bed. Thus the cohesion – moisture content relationship is

$$c = \phi_d' - (\phi_d')_m\,(1-M) + \left[\left(\frac{d\,\phi_d'}{dM}\right)_e (1-M)\right]_m (1-M) \tag{17}$$

where ϕ_d' equals $(dF_d/dV_w)_e$ or $-1/e\,V_B$ $(dF_d/dM)_e$ and the subscript m denotes a

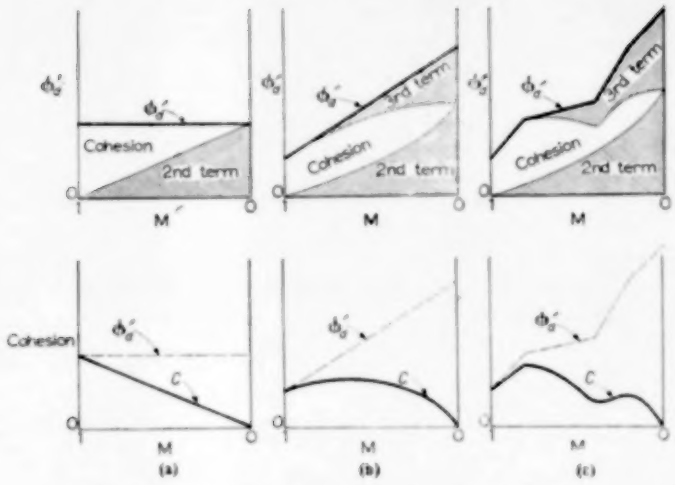

FIG. 10. Some cohesion vs. moisture relationships.

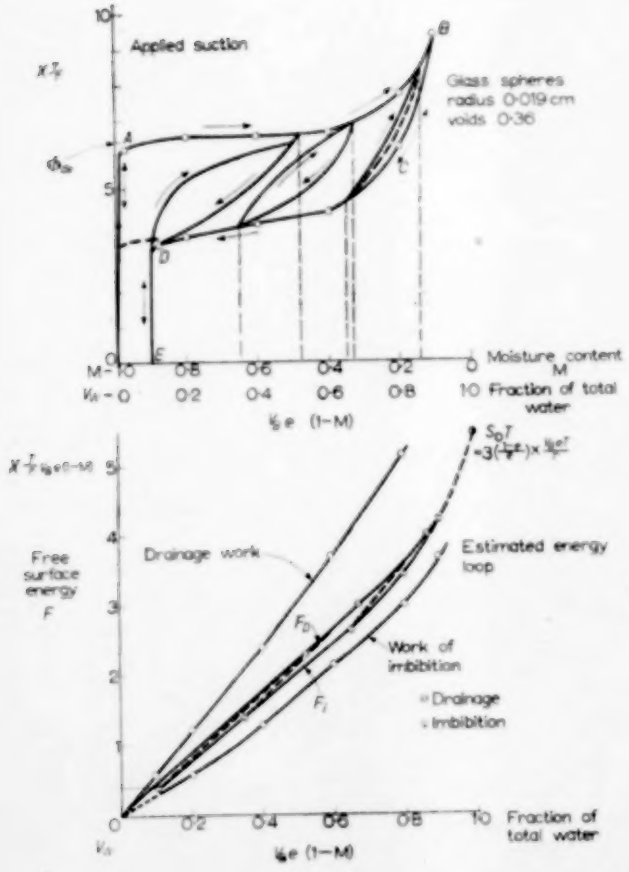

FIG. 11.

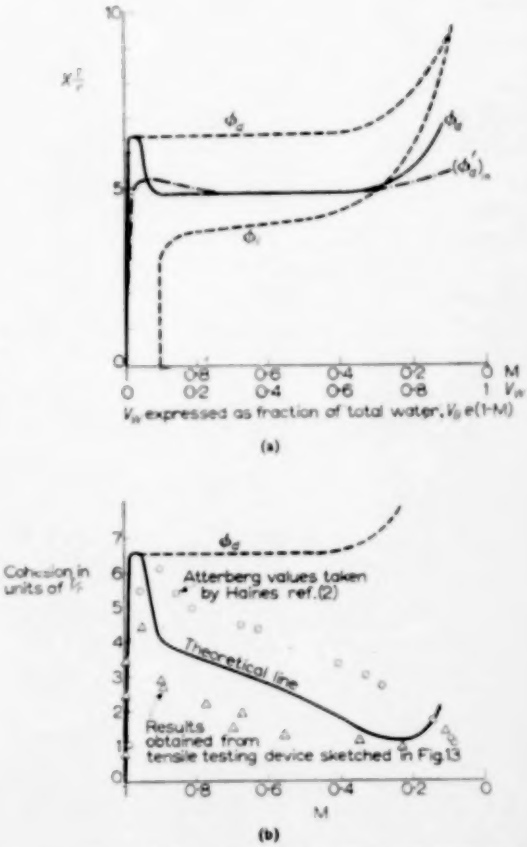

FIG. 12. The cohesion in a bed having uniform pores.

mean value over the moisture content range from 1 to M.

Discussion of the cohesion–moisture content equation

At saturation M equals one and so c becomes equal to ϕ_d'. Over the earliest part of the suction–moisture content curve the drainage process is reversible and therefore ϕ_d' is identical to ϕ_d the drainage suction. Hence at saturation the cohesion is equal to the applied suction.

In order to demonstrate the effects of the various terms in equation (17) three sample computations are illustrated in Fig. 10. As the ϕ_d' versus M curves bear a resemblance to their parent ϕ_d versus M curves the drawings illustrate the effects of pore size distribution on the cohesion. With beds having uniform pores the last term in in equation (17) is usually of little importance because the ϕ_d' versus M graph is flat (see Fig. 10 (a)). However, if pores of widely varying size are present, as is the case in Figs. 10 (b) and 10 (c) then the last term in equation (17) must be included ; the error incurred by omitting it is large at the lower moisture contents.

Graphs of F against M and ϕ_d' against M were estimated for a sample of glass spheres of diameter 360 μ from suction – moisture content data provided by HAINES. The original graph of ϕ_d and ϕ_i versus M has been corrected for the effect of bed thickness. Unfortunately only three minor hysteresis loops are given and so the determination of F and ϕ_d' is bound to be approximate. The results are shown in Figs. 11 and 12. When calculating the cohesion-moisture content relationship from the data in Fig. 12 (a) the last term in equation (17) was omitted. The omission was thought to be justified because over the majority of the moisture range the gradient of the ϕ_d' versus M graph was zero and just after air entry when the gradient had a large but uncertain value the factor $(1 - M)$ was small and appeared raised to the power two in equation (17). A plot of cohesion versus moisture content calculated from HAINES' data is given in Fig. 12 (b) together with HAINES' own measurements of cohesion taken from [2]. Also given in Fig. 12 (b) are measurements of cohesion taken with the special tensile testing apparatus depicted in

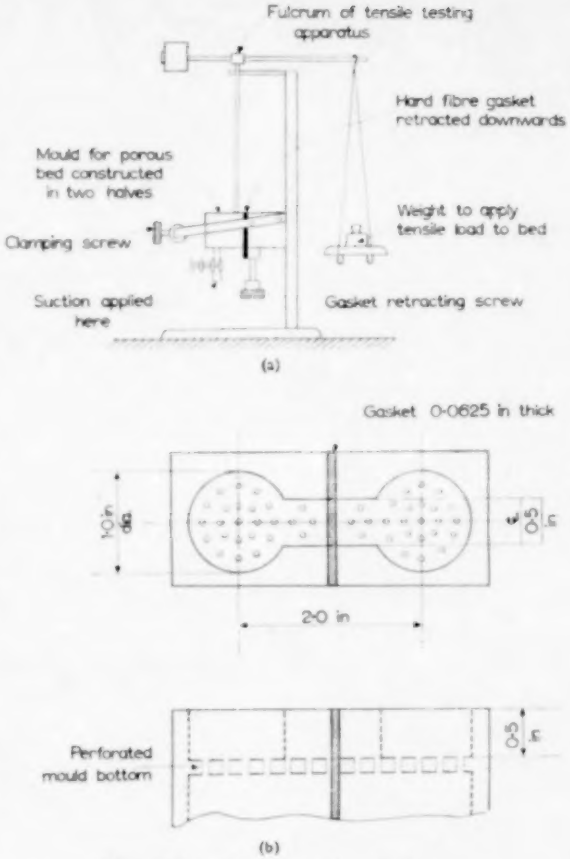

FIG. 13 (a) Tensile testing device.
FIG. 13 (b). Details of mould for porous bed.

Fig. 13. The tests were made upon moist beds of uniform glass spheres of 170 μ* diameter formed in a horizontal dumbell shaped mould which was constructed in two halves. Whilst water was being sucked from the bed of spheres the two halves of the mould were clamped together with a hard fibre gasket between them. When the bed had been partially dried the suction was stopped, the clamping pressure released and the gasket retracted. The bed of spheres was then stretched and broken by placing weights on the scale pan (see Fig. 13). Except with saturated samples, where some necking was observed before fracture, the beds broke cleanly across the centre. There

*Glass spheres of this size were conveniently available at the time of the experiments.

is wide disagreement between the two sets of experimental measurements presented in Fig. 12 (b) but no fruitful comments can be made about this at present because different types of porous bed and different pieces of apparatus were used in each set of experiments.

The results in Fig. 12 (b) shows that the theoretical cohesion–moisture content equation (equation 17) is basically of the right form; but clearly much more experimental work is necessary to obtain more accurate measurements of cohesion, and to obtain more information about the hysteresis loops in the suction potential moisture relationships of beds with uniform and non-uniform pore size distribution.

Conclusions

As a result of this study we may conclude that:

(i) the cohesion in a wetted porous bed is equal to the applied suction, when the bed is saturated,

(ii) the cohesion will fall below the applied suction after air entry into the bed, and

(iii) the precise relationship between cohesion and moisture content will depend on the pore size distribution in the bed.

Notation

a_i = the projection of the drained areas on the inside of the outermost layer of spheres, per unit area of bed exterior

A = the wetted area of one of a pair of parallel plates

A_e = the projection of the drained areas on the outside of the porous bed per unit area of bed exterior

B = the wetted perimeter of a water droplet on one of a pair of parallel plates

c = the cohesion in a porous bed

d = the distance between two parallel plates

e = the voidage or porosity of a porous bed

F_d = the free surface energy of a porous bed under drainage

F_i = the free surface energy of a porous bed during imbibition

H = the air–water interfacial area

M = the moisture content of a porous bed

n' = the fraction of solid surface that has been drained

P = the pull between two parallel plates caused by the presence of a water droplet between them

r = the radius of a sphere

r_f = the smaller principal radius of curvature of a water surface

R = the absolute temperature

R_f = the larger principal radius of curvature of a water surface

S_0' = the solid surface area in a porous bed

T = the surface tension of water

T_{Lg} = the liquid–gas interfacial tension

T_{sg} = the solid–gas interfacial tension

T_{sL} = the solid–liquid interfacial tension

V_B = the volume of a porous bed

V_w = the volume of water withdrawn from it

W_d = the work performed on the porous bed during a drainage process

W_i = the work performed by the porous bed whilst imbibing water

α = the angle of contact

ϕ_d = the drainage suction

ϕ_i = the imbibitional suction

$\delta\phi_d'$ = the gradient of the free surface energy vs. volume of water withdrawn graph

References

[1] Newman F. H. and Searle V. H. L. *The General Properties of Matter* p. 174, equation 151. Arnold 1957.

[2] Haines W. B. *J. Agric Sci.* 1925 **15** 529.

[3] Haines W. B. *J. Agric. Sci.* 1927 **17** 264.

[4] Haines W. B. *J. Agric. Sci.* 1930 **20** 97.

[5] Fisher R. A. *J. Agric. Sci.* 1926 **16** 492.

[6] Fisher R. A. *J. Agric. Sci.* 1928 **18** 406.

[7] Haines W. B. *J. Agric. Sci.* 1923 **13** 296.

[8] Pearce K. W. Ph.D.Thesis, London 1955.

VOL. 10 1959

Chemical Engineering Science, 1959, Vol. 10, pp. 225 to 228. Pergamon Press Ltd. London. Printed in Great Britain

Exact forms of the unrestricted Gibbs–Duhem equation

H. C. Van Ness*

Department of Chemical Engineering, Rensselaer Polytechnic Institute, Troy, New York

(*Received* 14 *October* 1958)

Abstract—The exact forms of the Gibbs–Duhem equation in terms of fugacities and activity coefficients, applicable to any multicomponent phase, are developed in a straightforward manner. Reduction to restricted equations valid for constant temperature, constant pressure, or constant composition becomes a simple matter of dropping terms.

Résumé—L'auteur développe de façon directe les formes de l'équation de Gibbs-Duhem en fonction des coefficients de fugacité et d'activité, applicable à n'importe quelle phase à plusieurs composants. Le passage aux équations restreintes, valables pour une température constante, une pression constante, ou une composition constante, se résume à une simple suppression de termes.

Zusammenfassung—Die exakten Formen der Gibbs-Duhem-Gleichung in Ausdrücken der Fugazitäten und Aktivitätskoeffizienten, die auf eine Phase mit mehreren Komponenten anwendbar ist, werden in einfacher Weise entwickelt. Die eingeschränkte Gleichung für konstante Temperatur, konstanten Druck, oder konstante Zusammensetzung erhält man durch einfaches Streichen von Ausdrücken.

The much-quoted paper by Ibl and Dodge [3] which appeared in this journal a few years ago presented derivations of the exact forms of the Gibbs–Duhem equation in terms of fugacities and activity coefficients for binary systems in phase equilibrium at (a) constant temperature, and (b) constant pressure. The object of this paper is to generalize these equations to apply to any phase, whether in equilibrium with another phase or not and without restriction as to the number of components or constancy of temperature or pressure. Moreover, the derivations are direct and without complication. Thus they allow a uniform, yet simple, treatment of all cases.

We start with the basic equation for an open system (see, for example, Denbigh [2]):

$$V\,dp - \underline{S}\,dT = \Sigma(n_i\,d\mu_i) \qquad (1)$$

This equation applies to the whole phase; indeed it applies to the whole of any multiphase system, provided that equilibrium exists throughout the system. However, for the purposes of this paper it will be applied to single phases, and will be put on a mole basis by dividing through by the total moles in the phase:

$$v\,dp - S\,dT = \Sigma(x_i\,d\mu_i) \qquad (2)$$

where v is the molal volume and S is the molal entropy of the solution. The x_i's represent mole fractions, and μ_i is the chemical potential of component i in solution. It is of course identical with the partial molal Gibbs free energy.

The defining equation for the fugacity of a component in solution is:

$$d\mu_i = RT\,d\ln\bar{f} \quad \text{(constant temperature)} \qquad (3)$$

This equation takes into account variations of μ_i as a result of pressure and composition changes *at constant temperature*, and hence cannot be substituted in equation (2) in the general case where $d\mu_i$ is the total derivative of μ_i as a result of changes in temperature as well as in pressure and composition. Rather, we integrate equation

*During 1958-59, Visiting Fulbright Lecturer in Chemical Engineering at King's College, University of Durham, Newcastle upon Tyne.

(3) at constant temperature from the low-pressure, ideal-gas reference state of the pure component to the actual state of the component in solution:

$$\mu_i - F_i^* = RT \ln \bar{f}_i - RT \ln f_i^*$$

where the asterisk designates the reference state for which, by definition, $f_i^* = p^*$. Hence

$$\mu_i = F_i^* + RT \ln \bar{f}_i - RT \ln p^* \qquad (4)$$

Since p^* is the constant reference-state pressure, general differentiation of equation (4) gives

$$d\mu_i = dF_i^* + RT d\ln \bar{f}_i + R \ln \bar{f}_i\, dT - R \ln p^*\, dT \qquad (5)$$

In this equation $d\mu_i$ is the required total derivative. Equation (5) may be simplified by the following substitutions. Since F_i^* is a function of temperature only

$$dF_i^* = -S_i^*\, dT$$

and by equation (4)

$$R \ln \bar{f}_i\, dT - R \ln p^*\, dT = \left(\frac{\mu_i - F_i^*}{T}\right) dT$$

Therefore

$$d\mu_i = -S_i^*\, dT + \left(\frac{\mu_i - F_i^*}{T}\right) dT + RT\, d\ln \bar{f}_i$$

or since $S_i^* + F_i^*/T = H_i^*/T$ from the defining equation for free energy,

$$d\mu_i = -(H_i^*/T)\, dT + (\mu_i/T)\, dT + RT\, d\ln \bar{f}_i \qquad (6)$$

If equation (6) is multiplied through by x_i and summed over all components i,

$$\Sigma(x_i\, d\mu_i) = \frac{-\Sigma(x_i H_i^*)}{T} dT + \frac{\Sigma(x_i \mu_i)}{T} dT + RT\, \Sigma(x_i\, d \ln \bar{f}_i)$$

But $\Sigma(x_i H_i^*) = H^*$, where H^* is the molal ideal-gas enthalpy of the solution, and $\Sigma(x_i \mu_i) = F$, where F is the actual molal free energy of the solution. Thus

$$\Sigma(x_i\, d\mu_i) = -(H^*/T)\, dT + (F/T)\, dT + RT\, \Sigma(x_i\, d \ln \bar{f}_i) \qquad (7)$$

Combining equation (7) and (2),

$$v\, dp - S\, dT = -(H^*/T)\, dT + (F/T)\, dT + RT\, \Sigma(x_i\, d \ln \bar{f}_i)$$

or since $S + F/T = H/T$

$$\frac{v}{RT} dp + \frac{(H^* - H)}{RT^2} dT = \Sigma(x_i\, d \ln \bar{f}_i) \qquad (8)$$

Equation (8) is the general equation relating pressure, temperature, and the fugacities for any liquid or vapour phase, whether in equilibrium with another phase or not. Reduction to the special cases of constant pressure or constant temperature or both is just a matter of dropping the appropriate terms.

Equation (8) may also be used as the starting point for the further development of both specific and general equations. Particularly useful is an equation relating pressure, temperature, and the activity coefficients for any phase. Equation (8) is of course valid for a pure material as well as for a solution. If it is written for pure i at the same temperature and pressure and in the same phase (liquid or vapour) as the solution in which i is a component, we have:

$$\frac{v_i}{RT} dp + \frac{(H_i^* - H_i)}{RT^2} dT = d \ln f_i$$

Multiplication by x_i and summation over all components of the solution gives:

$$\frac{\Sigma(x_i v_i)}{RT} dp + \frac{\Sigma(x_i H_i^*) - \Sigma(x_i H_i)}{RT^2} dT = \Sigma(x_i\, d \ln f_i) \qquad (9)$$

Subtracting equation (9) from equation (8) gives:

$$\frac{v - \Sigma(x_i v_i)}{RT} dp - \frac{H - \Sigma(x_i H_i)}{RT^2} dT = \Sigma\left(x_i d \ln \frac{\bar{f}_i}{f_i}\right)$$

But $v - \Sigma(x_i v_i)$ is the volume change of mixing Δv, $H - \Sigma(x_i H_i)$ is the heat of mixing ΔH, and $\Sigma[x_i d \ln (\bar{f}_i/f_i)] = \Sigma(x_i d \ln \gamma_i)$. The last equality results from the fact that $\Sigma(x_i\, d \ln 1/x_i) = 0$. Thus the final result is

$$\frac{\Delta v}{RT} dp - \frac{\Delta H}{RT^2} dT = \Sigma(x_i d \ln \gamma_i) \qquad (10)$$

Equation (10) applies to any phase provided that Δv, ΔH, and the γ_i's are all taken with respect to the pure components at the same

VOL. 10 1959

temperature and pressure and in the same physical state as the solution (often regarded as standard states). Applied to phases in vapour–liquid equilibrium, this usually requires the consideration of fictitious states for at least one of the pure components. In this case equation (10) is ordinarily written for the liquid phase. Since the properties of liquids are usually insensitive to changes is pressure, values of Δv and ΔH measured at pressures high enough so that all components are stable as liquids can be used in equation (10) at the equilibrium pressures in question without introducing sensible error. The equations resulting when equation (10) is restricted to conditions of constant pressure or temperature or both are obvious.

One additional step is of interest. Since

$$d(x_i \ln \gamma_i) = x_i \ln d\gamma_i + \ln \gamma_i dx_i$$

then $$\Sigma(x_i d \ln \gamma_i) = d\,\Sigma(x_i \ln \gamma_i) - \Sigma(\ln \gamma_i dx_i)$$

But $\Delta F^E/RT = \Sigma(x_i \ln \gamma_i)$ where ΔF^E is the excess free energy of mixing. Therefore, equation (10) may be written:

$$d\left(\frac{\Delta F^E}{RT}\right) = \frac{\Delta v}{RT}\,dp - \frac{\Delta H}{RT^2}\,dT + \Sigma(\ln \gamma_i dx_i) \quad (11)$$

There are several uses of this equation. Note first that $d(\Delta F^E/RT)$ is an exact differential. Hence the various reciprocity equations may be applied to give relationships between the differential coefficients. For example, it is easily shown that:

$$\left(\frac{\partial\,\Delta H}{\partial p}\right)_{T,x} = \Delta v - T\left(\frac{\partial\,\Delta v}{\partial T}\right)_{p,x} \quad (12)$$

This equation permits the determination of the effect of pressure on the heat of mixing from measurements of the volume change of mixing.

Another use of equation (11) is to derive the various "area" tests which may be used to examine data for thermodynamic consistency. Since $d(\Delta F^E/RT)$ is an exact differential, integration gives:

$$\left(\frac{\Delta F^E}{RT}\right)_2 - \left(\frac{\Delta F^E}{RT}\right)_1 = \int_1^2 \frac{\Delta v}{RT}\,dp - \int_1^2 \frac{\Delta H}{RT^2}\,dT + \Sigma \int_1^2 \ln \gamma_i\, dx_i \quad (13)$$

The limits 1 and 2 are here taken to represent any two states of an open system, and integration is of course carried out for some specific path for which data are available. This way of writing the equation illustrates the infinite possibilities, but in practice integration is ordinarily carried between limits and along paths which result in a considerable simplification of the equation. For example, if the composition of a binary solution is varied from $x_A = 0$ to $x_A = 1$ at constant temperature and pressure, equation (13) reduces to the Redlich and Kister [4] equation:

$$\int_0^1 \ln(\gamma_A/\gamma_B)\,dx_A = 0$$

If data are taken for a phase at constant composition, the last term of equation (11) is zero, and the equation may be solved for ΔH:

$$\Delta H = T\Delta v\left(\frac{\partial p}{\partial T}\right)_x - T^2\left[\frac{\partial(\Delta F^E/T)}{\partial T}\right]_x$$

This is the equation used by Ashley and Brown [1] to calculate heats of mixing from phase-equilibrium data for the HCl–C_2H_6 system.

The main object of this paper has been the development of the general relationships given by equations (8) and (10). In addition, a few illustrations of their use have been pointed out. However, no attempt has been made to exhaust the possibilities of their application to specific cases.

Notation

f_i = fugacity of pure component i at the T and p of the solution and in the same physical state
$\bar{f}_i$ = fugacity of component i in solution
F = molal free energy (Gibbs) of the solution
F_i = molal free energy of pure component i at the T and p of the solution and in the same physical state

F_i^* = molal free energy of pure component i in the reference state of an ideal gas at p^* and the T of the solution

ΔF^E = excess free energy change of mixing

H = molal enthalpy of the solution

H_i = molal enthalpy of pure component i at the T and p of the solution and in the same physical state

H_i^* = molal enthalpy of pure component i in the reference state of an ideal gas at p^* and the T of the solution

ΔH = enthalpy change of mixing at constant T and p; i.e., integral heat of mixing per mole of mixture formed

n_i = moles of component i

p = pressure

p^* = reference-state pressure where all gases are ideal

R = universal gas constant

$\underline{S}$ = total entropy of a phase or system

S = molal entropy of the solution

S_i^* = molal entropy of pure component i in the reference state of an ideal gas at p^* and the T of the solution

T = absolute temperature

V = total volume of a phase or system

v = molal volume of the solution

v_i = molal volume of pure i at the T and p of the solution and in the same physical state

Δv = volume change of mixing at constant T and p per mole of solution formed

x_i = mole fraction of component i in solution

γ_i = activity coefficient of component i in solution; equal to $\bar{f}_i/x_i f_i$

μ_i = chemical potential or partial molal Gibbs free energy of component i in solution

VOL. 10 1959

References

[1] Ashley J. H. and Brown G. M. *Chem. Engng. Progr. Symposium Series*, No. 10, 1954 **50** 129.

[2] Denbigh K. *The Principles of Chemical Equilibrium*, p. 91. Cambridge University Press 1955.

[3] Ibl N. V. and Dodge B. F. *Chem. Engng. Sci.* 1953 **2** 120.

[4] Redlich O. and Kister A. T. *Industr. Engng. Chem.* 1948 **40** 345.

Chemical Engineering Science, 1959, Vol. 10, pp. 229 to 233. Pergamon Press Ltd. London. Printed in Great Britain

Residence times and distribution of residence times in dispersed flow systems

J. G. VAN DE VUSSE

Koninklijke/Shell-Laboratorium, Amsterdam (N.V. De Bataafsche Petroleum Maatschappij)

(*Received* 3 *December* 1958)

Abstract—Mathematical expressions are derived for the residence time and the distribution of residence times of falling particles in a turbulent flow system.

Résume—L'auteur déduit des expressions mathématiques pour le temps de résidence et la répartition du temps de résidence de particules tombant dans un système à écoulement turbulent.

Zusammenfassung—Für die Verweilzeit und die Verteilung der Verweilzeit fallender Teilchen in einem turbulenten Strömungssystem werden mathematische Ausdrücke abgeleitet.

Introduction

The mixing and staging of flowing fluids are of interest in many physical and chemical processes. Various articles in this journal [2, 3, 4, 5, 6, 9] testify of significant progress in the analysis and understanding of these phenomena. In all these studies, however, only the mixing of a continuous phase in the flowing systems was considered. In many two-phase processes not only the mixing of the continuous phase is of interest but also the behaviour of the dispersed phase.

In the mathematical approach of the longitudinal mixing of continuous flow systems, the diffusion equation has been used. This equation can also be applied in dispersed flow systems [7, 8]. From this equation expressions can be derived for the residence time and for the distribution in residence times of dispersed particles. In particular the case will be considered where particles are falling in a fluid which is moving countercurrently. The particles are introduced into the system at the top and withdrawn at the bottom, below the continuous phase inlet. The rate of withdrawal can be influenced by physical means, for instance by controlling the settling rate and the rate of coalescence.

The Differential Equation

A vertical, one-dimensional flow system will be considered. The diffusion equation then can be written:*

$$\frac{\partial n}{\partial t} = \frac{\partial}{\partial y} D \frac{\partial n}{\partial y} - \frac{\partial (ny)}{\partial y}. \qquad (1)$$

It has been shown by Soo [7] that in turbulent systems the diffusion coefficient D of the dispersed particles is about equal to that of the continuous phase. Thus measurements of the diffusion coefficient obtained by tracer injection in the continuous phase, also can be used for determination of the dispersed phase diffusion coefficient.

For simplification of equation (1) two assumptions will be made:

1. D is independent of co-ordinate y, which will be true for homogeneous turbulence.
2. The particle velocity v is independent of co-ordinate y and also independent of particle concentration n. This is a rather sweeping assumption since it means that hindered settling effects are neglected, which is only permissible for a very low hold-up of the dispersed phase and low continuous phase velocity.

The differential equation for a system with the above mentioned assumptions will then be:

$$\frac{\partial n}{\partial t} = D \frac{\partial^2 n}{\partial y^2} - v \frac{\partial n}{\partial y} \qquad (2)$$

*See list of symbols used.

When we consider a state of equilibrium, where there is no variation of the concentration with time, equation (2) reduces to

$$D\frac{d^2n}{dy^2} - v\frac{\partial n}{dy} = 0, \text{ or} \qquad (3)$$

$$D\frac{dn}{dy} - vn = \text{constant} = -q$$

The constant q is the current of transportation of the particles (first boundary condition).

Average Residence Time

Integration of (3) yields: $n = \frac{q}{v} + Ce^{vy/D}$ (4)

The constant C can be found from the second boundary equation, which will depend on the manner in which the particles are removed. Since this can be done in different ways, it may be possible to influence the hold-up of the dispersed phase by the manner in which the removal of the particles is realized. Derivation of a mathematical expression for the second boundary condition, in the case of a countercurrent operation, will be given with reference to Fig. 1.

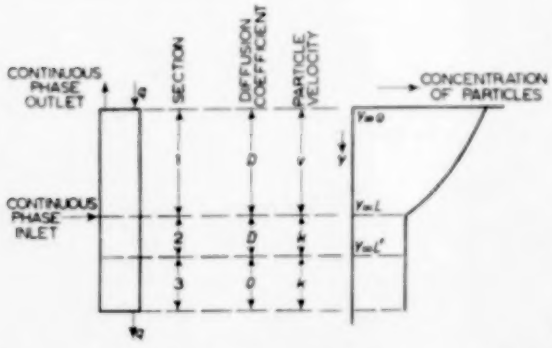

Fig. 1. Schematic situation of boundary conditions.

Dispersed phase is introduced at the top of the column ($y = 0$). The continuous phase is introduced at $y = L$. The particle velocity v for $0 \leqslant y \leqslant L$, will be the particle settling velocity k minus the fluid velocity. The value of the diffusivity will be D over the length of the sections 1 and 2 ($0 \leqslant y \leqslant L'$). At $y > L'$ (section 3) the diffusivity coefficient will be zero.

At the interface $y = L'$, it follows from the condition:

$$D\left[\frac{dn}{dy}\right]_{(y=L'-)} - kn = -kn,$$

that $$\left[\frac{dn}{dy}\right]_{(y=L'-)} = 0.$$

Hence for $L \leqslant y \leqslant L'$, $dn/dy = 0$ and the concentration equals q/k. At the interface $y = L$, the boundary condition becomes:

$$D\left[\frac{dn}{dy}\right]_{(y=L-)} - vn = D\left[\frac{dn}{dy}\right]_{(y=L+)} - kn = -kn$$

or $$D\left[\frac{dn}{dy}\right]_{(y=L-)} - vn = -kn \qquad (5)$$

We have assumed above that at L and L', the concentrations on each side of the boundary are equal. This assumption has been made, since we feel that continuity in the concentration will be ensured by the existence of diffusivity.

An analogous boundary equation can be derived for the case of coalescence of the dispersed phase at $y = L$. The value k will then represent the sedimentation velocity of the coalesced particles. Solving equation (4) with boundary condition (5) we obtain:

$$n = \frac{q}{v}\left[1 + \frac{v-k}{k}e^{v(y-L)/D}\right] \qquad (6)$$

For $y = L$ $\quad n_L = \frac{q}{v}\left[1 + \frac{v-k}{k}\right] = \frac{q}{k}.$ (7)

It can be seen that from (7) that $n_L < q/v$, if $k > v$. For large values of k, $n_L \to 0$. This condition may be considered as a limiting case. The particle concentration distribution along the axis then becomes:

$$n = \frac{q}{v}\left[1 - e^{v(y-L)/D}\right] \qquad (8)$$

The average concentration of n over the whole length L of the column will be:

$$n_{av} = \frac{q}{v}\left[1 - \frac{1}{Pe}(1 - e^{-Pe})\right], \qquad (9)$$

VOL. 10 1959

where $Pe = Lv/D$. The average residence time of the particlse Θ is given by $\Theta = (L/q)\, n_{av}$

or
$$\frac{v\Theta}{L} = \frac{Pe - 1 + e^{-Pe}}{Pe} \tag{10}$$

In Fig. 2 the relation between the residence time Θ and Pe, according to equation (10) is given.

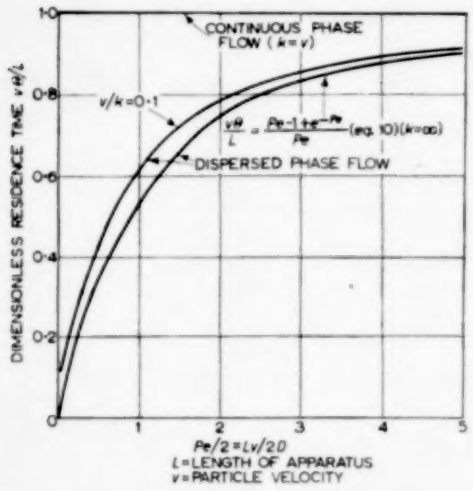

Fig. 2. Dimensionless residence time as a function of Péclet number.

Distribution of Residence Times, the Variance σ^2

The variance σ^2 will be used to characterize residence time distribution. The variance is calculated by van der Laan's method [5]. This is done with the aid of the transient differential equations. For section 1 ($0 < y \leqslant L$) we get:

$$\frac{\partial n}{\partial t} = D\frac{\partial^2 n}{\partial y^2} - v\frac{\partial n}{\partial y} \tag{2}$$

For section 2 ($L \leqslant y \leqslant L'$) the differential equation becomes:

$$\frac{\partial n}{\partial t} = D\frac{\partial^2 n}{\partial y^2} - k\frac{\partial n}{\partial y} \tag{2a}$$

For section 3 ($y \geqslant L'$) the diffusion coefficient D equals zero; hence

$$\frac{\partial n}{\partial t} = -k\frac{\partial n}{\partial y} \tag{2b}$$

At the entrance of the column ($y = 0$) a pulse of tracer mathematically described by the Dirac impulse function is introduced. The total quantity of injected material per unit cross-sectional area equals q^*.

The initial and boundary equations now become:

$$t = 0^- \quad y \geqslant 0 \quad n = 0 \tag{11}$$

$$y = 0 \quad vn - D\frac{\partial n}{\partial y} = q^*\,\delta(t)$$

$$y = L \quad \left(vn - D\frac{\partial n}{\partial y}\right)_{L-} = \left(kn - D\frac{\partial n}{\partial y}\right)_{L+} = q^*\,R(t)$$

$$n_{L-} = n_{L+}$$

$$y = L' \quad \left(kn - D\frac{\partial n}{\partial y}\right)_{L'-} = kn_{L+}$$

$$n_{L'-} = n_{L'+}$$

We are interested in the response $R(t)$ at $y = L$ to the $\delta(t)$ input. For the sake of simplicity we seek the solution for the case where $L' - L$ approaches zero. If $\overline{R}(p)$, the Laplace transform of $R(t)$, given by

$$\overline{R}(p) = \int_0^\infty e^{-pt}\,R(t)\,dt$$

is introduced, the solution of equations (2) taking into account the initial and boundary conditions (11) can easily be constructed. The solution $\overline{R}(p)$ reads:

$$\overline{R}(p) = \frac{k/v \,.\, 2Se^{-Pe(S-\frac{1}{2})}}{(S+\frac{1}{2})\left(S-\frac{1}{2}+\frac{k}{v}\right) - (S-\frac{1}{2})\left(S+\frac{1}{2}-\frac{k}{v}\right)e^{-2SPe}} \tag{12}$$

where

$$S = \sqrt{p\frac{L}{v}\cdot\frac{1}{Pe} + \frac{1}{4}} \qquad (13)$$

$$Pe = \frac{Lv}{D}$$

The average residence time Θ and the variance σ^2 can be calculated from (12) by means of simple differentiation [1, 5]

$$\Theta = \lim_{p\to 0} \frac{-dR(p)}{dp} \qquad (14)$$

$$\sigma^2 + \Theta^2 = \lim_{p\to 0} \frac{d^2}{dp^2}\bar{R}(p)$$

In this way we find:

$$\frac{\Theta\, Pe}{L/v} = Pe - 1 + \frac{v}{k} + \left(1 - \frac{v}{k}\right)e^{-Pe} \qquad (15)$$

$$\frac{\sigma^2\, Pe^2}{(L/v)^2} = 2Pe - 5 + 2\left(\frac{v}{k}\right) + \left(\frac{v}{k}\right)^2 + 2e^{-Pe} \times \left\{2 - \left(\frac{v}{k}\right)^2 + 2\left(1 - \frac{v}{k}\right)Pe\right\} + \left(1 - \frac{v}{k}\right)^2 e^{-2Pe} \qquad (16)$$

It is now possible to make a comparison with a system consisting of N ideal mixers. The comparison is based on the assumption of equal variance of the two distributions of residence times. For a system of N ideal mixers in series we may write:

$$\frac{\Theta^2}{\sigma^2} = N \qquad (17)$$

Dividing the square of (15) by (16) gives us the number of equivalent number of ideal mixers. For finite k, limiting cases are:

In the case of continuous phase flow, where $k = v$, (15) and (16) lead to the same solution as given by VAN DER LAAN [5].

It is of interest to note that the number of stages N approaches the value one, if $Pe \to 0$. The case of k infinite, which would lead to a value of 1·5 if $Pe \to 0$, is trivial. Fig. 3 gives

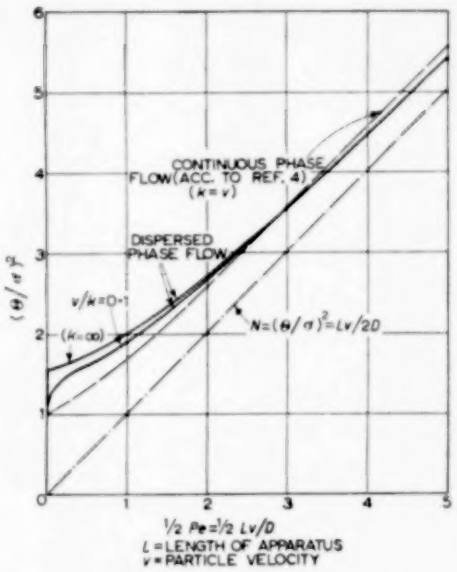

FIG. 3. Relation between $(\Theta/\sigma)^2$ and diffusivity (dimensionless).

$(\Theta/\sigma)^2$ as a function of the Péclet number. Deviations from the curve for the continuous phase flow are relatively small except for small values of Pe.

Acknowledgements—The author acknowledges with appreciation the valuable advice given by Mr. E. TH. VAN DER LAAN.

$Pe \ll 1$	$\frac{\Theta^2}{\sigma^2} \approx 1 + \frac{Pe}{3(v/k) + [2 - (3v/k)]\,Pe}$	$\frac{v\Theta}{L} \approx \frac{v}{k} + \frac{Pe}{2}\left(1 - \frac{v}{k}\right)$.
$Pe = 0$	$\frac{\Theta^2}{\sigma^2} = 1$	$\frac{v\Theta}{L} = \frac{v}{k}$.
$Pe \gg 1$	$\frac{\Theta^2}{\sigma^2} \approx \frac{Pe}{2} + \frac{1}{4} + \frac{1}{2}\frac{v}{k} - \frac{1}{4}\left(\frac{v}{k}\right)^2$	$\frac{v\Theta}{L} \approx 1 - \frac{[1 - (v/k)]}{Pe}$

Notation

D = longitudinal diffusion coefficient	$(L^2\,T^{-1})$	$\delta(t)$ = impulse function	(T^{-1})
k = particle settling velocity	(LT^{-1})	$R(t)$ = response function	(T^{-1})
L = length of tube	(L)	σ^2 = variance of the spread in residence times of the particles	(T^2)
N = number of mixing stages	—	Θ = average residence time of particles	(T)
n = particle concentration	(L^{-3})		
p = parameter in Laplace transformation	—		
q = current of transportation of particles	$(L^{-2}\,T^{-1})$	Pe = Péclet number $= \dfrac{vL}{D}$	—
q^* = total amount of injected tracer material	(L^{-2})		
t = time	(T)	bar over function designates the Laplace transform: $\overline{R}(p) = \int_0^\infty e^{-pt}\,R(t)\,dt.$	
v = particle velocity	(LT^{-1})		
y = length co-ordinate	(L)		

References

[1] Aris R. *Proc. Roy. Soc.* 1958 **A 245** 268.

[2] Danckwerts P. V. *Chem. Engng. Sci.* 1953 **2** 1.

[3] Klinkenberg A. and Sjenitzer F. *Chem. Engng. Sci.* 1956 **5** 258.

[4] Kramers H. and Alberda G. *Chem. Engng. Sci.* 1953 **2** 173.

[5] Laan E. Th. van der *Chem. Engng. Sci.* 1958 **7** 187.

[6] Levenspiel O. and Smith W. K. *Chem. Engng. Sci.* 1957 **6** 227.

[7] Soo S. L. *Chem. Engng. Sci.* 1956 **5** 57.

[8] Vusse J. G. van de *Proc. Symposium on Scaling up of Chemical Plant and Processes London*, 1957 S 41-6.

[9] Wehner J. F. and Wilhelm R. H. *Chem. Engng. Sci.* 1957 **6** 89.

Chemical Engineering Science, 1959, Vol. 10, pp. 234 to 242. Pergamon Press Ltd. London. Printed in Great Britain

The evaporation of two-component liquid mixtures

J. F. RICHARDSON

Department of Chemical Engineering, Imperial College, London, S.W.7.

(*Received* 14 *December* 1958)

Abstract—The diffusivities of acetone, carbon tetrachloride and water vapours in air have been determined experimentally using the method first developed by WINKELMANN and values have been obtained over a range of operating conditions to an accuracy of within ± 2 per cent. The evaporation of two-component liquid mixtures, consisting of a volatile and a non-volatile material has also been been studied in the same apparatus. It has been shown that, when the non-volatile liquid is the denser, the liquid remains completely mixed and the evaporation rate can therefore be simply calculated for an ideal mixture. When the non-volatile component is the less dense, convective mixing is negligible and the mass transfer in the liquid is a process of unsteady state molecular diffusion.

Résumé—L'auteur a déterminé expérimentalement les diffusibilités dans l'air des vapeurs d'acétone de tetrachlorure de carbone, et d'eau, en utilisant la méthode de WINKELMANN. Les valeurs obtenues dans certaines conditions d'opération ont une précision à + ou − 2%. Le même appareillage sert à étudier l'évaporation de mélanges liquides à deux constituants comprenant un produit volatil et un non volatil.

Quand le produit non volatil est le plus dense, l'auteur montre qui le liquide reste entièrement à l'état de mélange, et la vitesse d'évaporation peut donc être calculée simplement comme pour un mélange idéal. Quand le corps non volatil est le moins dense, le mélangeage par convection est négligeable et le transfert de masse dans le liquide est un procédé de diffusion moléculaire en régime transitoire.

Zusammenfassung—Die Diffusionskoeffizienten von Azeton, Tetrachlorkohlenstoff und Wasserdampf in Luft werden experimentell in einer von WINKELMANN angegebenen Apparatur mit einer Genauigkeit von ± 2% bestimmt. Die Verdampfung von flüssigen Gemischen aus zwei Komponenten, einer flüchtigen und einernichtflüchtigen, wurden ebenfalls in der gleichen Apparatur untersucht. Wenn die nichtflüchtige Flüssigkeit die grössere Dichte hat, dann bleibt die Flüssigkeit vollständig gemischt und die Verdampfungsgeschwindigkeit kann daher auf einfache Weise für ein ideales Gemisch berechnet werden. Wenn die nichtflüchtige Komponente die geringere Dichte hat, kann man die konvektive Vermischung vernachlässigen und den Stofftransport in der Flüssigkeit als einen nichtstationären Vorgang der molekularen Diffusion auffassen.

INTRODUCTION

WHEREAS there have been many investigations relating to the evaporation of a pure liquid into a gas stream, little attention has been paid to the evaporation of a liquid consisting of two or more components of differing volatilities. The more volatile components will then evaporate preferentially leaving a residual liquid which may be of greater or lower density than the original liquid, according to the values of the densities of the components. In the former case the heavy residue will sink into the bulk of the liquid and considerable mixing will occur, whereas in the latter, the residue will tend to concentrate in the upper layers and the more volatile liquid must diffuse through this region before it can evaporate.

For the present study, two simple two-component systems have been selected. Each contained a virtually non-volatile liquid (dibutyl phthalate); in the first mixture the volatile liquid was of lower density (acetone), and in the second the volatile liquid was of higher density (carbon

tetrachloride). The method of investigation which was adopted was to allow the mixture to evaporate at constant temperature in a vertical tube across the top of which was passed an air stream in which the vapour was carried away. The rate of evaporation was measured by observing the rate of fall of the liquid surface.

A series of preliminary experiments was carried out using the pure volatile liquid, in order to examine the reproducibility of results and the effect of experimental conditions. As a result of these experiments, values of the diffusivity of three vapours in air—acetone, carbon tetrachloride and water—have been obtained.

Apparatus and Experimental Method

The method adopted was based on that originally used by Stefan [1] and Winkelmann [2], and subsequently modified by a number of workers including Lee and Wilke [3]. The liquid to be evaporated was contained in the vertical limb of the tube shown in Fig. 1, the upper section *A*, serving merely for the introduction of the liquid.

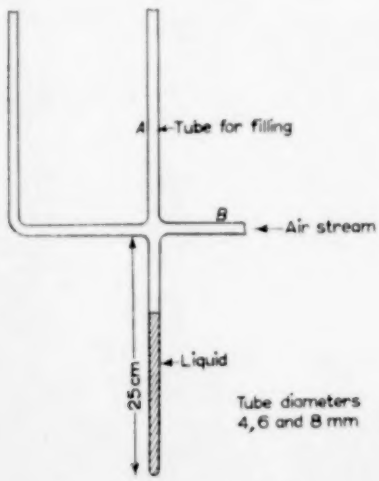

Fig. 1. Evaporation tube.

The tube was immersed in a thermostatically controlled bath. Air from a cylinder of compressed gas passed through a copper coil immersed in the bath and its temperature was raised to that of the bath. This air stream entered through the horizontal section *B* of the evaporation tube and the air leaving the tube was metered. The walls of the bath were of glass and the level of the liquid in the tube was measured by means of a cathetometer to within 0·002 cm. At the beginning of an experiment the liquid was introduced into the tube and allowed to reach the temperature of the bath before the passage of air was commenced. Readings of liquid level were then obtained as a function of time.

The effect of the operating variables was studied using acetone as the liquid. At a given temperature, the two important variables were the rate of passage of air and the diameter of the tube. The air rate was varied between 0·5 and 2·1 cm^3/sec and three tube diameters were used (4, 6 and 8 mm). The lower permissible limit of air rate is set by the necessity of maintaining an approximately zero concentration of vapour at the mouth of the tube, and the upper limit by the production of excessive turbulence in the upper parts of the diffusing vapour. In tubes of too small diameter, the overall rate of diffusion will be affected by the velocity profile over the cross-section, and in excessively large tubes, turbulence is induced too readily.

Evaporation of Pure Liquids

Theory

Under conditions of molecular diffusion, the rate of mass transfer per unit area of liquid surface is given by Stefan's law as :—

$$N = \rho \frac{dh}{dt} = D_v \frac{C_{vT}}{h} \ln \frac{P_{B2}}{P_{B1}} \qquad (1)$$

where h is the distance between the air stream and the liquid surface at time t, P_{B2}, P_{B1} are the partial pressures of air in the air stream and at the surface, ρ is the molar density of the liquid, D_v is the diffusivity of the vapour in air, and C_{vT} is the total molar concentration of gas and vapour in the diffusion region ; this will be constant and equal to the number of moles of gas plus vapour per unit volume in the tube. In a given experiment, h and t are the only variables and therefore on integration :

$$\frac{h^2 - h_0^2}{t} = \frac{2D_v C_{vT}}{\rho} \ln \frac{P_{B2}}{P_{B1}} \qquad (2)$$

where h_0 is the initial value of h.

Now the effective distance, h, over which molecular diffusion is occurring cannot be estimated accurately because of end-effects; the position of the liquid surface cannot be defined precisely because of the curvature of the meniscus, and at the upper end of the tube turbulence is induced in the diffusing vapour. On the other hand, values of $h - h_0$ can be measured very accurately and it is therefore convenient to rearrange equation (2) as:

$$\frac{(h - h_0)(h - h_0 + 2h_0)}{t} = \frac{2D_v C_{vT}}{\rho} \ln \frac{P_{B2}}{P_{B1}}$$

$$\text{i.e. } \frac{t}{h - h_0} = \frac{\rho}{2D_v C_{vT} \ln P_{B2}/P_{B1}} (h - h_0) + \frac{\rho h_0}{D_v C_{vT} \ln P_{B2}/P_{B1}} \qquad (3)$$

Thus, if $\frac{t}{h - h_0}$ is plotted against $h - h_0$, a straight line should be obtained. The diffusivity D_v can then be calculated from the slope s:

$$\text{i.e. } D_v = \frac{\rho}{2s C_{vT} \ln P_{B2}/P_{B1}} \qquad (4)$$

and the effective initial distance over which diffusion is occuring can be calculated from the intercept on the ordinate axis. A typical curve is shown in Fig. 2.

Results

The effect of tube diameter and air flow rate was studied using acetone at 30°C. In each case, the results were corrected to standard atmospheric pressure by multiplying by the factor $P/760$.

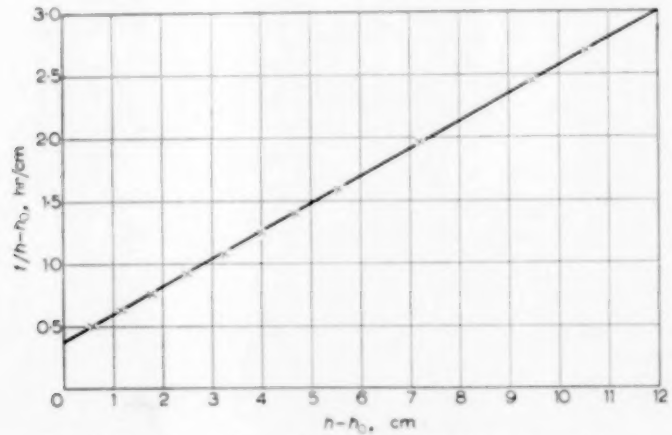

FIG. 2. Experimental results. Acetone at 50·9°C in 6 mm tube.

Table 1. *Effect of tube diameter and air flow rates on apparent diffusivity*

Tube diameter (mm)	*Air flow rate* (cm³/sec)	*Temp.* (°C)	*Slope of curve* (*s*) (hr/cm²)	D_v (cm²/sec)	*Pressure* P (mm Hg)	$D_v \frac{P}{760}$ (cm²/sec)
6	0·94	30·0	0·937	0·105	780	0·108
6	1·10	30·0	0·902	0·111	760	0·111
6	2·10	30·3	0·870	0·113	767	0·114
6	0·42	30·3	0·947	0·105	781	0·108
8	1·41	30·3	0·825	0·120	752	0·118
4	0·53	30·5	0·830	0·118	753	0·116
8	1·41	30·4	0·878	0·110	764	0·111

It will be seen that the results do not vary by more than ± 2 per cent from the mean value of 0·112 cm²/sec, and it is therefore concluded that neither tube diameter nor air rate has a critical effect for the ranges investigated. The succeeding experiments were all carried out in the 6 mm tube, with an air flow of about 1 cm³/sec. The variation of diffusivity D_T with temperature θ is seen in Fig. 3, and the diffusivities of acetone and carbon

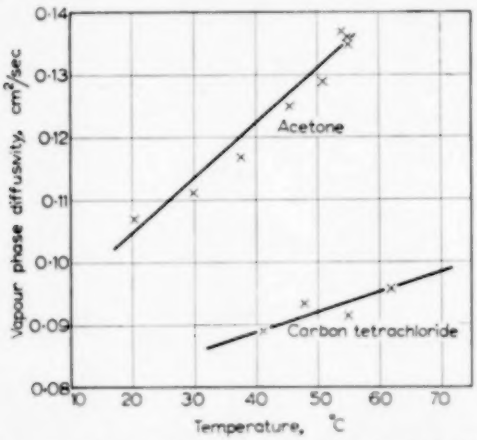

Fig. 3. Diffusivities of acetone and carbon tetrachloride in air as function of temperature.

tetrachloride vapours in air are given to within approximately 2 per cent by the relations:

$$\text{Acetone } D_v = 0{\cdot}087 + 0{\cdot}00086\,\theta \qquad (5)$$

$$\text{Carbon tetrachloride } D_v = 0{\cdot}076 + 0{\cdot}00032\,\theta \qquad (6)$$

Gush [5] obtained a value of 0·111 cm²/sec for the diffusivity of acetone for temperatures between 30 and 50°C.

No values for the diffusivities are quoted in the literature, but approximate values have been calculated from Gilliland's equation and compared below with those calculated from equations (5) and (6) at 42°C, the temperature at which the experiments with 2-component mixtures were carried out.

	Acetone	*Carbon tetrachloride*	
From equations (5) and (6)	0·123	0·090	cm²/sec
From Gilliland's equation	0·113	0·081	cm²/sec

An isolated measurement for water at 46°C gave a value of 0·258 cm²/sec.

In a number of the experiments in the 6 mm tube, the intercept on the $t/(h - h_0)$ axis was measured, and the effective position of the top of the region of molecular diffusion was determined.

Two-Component Mixtures—Volatile Liquid Less Dense

The evaporation of a mixture of equal volumes of acetone and dibutyl phthalate in the 6 mm tube was studied at 42°C. Measurements were taken in the same way as for single component liquids. Dibutyl phthalate can be considered as entirely non-volatile (vapour pressure at 42°C is 2×10^{-4} mm Hg), and on the assumption that the mixture is ideal, the relation between the partial pressure at the interface and the concentration of acetone in the liquid at the interface is given by Raoult's Law. As the residue is considerably denser than the evaporating liquid, it will be assumed that it mixes completely with the bulk of the liquid which will therefore be of uniform composition throughout at any given time, so that the partial pressure of acetone vapour at the interface, and hence the evaporation rate, can be calculated in terms of the amount of evaporation which has taken place up to that time. These various assumptions will be justified if the measured and calculated amounts of evaporation correspond during the whole course of the experiment. The calculated amount of evaporation is obtained as follows.

After time t, the number of moles of the more volatile component which have evaporated $= (h - h_0)\,\rho_v\,A$. Thus, if n_1 and n_2 are the numbers of moles of the volatile and non-volatile components initially, the mole fraction of the volatile liquid at time $t = \dfrac{n_1 - (h - h_0)\,\rho_v\,A}{n_1 + n_2 - (h - h_0)\,\rho_v A}$.

The molar concentration of vapour at the surface of the liquid is therefore

$$C_v = C_{v0}\left(\frac{n_1 - (h - h_0)\,\rho_v\,A}{n_1 + n_2 - (h - h_0)\,\rho_v\,A}\right) \qquad (7)$$

where C_{v0} is the corresponding value for the pure volatile liquid at the same temperature.

Now the rate of diffusion through the gas phase is strictly given by equation (1). However, the

ratio P/P_{Bm} was equal to 1·18 at the commencement of the experiment, and fell rapidly during the initial stages to a value of approximately unity. Since an algebraic relation between h and t can be obtained only when the ratio is unity, this simplification was introduced, because it was considered that the resulting errors would be less than those introduced by a graphical solution of the problem.

Thus, from Fick's Law,

$$\rho_v \frac{dh}{dt} = \frac{D_v C_{v0}}{h}\left(\frac{n_1 - (h - h_0)\rho_v A}{n_1 + n_2 - (h - h_0)\rho_v A}\right) \quad (8)$$

Rearranging, this gives

$$\frac{dt}{dh} = \frac{\rho_v}{D_v C_{v0}} h - \frac{n_2}{D_v C_{v0} A} + \frac{n_2}{D_v C_{v0} A}\left(\frac{n_1/\rho_v A + h_0}{n_1/\rho_v A + h_0 - h}\right)$$

On integration:

$$t = \frac{\rho_v}{2D_v C_{v0}}(h^2 - h_0^2) - \frac{n_2}{D_v C_{v0} A}(h - h_0) - \frac{n_2}{D_v C_{v0} A}\left(\frac{n_1}{\rho_v A} + h_0\right)\ln\left(1 - \frac{\rho_v A}{n_1}(h - h_0)\right) \quad (9)$$

The experiments were carried out at 42°C with mixtures consisting initially of equal volumes of dibutyl phthalate and acetone. Under these conditions, the values of the quantities in equation (9) were as follows:

$\rho_v = \frac{0{\cdot}764}{58} = 0{\cdot}0132$ g moles/cm³

$D_v = 0{\cdot}123$ cm²/sec $= 443$ cm²/hr (from equation 3)

$n_1 = 2 \times \frac{0{\cdot}764}{58} = 0{\cdot}0263$ g moles.

$n_2 = 2 \times \frac{1{\cdot}048}{278} = 0{\cdot}00753$ g moles.

$A = 0{\cdot}312$ cm²

$h_0 = 1{\cdot}15$ cm

$C_{v0} = \frac{455}{760} \times \frac{273}{315} \times \frac{1}{22{,}400}$

$= 2{\cdot}32 \times 10^{-5}$ g moles/cm³.

On substitution and simplification, the relation between t and h (in hours and centimetres respectively) becomes:

$$t = 0{\cdot}641h^2 - 2{\cdot}40h + 35{\cdot}6 - 41{\cdot}8\log_{10}(7{\cdot}56 - h) \quad (10)$$

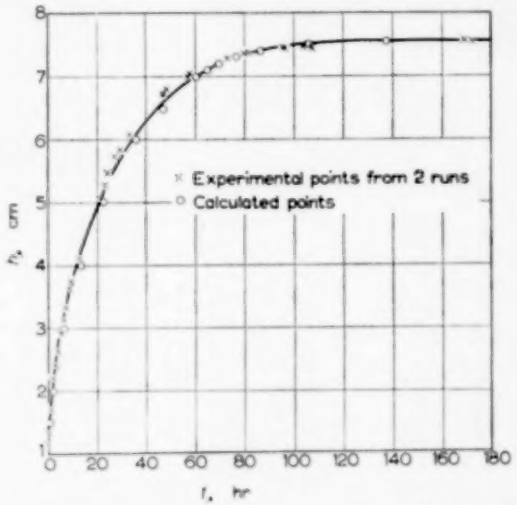

FIG. 4. Experimental and calculated results for evaporation of equivolume mixtures of acetone and dibutyl phthalate at 42°C.

In Fig. 4 is shown the experimentally determined relationship between h and t together with that calculated from equation (10). The agreement is seen to be within 4 per cent over the whole range, with the theoretical curve slightly below the experimental one. This small difference could be attributed to small inaccuracies in experiment or to the assumption that P/P_{Bm} is equal to unity.

TWO-COMPONENT MIXTURES—VOLATILE LIQUID DENSER

When the volatile liquid is denser than the non-volatile component, the residue after evaporation is of relatively low density and therefore shows little tendency to mix with the bulk of the liquid. Under these circumstances, therefore, diffusion must take place through the bulk of the liquid phase before further evaporation can occur. Since the capacity of the vapour phase is very much less than that of the liquid phase, it will be assumed that in the gas phase the rate of transfer is proportional to the overall concentration

VOL. 10 1959

gradient and that in the liquid phase the transfer is an unsteady state diffusional process. The liquid depth was assumed to be effectively infinite. Measurements of the rate of evaporation of a mixture of equal volumes of carbon tetrachloride and dibutyl phthalate in the 6 mm tube at 42°C, should then enable the liquid phase diffusivity, D, to be calculated. If the calculated value of D over the whole duration of the experiment remains constant the above assumptions concerning the mechanism of the process would appear to be justified.

The rate of diffusion in the gas phase is given by:

$$\rho_v \frac{dh}{dt} = \frac{D_v C_v}{h} \qquad (11)$$

where C_v is the molar concentration of vapour at the liquid surface at time t. If the mixture is ideal, Raoult's Law will be applicable and the molar concentration of the volatile component in the liquid at the surface C_L will be proportional to the concentration in the vapour.

$$\text{i.e. } C_L = kC_v \qquad (12)$$

$$\text{Thus } C_L = \frac{k\rho_v}{D_v} \cdot h\frac{dh}{dt} = bh\frac{dh}{dt} \text{ (say)} \qquad (13)$$

For diffusion in the liquid:

$$\frac{\partial C}{\partial t} = D\frac{\partial^2 C}{\partial y} \qquad (14)$$

where C is the molar concentration of the volatile liquid at a depth y below the surface.

This equation must be solved to give the concentration gradient at the surface for the following boundary conditions:

$t = 0,\ 0 < y < \infty,\ C = C_0$ (uniform constant value)

$t > 0,\ y = \infty,\quad \dfrac{\partial C}{\partial y} = 0$

$y = 0,\ t = t_1,\quad C = C_1$

$t = t_2,\quad C = C_2$

$t = t_n,\quad C = C_n$ etc.

where $C_1, C_2 \ldots C_n$ are values of C_L calculated from equation (13), using the experimentally determined values of h and dh/dt at regular time intervals. This procedure was necessary because it was not found possible to express C_L as a simple algebraic function of t.

The solution of equation (14) is given in Appendix 2 as:

$$\left(\frac{\partial c}{\partial y}\right)_{y=0} = \frac{1}{2\sqrt{\pi D}} \left(\sum_1^n \left[\frac{C_{n-1} - C_{n+1}}{\sqrt{t - t_n}}\right] + \frac{C_0 - C_1}{\sqrt{t}}\right) \quad (\text{for } t > t_n) \qquad (15)$$

At time t, the molar rate of evaporation per unit area is given by

$$\left(D\frac{\partial C}{\partial y}\right)_{y=0} = \rho_v \frac{dh}{dt} \qquad (16)$$

Then from equations (13), (15) and (16), at time t,

$$\tfrac{1}{2}\sqrt{\frac{D}{\pi}}\, b \left(\sum_1^n \left[\frac{(h\,dh/dt)_{n-1} - (h\,dh/dt)_{n+1}}{\sqrt{t - t_n}}\right] + \frac{(h\,dh/dt)_0 - (h\,dh/dt)_1}{\sqrt{t}}\right) = \rho_v \frac{dh}{dt} \qquad (17)$$

From equations (12) and (13),

$k = C_L/C_v$ for pure carbon tetrachloride, and $b = k\,\rho_v/D_v$.

Under the conditions of the experiment—atmospheric pressure and 42°C—the vapour pressure of carbon tetrachloride is 251 mm Hg, so that

$$k = \frac{1{\cdot}54/155}{1/22{,}400 \times 273/315 \times 251/760} = 780$$

and $\dfrac{b}{\rho_v} = \dfrac{780}{324} = 2{\cdot}4$ hr/cm²

[$D_v = 0{\cdot}090$ cm²/sec = 324 cm²/hr from equation (6)]

Substituting in equation (17),

$$D = 2{\cdot}2\left(\frac{dh}{dt}\right)^2 \left(\sum_1^n \left[\frac{(h\,dh/dt)_{n-1} - (h\,dh/dt)_{n+1}}{\sqrt{t - t_n}}\right] + \frac{(h\,dh/dt)_0 - (h\,dh/dt)_1}{\sqrt{t}}\right)^{-2} \qquad (18)$$

(units of centimetres and hours) $(t > t_n)$

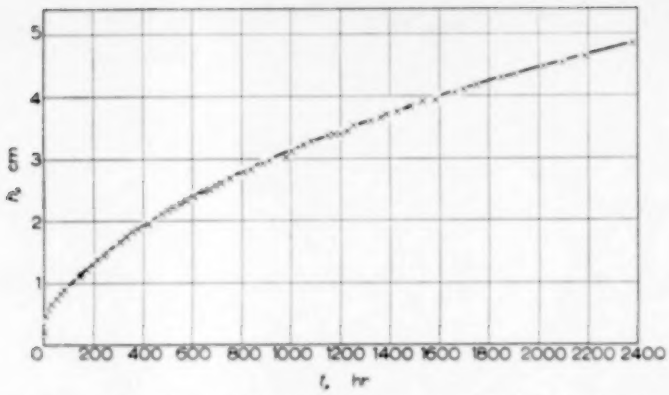

Fig. 5. Experimental figures for the evaporation of equi-volume mixture of carbon tetrachloride and dibutyl at 42°C.

$$= 2{\cdot}2\left(\frac{dh/dt}{\sigma}\right)^2 \text{ (say)} \qquad (19)$$

Experimental measurements of a mixture of equal volumes of carbon tetrachloride and dibutyl phthalate were made over a period of 4400 hr and values of σ were calculated at various times from the experimental results. The results are given in Fig. 5 and Table 2.

Table 2. *Calculation of liquid phase diffusivity for carbon tetrachloride in dibutyl phthalate*

Time, t (hr)	dh/dt (cm/hr)	σ ($cm^2/hr^{1.5}$)	$\frac{dh/dt}{\sigma}$
10	0·0095	0·138	0·069
20	0·0070	0·0943	0·074
50	0·0060	0·0585	0·103
100	0·0052	0·041	0·127
500	0·0022	0·0204	0·108
1000	0·0016	0·0133	0·120
2000	0·0011	0·0094	0·117
2600	0·00085	0·00824	0·103
3000	0·00072	0·00768	0·094
4000	0·00052	0·00688	0·076

Over the period from 50 to 2600 hr, the value of $(dh/dt)/\sigma$ remained substantially constant. For lower values of time, the gradient dh/dt was changing very rapidly so that accurate measurements were difficult to obtain. After more prolonged periods than about 2600 hr, the concentration was starting to change rapidly at the bottom of the tube and it was no longer justifiable to consider the liquid depth as infinite. A rough calculation has shown that the concentration at the bottom of the tube would have changed by about 20 per cent after 1000 hr. The mean value of $(dh/dt)/\sigma$ over the period was 0·113 $hr^{\frac{1}{2}}$/cm. Hence the mean value for the diffusivity for the carbon tetrachloride – dibutyl phthalate system was given by equation (19) as 0·028 cm^2/hr.

Conclusions

The Winkelmann method has been used with varying experimental conditions to determine the diffusivity of a vapour in air. It has been concluded that the results obtained are substantially independent of both air rate and tube diameter, over the range investigated. Values of diffusivities have been obtained for acetone, carbon tetrachloride and water vapours to within an estimated accuracy of $\pm$ 2 per cent.

The evaporation of a mixture of acetone and dibutyl phthalate has been studied in the same apparatus and it has been shown that the heavy residue sinks and completely mixes with the remaining liquid. The levels of the liquid surface calculated on this assumption were found to agree closely with the experimental values throughout the course of the experiment.

When a mixture of carbon tetrachloride and dibutyl phthalate evaporates, the evaporation rate falls off very rapidly with time because the residual

liquid is of a lower density and therefore remains close to the surface. The value of the liquid phase diffusivity has been calculated at various times during the process, on the assumption that the amount of mixing in the liquid due to convection is negligible and that the transfer process in the liquid approximates to that which would occur under conditions of molecular diffusion in a liquid of infinite depth. The value of the diffusivity so calculated was constant for a period of over 2500 hr. At the beginning of the experiment, accurate values were difficult to obtain because of the rapid change in the evaporation rate. Towards the end of the experiment, low values of diffusivity were obtained because the concentration was changing appreciably in the liquid at the lower end of the tube.

In this study, the behaviour of two simple ideal systems has been elucidated. Further investigations are needed in order to determine the behaviour of the more complex mixtures which are normally encountered in the petroleum and chemical industries, both under conditions of natural evaporation and during the combustion of the liquid in bulk.

Acknowledgements—The author is indebted to Professor D. M. Nevitt for providing facilities for the experimental work.

Appendix—1

Physical Properties of Materials Used

Carbon tetrachloride

Density (g/cm^3)

$$= 1{\cdot}63255 - 1{\cdot}9110 \times 10^{-3}\theta - 6{\cdot}90 \times 10^{-5}\theta^2$$

Vapour pressure (P_v — mm Hg) is given by:

$$\log_{10} P_v = 79{\cdot}875 - \frac{1769}{T}$$

Acetone

Density (g/cm^3)

$$= 0{\cdot}81248 - 1{\cdot}1 \times 10^{-3}\theta - 8{\cdot}58 \times 10^{-5}\theta^2$$

Vapour pressure (P_v — mm Hg) is given by:

$$\log_{10} P_v = 7{\cdot}930 - \frac{1660}{T}$$

Dibutyl phthalate

Density (g/cm^3) at 42°C = 1·048

Appendix—2

Solution of the Liquid Phase Diffusion Equation

$$\frac{\partial C}{\partial t} = D\frac{\partial^2 C}{\partial y^2} \tag{14}$$

When $t = 0$, $C = C_0$ $\qquad 0 < y < \infty$

Put $c = C - C_0$

Then $$\frac{\partial c}{\partial t} = D\frac{\partial^2 c}{\partial y^2} \tag{20}$$

and when $t = 0$, $c = c_0 = 0$. $\qquad (0 < y < \infty)$

When $y = \infty$, $\dfrac{\partial C}{\partial y} = \dfrac{\partial c}{\partial y} = 0 \quad (t > 0)$

When $y = 0$, $\quad C = C_1$ and $c = c_1$ at $t = t_1$

$C = C_n$ and $c = c_n$ at $t = t_n$ etc.

Mean value of c over time interval t_{n-1} to $t_n = \frac{1}{2}(c_{n-1} + c_n)$ $= a_n$ (say).

Taking Laplace Transforms of both sides of equation (20),

$$\int_0^\infty \frac{\partial c}{\partial t} e^{-pt}\, dt = D\int_0^\infty \frac{\partial^2 c}{\partial y^2} e^{-pt}\, dt$$

$$\therefore \quad (-c)_{t=0} + p\bar{c} = D\frac{\partial^2 \bar{c}}{\partial y^2}$$

i.e. $$\frac{\partial^2 \bar{c}}{\partial y^2} - \frac{p}{D}\bar{c} = 0$$

$$\therefore \quad \bar{c} = B_1 e^{y\sqrt{p/D}} + B_2 e^{-y\sqrt{p/D}} \tag{21}$$

and $$\frac{\partial \bar{c}}{\partial y} = B_1\sqrt{p/D}\, e^{y\sqrt{p/D}} - B_2\sqrt{p/D}\, e^{-y\sqrt{p/D}} \tag{22}$$

When $y = \infty$, $\dfrac{\partial c}{\partial y} = 0$, and $\dfrac{\partial \bar{c}}{\partial y} = 0$.

$$\therefore \quad B_1 = 0$$

$$\therefore \quad \text{when } y = 0,\ \bar{c} = B_2,$$

and $$\frac{\partial \bar{c}}{\partial y} = -B_2\sqrt{p/D}$$

Thus $$B_2 = \int_0^\infty c\, e^{-pt}\, dt$$

$$= \int_0^{t_1} a_1 e^{-pt}\, dt + \int_{t_1}^{t_2} a_2 e^{-pt} + \ldots. + \int_{t_{n-1}}^{t_n} a_n e^{-pt}\, dt + \ldots$$

$$= \frac{a_1}{p}(1 - e^{-pt_1}) + \frac{a_2}{p}(e^{-pt_1} - e^{-pt_2}) + \ldots.$$

$$+ \frac{a_n}{p}(e^{-pt_{n-1}} - e^{-pt_n}) + \ldots.$$

$$= \frac{1}{p} a_1 + \frac{1}{p} e^{-pt_1} (a_2 - a_1) + \ldots .$$

$$+ \frac{1}{p} e^{-pt_n} (a_{n+1} - a_n) + \ldots .$$

$$= \frac{1}{2p} (c_0 + c_1) + \frac{1}{2p} e^{-pt_1} (c_2 - c_0) + \ldots$$

$$+ \frac{1}{2p} e^{-pt_n} (c_{n+1} - c_{n-1}) + \ldots .$$

$$= \frac{1}{2p} (C_1 - C_0) + \sum_{n=1}^{n=\infty} \left[\frac{1}{2p} e^{-pt_n} (C_{n+1} - C_{n-1}) \right]$$

Substitution in equations (21) and (22) gives :

$$\bar{C} = \frac{1}{2p} (C_1 - C_0) e^{-y\sqrt{p/D}} +$$

$$+ \sum_{n=1}^{n=\infty} \left[e^{-pt_n} \frac{1}{2p} (C_{n+1} - C_{n-1}) e^{-y\sqrt{p/D}} \right] \quad (23)$$

and $$\frac{\partial \bar{C}}{\partial y} = - \frac{1}{2\sqrt{pD}} (C_1 - C_0) e^{-y\sqrt{p/D}} -$$

$$- \sum_{n=1}^{n=\infty} \left[\frac{1}{2\sqrt{pD}} e^{-pt_n} (C_{n+1} - C_{n-1}) e^{-y\sqrt{p/D}} \right] \quad (24)$$

Taking the inverse transform [4] of equation (24),

$$\frac{\partial C}{\partial y} = - \frac{1}{2\sqrt{\pi D t}} (C_1 - C_0) e^{-y^2/4Dt} -$$

$$- \sum_{n=1}^{n=n} \left[\frac{1}{2\sqrt{\pi D (t - t_n)}} (C_{n+1} - C_{n-1}) e^{-y^2/4D(t-t_n)} \right]$$

(for $t > t_n$) (25)

When $t = t_n$, the corresponding term is zero for all value of y.

Thus, when $y = 0$,

$$\frac{\partial C}{\partial y} = \frac{1}{2\sqrt{\pi D}} \left\{ \sum_{n=1}^{n=n} \left[\frac{C_{n-1} - C_{n+1}}{\sqrt{(t - t_n)}} \right] + \frac{C_0 - C_1}{\sqrt{t}} \right\}$$

(for $t > t_n$) (26)

NOTATION

A = cross-sectional area of evaporating surface
a_n = mean value of c over internal t_{n-1} to t_n
B_1, B_2 = integration constants
$b = k\rho_v / D_v$
C = molar concentration of volatile liquid at time t, depth y below surface
C_0 = uniform constant value of C at $t = 0$
C_L = molar concentration of volatile liquid at surface
C_n = value of C at $t = t_n$
C_v = molar concentration of vapour at liquid surface
C_{v0} = molar concentration of vapour at surface of pure liquid
C_{vT} = total molar concentration of gas and vapour
$c = C - C_0$
D = liquid phase diffusivity
D_v = vapour phase diffusivity
h = distance over which vapour is diffusing at time t
h_0 = initial value of h
k = Henry's constant C_L / C_v
N = molar rate of transfer per unit area
n_1 = number of moles of volatile component initially
n_2 = number of moles of non-volatile component initially
P = total pressure
P_B = partial pressure of air
P_{Bm} = logarithmic mean partial pressure of air
P_v = vapour pressure
p = parameter in Laplace transformation
s = slope of curve in single component experiments
T = absolute temperature
t = time
y = distance below surface
ρ = molar density of single component liquid
ρ_c = molar density of more volatile component in liquid form
σ = function of h, t, dh/dt as defined by equations (18) and (19)
θ = temperature in degrees centigrade

REFERENCES

[1] STEFAN J. *Wien Ber. II* 1873 **68** 385.

[2] WINKELMANN A. *Ann. Phys.* 1884 **22** 1, 154 ; **36** 1889 93.

[3] LEE C. Y. and WILKE C. R. *Industr. Engng. Chem.* 1954 **46** 2381.

[4] MICKLEY H. S., SHERWOOD T. K. and REED C. E. *Applied Mathematics in Chemical Engineering* p. 284. McGraw Hill, New York 1957.

[5] GUSH L. L. *Trans. Inst. Chem. Engrs.* 1958 **26** 142.

Chemical Engineering Science, 1959, Vol. 10, pp. 243 to 253. Pergamon Press Ltd. London. Printed in Great Britain

Liquid mixing on bubble-cap and sieve plates

T. J. GILBERT

Imperial Chemical Industries Ltd., Central Instrument Laboratory, Whitchurch Hill, Reading, Berks.*

(*Received* 15 *December* 1958)

Abstract—Experimental frequency-response results and their interpretation by the diffusion equation lead to a correlation of liquid mixing with operating conditions for large-scale bubble-cap and sieve plates, in terms of a modified Péclet number and the liquid hold-up and froth density. Other mixing concepts are critically discussed. A simple method of predicting the effect of liquid mixing on plate efficiency is proposed, assuming complete mixing of the vapour between plates.

Résumé—Les résultats expérimentaux fréquence-réponse et leur interprétation par l'équation de diffusion conduisent à une relation entre le mélange liquide et les conditions d'opération pour les barbotteurs à champignons et les plateaux perforés à grande échelle en fonction du nombre de Péclet modifié, de la retention liquide et de la densité de la mousse. L'auteur discute et critique d'autres concepts du mélangeage. Il propose une méthode simple pour prévoir l'influence du mélange liquide sur l'efficacité du plateau, en supposant un mélange complet de la vapeur entre les plateaux.

Zusammenfassung—Versuchsergebnisse des Frequenzganges und ihre Interpretation durch die Diffusionsgleichung führt zu einer Beziehung zwischen der Durchmischung der Flüssigkeit und den Arbeitsbedingungen von grossen Glocken-und Siebböden in Ausdrücken einer modifizierten Péclet-Zahl des flüssigen Inhalts und der Schaumdichte. Andere Vorstellungen über die Durchmischung werden kritisch diskutiert. Um die Wirkung der Durchmischung der Flüssigkeit auf den Bodenwirkungsgrad vorauszusagen, wird eine einfache Methode vorgeschlagen, bei der vollständige Durchmischung des Dampfes zwischen den Böden angenommen ist.

INTRODUCTION

ALTHOUGH methods have long been in use [1] for calculating the effect of vapour mixing on plate efficiency, the effect of longitudinal mixing in the liquid has been relatively neglected. In small laboratory columns perfect mixing can be assumed with negligible error; however, the effect of liquid mixing increases in importance with increasing path length, and only on very large plates is it justifiable to assume no mixing, as is usually done when calculating the vapour-mixing effect [1]. It has been shown [2] that on plates having a length of liquid path greater than about 5 ft, the liquid-mixing effect tends to become the more important.

The existence of the liquid-mixing effect has long been recognized [3], but the lack of a suitable quantitative mixing parameter prevented its experimental determination until recently [4, 5]. The need for such a parameter in a rigorous treatment of the non-steady state behaviour of distillation columns was the original reason for this investigation. In this paper a simple method is presented for characterizing liquid mixing on large plates in terms of an assumed eddy-diffusion mechanism, for predicting the value of the mixing parameter from the operating conditions, and for using this parameter to predict the true plate efficiency. Complete mixing of the vapour between plates is assumed.

THEORETICAL APPROACH

Most previous work on mixing on plates has aimed at a correlation of point and overall Murphree plate efficiencies in terms of a quantitative mixing parameter. Plates have been regarded

*Present Address: Imperial Chemical Industries Ltd., Dyestuffs Division, Division Engineering Department, Dalton Works, Huddersfield, Yorks.

as consisting of a number of perfectly mixed stages [2] which has been related to the point and overall efficiencies, but which has not been related experimentally to the plate size or the operating conditions. Data which are based on column overall-efficiency determinations and correlation with point efficiencies calculated from relative volatility [6], indicate that for liquid paths less than about 10 ft the equivalent number of perfectly mixed stages is roughly equal to the number of feet. Some step-response experiments performed with a single row of bubble caps [7], however, indicate that the number of stages is approximately equal to the number of caps – or rows of caps – traversed by the liquid.

Other mixing parameters have been defined [8, 9] as functions of the concentration jump at the inlet weir. Their experimental determination, unfortunately, depends on concentration samples taken from the unstable "entrance length" of the plate close to the inlet weir; their use in relating overall plate efficiency to point efficiency is discussed by CROZIER [10].

Dispersion on bubble-cap and sieve plates is more realistically treated as a continuous-flow phenomenon. In recent years considerable thought has been given to longitudinal dispersion in continuous-flow systems [11, 12, 13, 14, 15], specifically in pipes [16, 17], in fluidized beds [18], in packed beds [19, 20, 21, 22, 23, 24, 25, 26] and in reactors [27, 28].

Several workers under GILLILAND at the Massachusetts Institute of Technology have supposed liquid mixing on bubble-cap and sieve plates to take place by an eddy-diffusion mechanism. Longitudinal eddy-diffusion coefficients have been measured over a limited range of operating conditions [29] and a relation between point-and overall Murphree plate efficiencies has been developed [30] in terms of an eddy diffusivity. Similar relations have also been derived elsewhere [31, 32, 33].

More recently, in a significant contribution by Foss [4, 5], liquid mixing and its effect on plate efficiency have been characterized in terms of liquid residence-time distribution functions based on the response to step changes in concentration of a tracer. The residence-time distribution approach yields the maximum useful information about continuous-flow systems, and can be used even when channelling and by-passing occur; it is considerably more complicated than the assumption of an eddy-diffusion mechanism. If the mixing can be shown to obey the diffusion equation, this simplifies both the experiments and the interpretation and subsequent use of the results.

The diffusion model is likely to be adequate so long as the turbulent intensity is uniform and as long as no channelling or stagnation of liquid occurs on the plate. It would be expected to break down where the eddies are comparable in scale with the vessel in which they are formed. On a distillation plate of conventional design it can be assumed that the eddies are small compared with the vessel dimensions and that no concentration gradient exists in a direction perpendicular to that of liquid flow. The effects of velocity and concentration gradients resulting from the changing cross-sectional area perpendicular to the direction of flow on circular plates are unlikely to be significant: the mean width differs very little from the width of the weirs.

In the present work it was therefore decided to assume a diffusion model and to use frequency response, which, of the possible methods of dynamic analysis, is in some ways the most attractive [34, 35]. It has been shown by KRAMERS *et al.* [12] that a characteristic mixing parameter can be determined for a continuous-flow system by comparison of the experimental and theoretical frequency responses, provided it is valid to assume that the mixing process can be represented mathematically by a combination of piston flow and longitudinal diffusion.

THEORETICAL FREQUENCY RESPONSE

From the unsteady-state material balance in time dt about an element of length ds of unit cross-sectional area, assuming a constant longtudinal diffusivity D, it follows that:

$$\frac{\partial^2 c}{\partial s^2} - \frac{u}{D} \cdot \frac{\partial c}{\partial s} \cdot - \frac{1}{D} \cdot \frac{\partial c}{\partial t} = 0 \qquad (1)$$

The transfer function of exit, with respect to inlet concentrations for this system, is derived

VOL. 10 1959

and its significance explained elsewhere [12]. If the concentration vectors measured are those upstream of the inlet (X_i) and at a point distance s from the inlet (X_s)' where

$$s = a\Sigma,$$

the transfer function can be shown to become:

$$\frac{X_s}{X_i} = \frac{(p+1)\exp az\left[p\,(2/a-1)+1\right] + (p-1)\exp az\,(p+1)}{\frac{1}{2}[(p+1)^2\exp 2zp - (p-1)^2]} \qquad (2)$$

$$\text{where } p = \left[1 + \frac{4\pi i}{(P/T)\,.\,z}\right]^{\frac{1}{2}}$$

$$\text{and} \quad z = \frac{u\Sigma}{2D}.$$

This was solved for attenuations with the aid of a digital computer, and the computed curves are shown in Figs. 2 and 3. The quantity "z," which is a measure of the departure from perfect mixing, can be regarded as the ratio of the diffusion time-constant, or mixing time, to the mean residence time. It can be shown [12] that it is numerically approximately equal to the number of equivalent perfectly mixed stages (when this exceeds five) and is thus analogous to the number of transfer units.

The dimensionless group $u\Sigma/D$ is a form of modified Péclet number.

Apparatus

Several requirements were recognized:

(a) The plates should be typical of full-scale plant, but a rectangular design facilitates interpretation of the results.

(b) A tracer is necessary for following concentration changes. It should be well dispersed on reaching the inlet weir, where uniform lateral distribution is required. It was decided to use electrical conductivity as an inferential measure of concentration because of its convenience and the ease with which it can be measured continuously. Sodium thiosulphate was selected as the tracer: its resistivity is nearly linear with concentration over the range used, and it was readily available.

(c) The boundary conditions must correspond to those assumed in the theoretical treatment, but both upstream- and downstream measurements should be made using cells of identical design to enable measuring lags to be neglected, since these are not always small compared with the residence time of the liquid on the plate. This can be achieved by building both cells into the plate. The down-stream cell then replaces a cap or a number of perforations; the upstream cell, however, is required to sample the solution from above the inlet weir, with which it must therefore be supplied to the exclusion of the surrounding froth.

(d) The sampling time-lag should be reduced to a minimum consistent with the necessity for deaeration prior to the continuous measurement of conductivity. This lag places a lower limit on the liquid residence-time on the plate, which should be greater than the cell time-constant. Conversely, as was found later, a lower limit of liquid-flow rate is reached when the output signal is masked to such an extent by "noise" as to be unrecognizable as a sine wave. The velocities of the large-scale eddies are then presumed to have become comparable in magnitude with the mean liquid velocity, the flow being no longer predominantly in one direction but becoming increasingly random as the mean velocity tends to zero.

Fig. 1 is the flow diagram. The plates are rectangular sections 1 ft wide and of 3 ft active length. Mains water mixes in the downcomer with a slow stream of concentrated sodium thiosulphate solution, the flow rate of which is modulated sinusoidally by applying a sinusoidally-changing air pressure through a valve positioner to a control valve. The amplitude, mean point and frequency of the oscillations are adjustable.

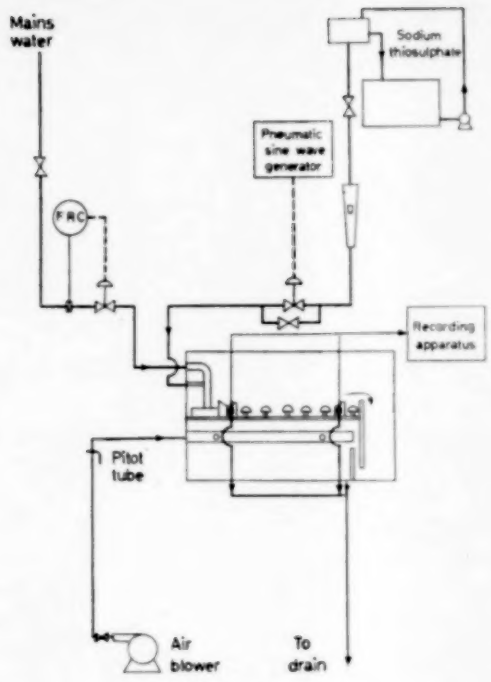

FIG. 1. Flow diagram.

Stirrers in the inlet weir box reduce segregation to a minimum before the solution crosses the weir onto the plate. A small quantity is continuously diverted from the weir through a cell containing two platinum electrodes. A similar conductivity cell is placed centrally at a convenient point downstream about three-quarters of the way towards the end of the active bed. Several sampling arrangements were tried before a satisfactory system was found. Both cells are connected to a fast and sensitive strip-chart galvanometer-recorder which also supplies a high-frequency excitation voltage to the electrodes, thus precluding polarization.

The layout of both plates is conventional: 7 rows, consisting alternately of 2 and 3 slotted caps, 3 in. diameter, mounted with a skirt height of $\frac{7}{16}$ in. on 2 in. diameter risers on an equilateral pitch of $4\frac{1}{4}$ in. The sieve plate has 41 rows consisting alternately of 14 and 15 holes $\frac{3}{16}$ in. diameter drilled in $\frac{1}{4}$ in. thick perspex on an equilateral pitch of $\frac{3}{4}$ in. Both plates are installed in a tank with perspex walls which enable visual tests to be made with traces of dye to ensure that all dead space has been eliminated over the range of liquid velocities used, and that interference of the cells with the flow pattern on the plate is negligible.

EXPERIMENTAL PROCEDURE AND RESULTS

Experiments with both plates were done at water flow rates of approximately 80–320 ft^3/hr. ft width, superficial air velocities between $1\frac{1}{2}$ and 3 ft/sec, and weir heights between 1 and 4 in. For every combination of weir height and liquid rate a series of frequency responses was recorded for each of two gas rates.

Owing chiefly to the large magnitude of the phase lags involved (many cycles long), it was found to be more accurate and more convenient to measure only the attenuations, the amplitude being taken to be the average value for a number of oscillations. The flow rates through the cells were equalized and adjusted to prevent air bubbles from being drawn down through the electrodes.

It was found to be important to know accurately the residence time of the clear liquid on the plate. In a separate series of experiments this was determined for each set of operating conditions by simultaneously shutting off the water supply and blocking the exit weir, thus trapping the froth on the plate, and then collecting and measuring the volume of the clear water (still supported by the gas) by draining the plate through the holes left after removal of the samplers. Loss by spray and leakage were reduced to an acceptable minimum. Pressure probes were believed to be subject to large errors and were not used to measure clear-liquid depths. At the same time it was found that froth heights could also be measured with consistency and this was done for each combination of operating conditions.

Calculations of mean liquid velocity and residence time are based on the volume of clear liquid on the plate. To show the dependence of this quantity on the gas-and liquid rates and the weir height (which for the purpose of this paper will be referred to hereafter as the operating conditions), an aeration factor "f_a" (defined here as the ratio of "h," the clear liquid height after collapse of the foam, to "$h_w + h^*$," the sum of the weir height and crest over the weir as deduced from the Francis formula) is plotted in Figs. 4 and 5 against liquid rate for different combinations of weir height and gas rate (expressed as a superficial air velocity). The ratio f_a is in fact the ratio of the depth of liquid after collapse of the foam to the depth which the liquid would attain when flowing across the plate at the same flow rate in the absence of aeration.

The results derived from the bubble-cap and sieve plate runs are given in Tables 1 and 2. The value of the quantity "z" for a given run is that corresponding to the best curve through the experimental attenuations, which are superimposed for interpolation on graphs (Figs. 2 and 3) computed from equation (2), with "a" equal to 0·81.

Tables 1 *and* 2. *Experimental results.*

Weir height	*Superficial gas velocity*	*Liquid rate*	*Clear-liquid height*	*Froth height*	*Mean residence time*	*Mean velocity*		*Eddy diffusivity*	*Froth "density"*			*Run no.*
h_w'		—	h	h_f	T	u	z	$D = \frac{u\Sigma}{2z}$	$= \phi \frac{h}{h_f}$	ϕu	$\frac{2D}{u^3 h}$	
in.	ft/sec	ft³/hr	cm	cm	sec	cm/sec		cm²/sec		g/sec cm²	cm²/sec²	
			Bubble-cap plate $w = 34{\cdot}3$ cm, $\Sigma = 89{\cdot}0$ cm									
1·69	1·4	320	6·50	11·4	6·05	14·7	6·5	101	0·57	8·40	0·0097	B1
	2·8	320	6·18	12·4	5·65	15·7	6·0	117	0·50	7·85	0·0097	B2
2¼	1·4	320	7·53	11·4	7·3	12·2	6·5	84	0·66	8·05	0·0121	B3
	2·8	320	7·43	12·7	7·15	12·4	6·0	92	0·59	7·25	0·0129	B4
2¾	1·4	80	6·55	10·1	24·5	3·62	7·0	23	0·65	2·34	0·1480	B5
		160	7·28	11·4	14·0	6·35	8·5	33	0·65	4·10	0·0352	B6
		240	8·00	12·1	10·4	8·60	8·5	45	0·66	5·65	0·0180	B7
		320	8·40	12·7	8·3	10·7	9·0	53	0·66	7·05	0·0103	B8
3¼	1·4	80	7·15	11·4	27·3	3·24	5·0	29	0·63	2·03	0·2370	B9
		160	8·00	12·4	15·7	5·60	8·0	31	0·65	3·61	0·0444	B10
		320	9·20	14·0	9·3	9·50	7·0	61	0·66	6·20	0·0154	B11
	2·8	80	6·60	12·1	24·7	3·60	6·5	25	0·55	1·97	0·1560	B12
		160	7·30	14·0	14·0	6·30	8·5	33	0·52	3·28	0·0360	B13
		320	8·55	15·2	8·5	10·4	7·5	62	0·56	5·80	0·0127	B14
3¾	1·4	160	8·55	14·0	17·0	5·22	7·0	33	0·61	3·16	0·0543	B15
		320	9·70	15·9	10·0	8·90	7·0	57	0·61	5·43	0·0166	B16
	2·8	160	8·00	14·9	15·8	5·60	8·0	31	0·54	3·02	0·0445	B17
		320	9·00	16·5	9·1	9·80	9·0	49	0·55	5·34	0·0115	B18
			Sieve plate $w = 29{\cdot}2$ cm, $\Sigma = 77{\cdot}5$ cm									
1	1·9	80	2·07	5·7	7·45	10·4	16	25·3	0·364	3·78	0·0217	S1
	3·8	80	1·89	6·35	6·82	11·4	8	55·5	0·297	3·38	0·0398	S4
2	1·9	80	2·77	8·9	10·0	7·8	11	27·6	0·311	2·44	0·0418	S7
		160	3·15	10·2	5·64	13·8	10	53·5	0·309	4·25	0·0130	S8
	3·8	80	2·40	9·2	8·73	8·9	7	49·5	0·261	2·32	0·0584	S10
		160	2·67	10·8	4·80	16·2	6	105	0·247	4·00	0·0185	S11

Tables 1 *and* 2. *Experimental results.*

Weir height	*Superficial gas velocity*	*Liquid rate*	*Clear-liquid height*	*Froth height*	*Mean residence time*	*Mean velocity*		*Eddy diffusivity*	*Froth "density"*			*Run no.*
h_w'		—	h	h_f	T	u	z	$D = \frac{u\Sigma}{2z}$	$= \phi \frac{h}{h_f}$	ϕu	$\frac{2D}{u^3 h}$	
in.	ft/sec	ft³/hr	cm	cm	sec	cm/sec		cm²/sec		g/sec cm²	cm²/sec²	
			Bubble-cap plate $w = 34{\cdot}3$ cm, $\Sigma = 89{\cdot}0$ cm									
1·69	1·4	320	6·50	11·4	6·05	14·7	6·5	101	0·57	8·40	0·0097	B1
	2·8	320	6·18	12·4	5·65	15·7	6·0	117	0·50	7·85	0·0097	B2
2¼	1·4	320	7·53	11·4	7·3	12·2	6·5	84	0·66	8·05	0·0121	B3
	2·8	320	7·43	12·7	7·15	12·4	6·0	92	0·59	7·25	0·0129	B4
2¾	1·4	80	6·55	10·1	24·5	3·62	7·0	23	0·65	2·34	0·1480	B5
		160	7·28	11·4	14·0	6·35	8·5	33	0·65	4·10	0·0352	B6
		240	8·00	12·1	10·4	8·60	8·5	45	0·66	5·65	0·0180	B7
		320	8·40	12·7	8·3	10·7	9·0	53	0·66	7·05	0·0103	B8
3¼	1·4	80	7·15	11·4	27·3	3·24	5·0	29	0·63	2·03	0·2370	B9
		160	8·00	12·4	15·7	5·60	8·0	31	0·65	3·61	0·0444	B10
		320	9·20	14·0	9·3	9·50	7·0	61	0·66	6·20	0·0154	B11
	2·8	80	6·60	12·1	24·7	3·60	6·5	25	0·55	1·97	0·1560	B12
		160	7·30	14·0	14·0	6·30	8·5	33	0·52	3·28	0·0360	B13
		320	8·55	15·2	8·5	10·4	7·5	62	0·56	5·80	0·0127	B14
3¾	1·4	160	8·55	14·0	17·0	5·22	7·0	33	0·61	3·16	0·0545	B15
		320	9·70	15·9	10·0	8·90	7·0	57	0·61	5·43	0·0166	B16
	2·8	160	8·00	14·9	15·8	5·60	8·0	31	0·54	3·02	0·0445	B17
		320	9·00	16·5	9·1	9·80	9·0	49	0·55	5·34	0·0115	B18
			Sieve plate $w = 29{\cdot}2$ cm, $\Sigma = 77{\cdot}5$ cm									
1	1·9	80	2·07	5·7	7·45	10·4	16	25·3	0·364	3·78	0·0217	S1
	3·8	80	1·89	6·35	6·82	11·4	8	55·5	0·297	3·38	0·0398	S4
2	1·9	80	2·77	8·9	10·0	7·8	11	27·6	0·311	2·44	0·0418	S7
		160	3·15	10·2	5·64	13·8	10	53·5	0·309	4·25	0·0130	S8
	3·8	80	2·40	9·2	8·73	8·9	7	49·5	0·261	2·32	0·0584	S10
		160	2·67	10·8	4·80	16·2	6	105	0·247	4·00	0·0185	S11

The results are plotted as normalized attenuations, obtained by dividing the attenuation or amplitude ratio at any period by that at infinite period.

The results are correlated as a plot of $2D/u^3 h$ against uh/h_f as proposed by Foss [4, 5] whose results, which also followed the diffusion law, were obtained by determining the residence-time distributions of liquid on sieve trays. For comparison, the best line through Foss' results is reproduced alongside the author's results in Fig. 6.

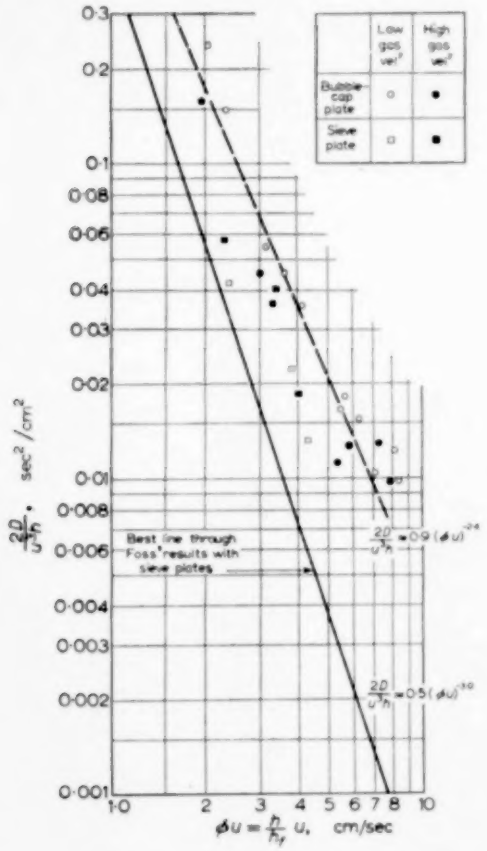

FIG. 6. Correlation of results.

DISCUSSION

That the observed aeration factors for the sieve tray are lower than those for the bubble-cap tray, indicating greater aeration on the sieve tray, is attributed to more effective dispersal of the air on the sieve tray and also to the inclusion of the unaerated layer in the calculation of aeration on the bubble-cap tray.

The difference between the bubble-cap and sieve plate lines in Fig. 6 may be due to differences in turbulent mechanism and scale and the stratification into aerated- and unaerated layers on the bubble-cap plate, resulting in higher mean froth densities. No obvious explanation suggests itself of the slight deviation of the plotted sieve-plate points from the best line through Foss' results. The lines fit the equation:

$$\frac{2D}{u^3 h} = c_1 (\phi u)^{-c_2} \tag{3}$$

where $c_1 \approx 0{\cdot}9$, $c_2 \approx 2{\cdot}4$ for the author's bubble-cap plate and $c_1 \approx 0{\cdot}5$, $c_2 \approx 3{\cdot}0$ for Foss' sieve plate. "ϕ" is the ratio h/h_f and will be referred to as the froth "density."

Hence, over the range of operating conditions investigated, for the author's bubble-cap plate:

$$\frac{D}{uh} = 0{\cdot}9 \left(\frac{h_f}{h}\right)^{2{\cdot}4} \cdot \left(\frac{1}{u}\right)^{0{\cdot}4} \tag{4}$$

and for Foss' sieve plate

$$\frac{D}{uh} = 0{\cdot}25 \left(\frac{h_f}{h}\right)^{3} \cdot \frac{1}{u} \tag{5}$$

The group uh/D is another form of the Péclet number, with "h" as the characteristic linear dimension. It is not possible to write complete dimensionless equations because the relevant physical properties of the liquid such as density and viscosity were not varied in either set of experiments. It may be noted that Foss found D to be independent of u, and that in the present experiments with the bubble-cap plate it varied only as the 0·6 power of u. The effect of gas velocity on the diffusivity appears to manifest itself only in so far as it affects the froth "density" (h/h_f). The underlying physical mechanism responsible for longitudinal mixing is not yet clearly understood.

EFFECT ON PLATE EFFIENCY

It will be assumed that the Murphree point efficiency, defined by:

$$\eta = \frac{y - Y}{y^* - Y} = \frac{y_e - Y}{y_e^* - Y}$$

is constant over the plate, that the composition

of vapour entering a plate is constant over the column cross-section, that the equilibrium curve is a straight line over the concentration range involved, i.e.

$$y^* = y_e + kx$$

$$\text{and } y_e^* = y_e + kx_e,$$

that the molar volume $1/\rho$, where $c = \rho x$, and the clear-liquid height, "h," are constant over the plate, and that liquid mixing can be characterized by an eddy diffusivity. For convenience, the following equations are derived in terms of "h" and "ρ," the height and density of clear liquid, rather than the height and density of the froth. The products $h\rho'$ and $h_f \phi \rho'$, where $\phi = h/h_f$, represent liquid loading and are equal.

Making the above assumptions, a steady-state material balance on an element of thickness ds at distance s from the inlet gives:

$$\frac{d^2x}{ds^2} - \frac{L}{h\rho D}\cdot\frac{dx}{ds} = \frac{G\eta kx}{h\rho D} = \frac{G\eta (y_e - Y)}{h\rho D} \qquad (6)$$

The boundary conditions, the same as those assumed in deducing equation (2), are as follows [11, 36]:

$$\frac{dx}{ds} = \frac{L}{h\rho D}(x - x_i); \quad s = 0. \qquad (7)$$

$$\frac{dx}{ds} = 0; \quad s = \Sigma. \qquad (8)$$

By a mass balance over the whole plate:

$$y_{av} = Y + \frac{L}{G\Sigma}(x_i - x_e) \qquad (9)$$

and by solving for the arbitrary constants in the general solution of equation (6) it can be shown [30, 32] that the ratio of the Murphree overall vapour-phase plate efficiency to the point efficiency is given by:

$$\frac{\eta_{plate}}{\eta} = \frac{1}{4p'\beta\eta}\{(1+p')^2 \exp -z(1-p') - (1-p')^2 \exp -z(1+p') - 4p'.\} \qquad (10)$$

where $p' = \left(1 + \frac{4\beta\eta}{\alpha\Sigma}\right)^{\frac{1}{2}}$

and $\alpha\Sigma$ (the modified Péclet number) $= 2z$.

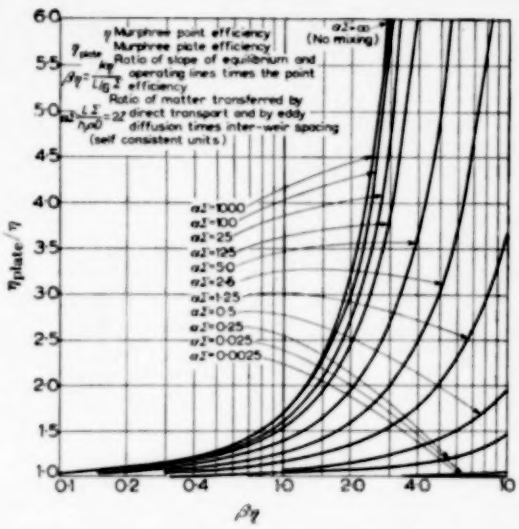

FIG. 7. Correlation of Murphree plate vs. point efficiences. ((The graph is due to S. P. S. Andrews and R. W. Mackay, I.C.I. Ltd., Billingham Division).

Fig. 7 was constructed from equation (10). When $D \to 0$, this expression for the efficiency ratio reduces to the LEWIS [1] equation:

$$\frac{\eta_{plate}}{\eta} = \frac{\exp \beta\eta - 1}{\beta\eta}; \qquad (11)$$

it reduces to unity when $D \to \infty$.

The Murphree overall liquid-phase plate efficiency can similarly be related to point efficiency, which can be calculated from physical data and the operating conditions [30].

Once "β" is known, it should be possible, therefore, to predict the overall plate efficiency from Fig. 7 by the following procedure: ϕu is estimated from the operating conditions and plate dimensions using the graphs of aeration factors of Figs. 2 and 3 to obtain "h" and hence "u." The relation due to CROZIER [10]:

$$-\ln \phi = 0{\cdot}715\, v\sqrt{\rho_g} + 0{\cdot}45 \qquad (12)$$

which implies dependence on gas rate only, can be used to predict an approximate value of "ϕ." u/D which determines the value of the parameter $\alpha\Sigma$ in Fig. 7, is now obtained from Fig. 6 for either a bubble-cap or sieve plate. This

graph is valid provided the operating conditions do not necessitate extrapolation to $\phi u > 12$ or $\phi u < 1$.

No conclusive tests of this proposed calculation have been possible with data reported for experimental plates. It is intended to apply it to large plates working under typical conditions with binary systems in which both vapour- and liquid-phase resistances are important.

Conclusions

(a) Assuming a diffusion mechanism, and using frequency response, a relation has been obtained from which the value of a mixing parameter (a modified Péclet number, which represents the ratio of the transfer rates due to bulk flow and to diffusion) can be predicted from the operating conditions on bubble-cap and sieve plates. The mechanism of the dispersion process is not understood, but longitudinal eddy-diffusivity has been correlated with liquid velocity, liquid hold-up and froth "density," which have themselves been related to operating conditions over a range typical of industrial practice.

(b) Gas rate has no significant effect on the mixing parameter distinct from its effect on froth "density" and on hold-up.

(c) Values of longitudinal eddy-diffusivity vary between 25 and about 120 cm²/sec, over the range of operating conditions investigated on both plates.

(d) The overall Murphree plate efficiency for a binary mixture can be related to the point efficiency through the modified Péclet number. The effect of longitudinal liquid mixing on the overall efficiency can therefore be calculated given the relevant physical properties of the components, the plate dimensions and the operating conditions. The effect increases in importance with increasing length of liquid path.

(e) It is suggested that for the more common organic and inorganic distillates the density, viscosity and surface tension of the liquid and vapour are likely to be of only secondary importance compared with the operating conditions and that the relations found here for water can be expected to hold for other liquids.

(f) It is probable that, as Foss' relation for sieve plates was found to be independent of hole spacing, so the relation found here will hold for different designs of bubble-cap plate.

Acknowledgements—Thanks are due to Mr. A. J. Young, Head of the Central Instrument Laboratory, Imperial Chemical Industries Ltd., to Mr. J. McMillan for his advice throughout this work, to Professor Danckwerts for his advice in the interpretation of the results, to Mr. F. P. Lees, who carried out the experiments and many of the calculations, and to others who helped in many ways. Figure 7 was computed at I.C.I. Billingham Division, where the author is also indebted for discussions with Mr. S. P. S. Andrew and Mr. R. W. Mackay in the early stages of the work.

Notation

$a = s/\Sigma$

c = deviation of a sinusoidal signal of tracer concentration from its mean value (g mol/cm³)
$= Xe^{i\omega t}$

c_1, c_2 = constants in the correlation of u, D, h and ϕ

D = longitudinal eddy diffusivity in the liquid (cm²/sec)

D_g = eddy diffusivity in the vertical plane due to gas bubbles

f_a = aeration factor
$= \dfrac{h}{h_w + h^*}$

G = vapour flow rate per unit area of plate (g mol/sec cm² plate area)

g = liquid flow rate per unit weir width (ft³/hr. ft weir width)

h = clear-liquid height (after collapse of froth) (cm)
$= V/w\,\Sigma$

h_f = height of froth

h_w = weir height (cm)

h_w' = weir height (in)

h^* = crest over weir (cm)
$= 0{\cdot}0585\ g^{0{\cdot}67}$

$i = \sqrt{-1}$

k = slope of vapour–liquid equilibrium line

L = liquid flow rate per unit weir width (g mol/sec cm weir width)

P = forcing period (sec)

$$p = \left(1 + \frac{4\pi i T/P}{z}\right)^{\frac{1}{2}}$$

$$p' = \left(1 + \frac{4\beta\eta}{\alpha\Sigma}\right)^{\frac{1}{2}}$$

Q = liquid volume flow rate (cm³/sec)

s = distance along plate from inlet weir or first cell (cm)

T = mean liquid residence time (sec)
$= V/Q$

t = time

u = mean liquid velocity (cm/sec)
$= \Sigma/T$
V = clear-liquid volume hold-up (cm^3)
v = superficial air velocity, based on total area between weirs (ft/sec)
w = plate width (cm)
X = complex concentration vector
x = mol fraction in the liquid of the more volatile component of a binary mixture
Y = mol fraction—in the vapour entering the plate—of the more volatile component
y = mol fraction—in the vapour leaving the plate—of the more volatile component
y^* = value of y for vapour in equilibrium with liquid of composition x
$z = u\Sigma/2D = \alpha\Sigma/2$
$\alpha = L/h\rho\ D = u/D\ (cm^{-1})$
β = ratio of slopes of equilibrium and operating lines
$= \dfrac{k}{L/G\Sigma}$

η = vapour-phase Murphree point efficiency
$= \dfrac{y - Y}{y^* - Y} = \dfrac{y_e - Y}{y_e^* - Y}$
η_{plate} = overall vapour-phase Murphree plate efficiency
$= \dfrac{y_{av} - Y}{y_e^* - Y}$
ρ = molar density of unaerated binary mixture (g mol/cm^3)
ρ_g = vapour density (lb/ft^3)
Σ = total effective plate length (cm)
σ^2 = variance of the distribution curve about its mean (sec^2)
$= 2Ds/u^3$
$\phi = h/h_f$ (air-water froth "density")
$\omega/2\pi$ = frequency (c/s)
$= 1/P$

Subscripts
e = exit (when $s = \Sigma$)
i = inlet (upstream of the weir, not when $s = 0$)

VOL. 10 1959

REFERENCES

[1] LEWIS W. K. *Industr. Engng. Chem.* 1936 **28** 399.
[2] GAUTREAUX M. F. and O'CONNELL H. E. *Chem. Engng. Progr.* 1955 **51** 232
[3] MACMULLIN R. B. and WEBER M. *Trans. Amer. Inst. Chem. Engrs.* 1935 **31** 409.
[4] FOSS A. S. Ph.D. Thesis, University of Delaware 1957.
[5] FOSS A. S. GERSTER J. A. and PIGFORD R. L. *Amer. Inst. Chem. Engrs. J.* 1958 **4** 231.
[6] O'CONNELL H. E. *Trans. Amer. Inst. Chem. Engrs.* 1946 **42** 741.
[7] ARMSTRONG W. D. University of Cambridge, personal communication, Oct. 1957.
[8] OLIVER E. D. and WATSON C. C. *Amer. Inst. Chem. Engrs. J.* 1956 **2** 18.
[9] WARZEL L. A. Ph.D.Thesis, University of Michigan 1955.
[10] CROZIER R. D. Ph.D. Thesis, University of Michigan 1956.
[11] DANCKWERTS P. V. *Chem. Engng. Sci.* 1953 **2** 1.
[12] KRAMERS H. and ALBERDA G. *Chem. Engng. Sci.* 1953 **2** 173.
[13] LEVENSPIEL O. and SMITH W. K. *Chem. Engng. Sci.* 1957 **6** 227.
[14] VAN DER LAAN E. T. *Chem. Engng. Sci.* 1958 **7** 187.
[15] LEVENSPIEL O. *Industr. Engng. Chem.* 1958 **50** 343.
[16] TAYLOR G. I. *Proc. Roy. Soc.* 1954 **A223** 446.
[17] TICHACEK L. J. *et al. Amer. Inst. Chem. Engrs. J.* 1957 **3** 439.
[18] GILLILAND E. R. and MASON E. A. *Industr. Engng. Chem.* 1949 **41** 1191.
[19] BERNARD R. A. and WILHELM R. H. *Chem. Engng. Progr.* 1950 **46** 233.
[20] DEISLER P. F. and WILHELM R. H. *Industr. Engng. Chem.* 1953 **45** 1219.
[21] MCHENRY K. W. and WILHELM R. H. *Amer. Inst. Chem. Engrs. J.* 1957 **3** 83.
[22] ARIS R. and AMUNDSON N. R. *Amer. Inst. Chem. Engrs. J.* 1957. **3** 280.
[23] EBACH E. A. Ph.D. Thesis, University of Michigan, 1957.
[24] EBACH E. A. and WHITE R. R. *Amer. Inst. Chem. Engrs. J.* 1958 **4** 161.
[25] STRANG D. A. and GEANKOPLIS C. J. *Industr. Engng. Chem.* 1958 **50** 1305.
[26] TURNER G. A. *Chem. Engng. Sci.* 1958 **7** 156.

[27] Wilhelm R. H. *Chem. Engng. Progr.* 1953 **49** 150.

[28] Danckwerts P. V. *Chem. Engng. Sci.* 1958 **8** 93.

[29] Wharton L. B.S. Thesis, Massachusetts Institute of Technology 1955.

[30] Anderson J. E. Sc.D. Thesis, Massachusetts Institute of Technology 1954.

[31] Ruckenstein E. *Commun. Acad. Rep. Pop. Romine (Fiz)* 1956 **6** 1085.

[32] Ruckenstein E. *Zh. prikl. Khim.* 1957 **30** 1012.

[33] Hutchinson R. C. Mackay R. W. and Andrew S. P. S. I.C.I. Billingham Division, 1957, (unpublished).

[34] McMillan J. *Trans. Inst. Chem. Engrs.* 1955 **33** 168.

[35] Young A. J. *An Introduction to Process Control System Design.* Longmans, London 1956.

[36] Wehner J. F. and Wilhelm R. H. *Chem. Engng. Sci.* 1956 **6** 89.

Chemical Engineering Science, 1959, Vol. 10, pp. 254 to 267. Pergamon Press Ltd. London. Printed in Great Britain

The performance of rotary concentric cylinder fractionating columns—1

N. MACLEOD* and K. J. MATTERSON†
Chemistry Department, University of Leicester

(*Received* 16 *December* 1958)

Abstract—A type of laboratory fractionating column is described, consisting essentially of two concentric glass cylinders of which the inner one rotates. This apparatus is of general use in preparative work, giving an exceptionally low hold-up, pressure drop and H.E.T.P., and having no bearings or shaft seals in the working section. It also offers a convenient means of studying the general properties of film-type rectifying systems; it functions as a wetted-wall column in which the vapour flow regime may be changed in a predictable way without alteration of throughput by changing the form and speed of the rotor.

A technique is described for determining liquid and vapour side mass transfer resistances. In experiments at atmospheric pressure with a mixture of *n*-heptane and methyl cyclohexane it is shown that the separating power of the column is controlled by the vapour phase mass-transfer resistance, the liquid side resistance being negligible. Attempts are made to relate the overall column characteristics to the fluid mechanical properties of the vapour stream under various conditions of operation.

Résumé—Les auteurs décrivent une colonne à fractionner de laboratoire, formée essentiellement de deux cylindres de verre concentriques dont le cylindre intérieur tourne. Cet appareil peut être utilisé d'une façon générale pour les travaux pratiques car il donne une faible rétention, des pertes de charge et un H.E.T.P. très bas et qu'il n'a pas de palier ou joints de l'axe dans la section de travail. Il permet d'effectuer commodement l'étude des propriétés générales des systémes de rectification de type film. Il fonctionne comme une colonne à paroi mouillée dans laquelle le régime d'écoulement de la vapeur peut être modifié de façon prévisible sans altération de débit, en changeant la forme et la vitesse du rotor. Les auteurs donnent une technique de détermination des résistances de transfert de masse du liquide et de la vapeur. Pour les expériences à la pression atmosphérique avec un mélange de *n*-heptane et methyl cyclohexane, le pouvoir de séparation de la colonne est déterminé par la résistance de transfert de masse de la phase vapeur, la résistance du coté liquide étant négligeable. Les auteurs ont essayé de rattacher les caractéristiques globales de la colonne aux propriétés mécaniques du courant de vapeur sous diverses conditions d'opération.

Zusammenfassung—Es wird der Typ einer Laboratoriums-Fraktionierkolonne beschrieben, die hauptsächlich aus zwei konzentrischen Glaszylindern besteht, von denen der innere rotiert. Dieser Apparat ist im allgemeinen Gebrauch bei präparativen Arbeiten und gibt einen besonders geringen Flüssigkeitsinhalt, Druckabfall und H.E.T.P.; er hat weder Lager noch Wellendichtungen im Arbeitsteil. Man kann mit ihm bequem das allgemeine Verhalten von Rektifiziersystemen vom Filmtyp studieren; er arbeitet als Kolonne mit benetzter Wand, bei der man die Dampfströmung in definierter Weise bei gleichem Durchsatz verändern kann durch Veränderung von Form und Geschwindigkeit des Rotors.

Zur Bestimmung der Stoffübergangswiderstände auf der Flüssigkeits- und Dampfseite wird eine Versuchstechnik beschrieben. In Versuchen bei Atmosphärendruck mit einer Mischung von *n*-Heptan und Methylcyclohexan wird gezeigt, dass die Trennwirkung der Kolonne durch den Übertragungswiderstand auf der Dampfseite bestimmt wird, während der flüssigkeitsseitige Widerstand vernachlässigt werden kann. Es wird versucht, zwischen dem gesamten Verhalten der Kolonne und den Daten der Dampfströmung unter verschiedenen Arbeitsbedingungen eine Beziehung herzustellen.

*Present address: Chemical Engineering Laboratories, University of Edinburgh and Heriot Watt College, Edinburgh 1.
†Present address: Plessey Ltd., Northampton.

Introduction

In fractionating columns of the type discussed here the vapours from the stillpot are made to pass through the annular space between two vertical concentric cylinders, of which the inner cylinder rotates while the outer one is stationary. Reflux from a condenser at the column top returns as a falling film down the stationary outer wall, from which heat loss is as far as possible prevented by lagging and compensating heaters. This kind of column is of interest for two main reasons. First, in comparison with other columns of similar dimensions and throughput, the H.E.T.P., pressure drop and hold-up may be made small, so that the rotary concentric cylinder column promises to be of great practical use, particularly for low pressure batch operation. Second, this type of column is essentially a wetted wall system into which an additional degree of freedom is introduced by the presence of the rotor, whose effects, unlike those of a spinning band, for example, are sufficiently determinate for theoretical treatment. The rotor surface can be assumed to be dry under ordinary running conditions, for any reflux deposited on it from the condenser would quickly be thrown off by centrifugal force at the operating speeds used. It may therefore be supposed that mass transfer between the liquid and vapour phases in the rectifying section occurs at the relatively stable and well-defined surface of the film of reflux on the stationary outer wall of the annulus. Results obtained with such apparatus would thus be expected to throw light on some general aspects of the mass transfer processes occurring in wetted wall columns.

The first published account of a rotary concentric cylinder fractionating column was that of Willingham *et al.* [1], who described in 1947 an extensive series of trials with such an apparatus in the U.S. National Bureau of Standards. This machine was not designed for use as a practical still, but was well adapted for investigations of the rectifying properties of the rotary concentric cylinder system. In the course of this work it was found that the separating power increased as the rotor speed was raised; beyond a certain critical speed of rotation the rise in separating power was very abrupt. It was supposed that this critical speed corresponds to the onset of turbulence in the vapour, resulting in increased radial diffusion. If the resistance to mass transfer between the liquid and vapour phases is predominantly in the vapour phase, it would be expected that the sudden development of vapour turbulence would explain the observed sharp improvement in column performance at a critical speed of rotation.

It was found that the critical rotor speed corresponds to a Reynolds number for the vapour stream (based on annular thickness and mean vapour velocity) near that which would be expected to mark the transition between laminar and turbulent regimes for flow between flat plates;* i.e. assuming that the surfaces of the rotor and outer cylinder (radii approx. 3·7 cm and 3·8 cm respectively) can be treated as parallel planes. However, an attempt to calculate the H.E.T.P. of the column at various rotor speeds on this basis was not very successful [1].

Several papers describing rotary concentric cylinder fractionating columns have since appeared ([2], [3], [4], [5]) but no further serious attempt seems to have been made to elucidate the theory of operation. In particular, it has not been established to what extent the mass transfer resistance in the system studied by Willingham *et al.* resides in the vapour phase. Evidently this must be known before the influence of rotor speed on the performance of the column can be interpreted quantitatively in terms of the effect of the rotor on the vapour stream. Furthermore, the effect of the rotor on the character of the vapour flow has not been made clear. Whatever may be the criterion determining the transition to turbulence, it does not seem to have been pointed out that the motion of the annular vapour stream probably differs from the assumed Couette flow in at least one important respect; viz., that at rotor speeds well below that for the onset of general turbulence Taylor vortices [6] would be expected to be present. Inasmuch as these

*From [1], the critical value of $V_s b \rho/\eta$ found experimentally is about 3000.

Willingham *et al.* give the observed critical Reynolds number as 2500; they define Re as $0{\cdot}84 \times \frac{V_s b \rho}{\eta}$.

regular vortices would be expected to promote radial diffusion in the vapour one might expect their appearance to be marked by an abrupt improvement in column performance like that now ascribed to the onset of turbulence. No such low-speed effect is reported in the literature, however. There is thus some uncertainty about the relation between the fluid mechanics of these columns and their rectifying properties. In the present work an attempt has been made to throw some light on this.

The potential practical value of rotary concentric cylinder fractionating columns is evidently very great. The apparatus described by WILLINGHAM *et al.* was shown to give (at total reflux) an efficiency factor, defined [1] as:

$$\frac{\text{No. of plates per unit length} \times \text{Throughput}}{\text{Hold-up per unit length}}$$

of the order 10,000 plates/hr, several times greater than that for any type of column previously reported. In spite of this, little progress seems to have been made in adapting the pioneer machine for general preparative purposes. The original apparatus and all its variants so far described have a rotor bearing at the lower end of the working section, immediately above the still pot, fully exposed to the hot vapour stream and the returning reflux. Even when this is a plain journal bearing of inert material, as in the column of IRLIN and BRUNCE [2], its presence introduces lubrication difficulties at the relatively high rotor speeds required, and limits the range of substances which the column can handle.

In the work to be described, two rotary concentric cylinder fractionating columns were employed. One of these was designed primarily for experimental purposes; the other, a larger machine, was designed later for general preparative work on a laboratory scale. This apparatus has an all glass working section containing no exposed bearings or shaft seals, and has proved entirely suitable for general use as a laboratory column of exceptionally high separating power, low hold-up and low pressure drop.

EXPERIMENTAL

Figures 1 and 2 (a) show the general arrangement of the larger column, which will be referred to as Column 2. The rotor, R, is a Chance "Veridia" tube, specially selected by the makers for straightness and exterior uniformity, 2.6 cm nominal outside diameter and approximately 74 cm long. It is driven as shown in Fig. 2 (b) by means of a B.T.H. "canned" squirrel cage motor, the squirrel cage (an aluminium casting with copper inserts) being actuated through the

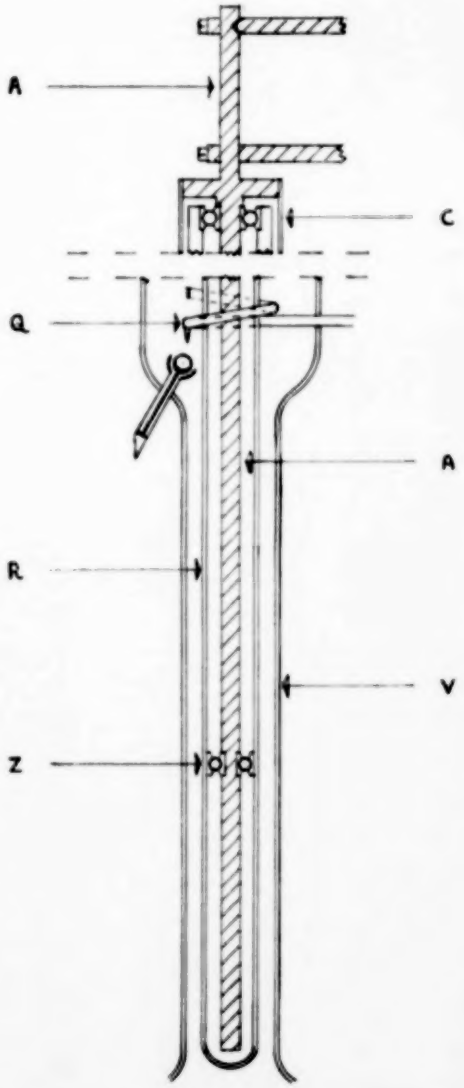

FIG. 1. Column 2. General mechanical arrangement. Schematic. Horizontal scale much distorted and enlarged.

VOL. 10 1959

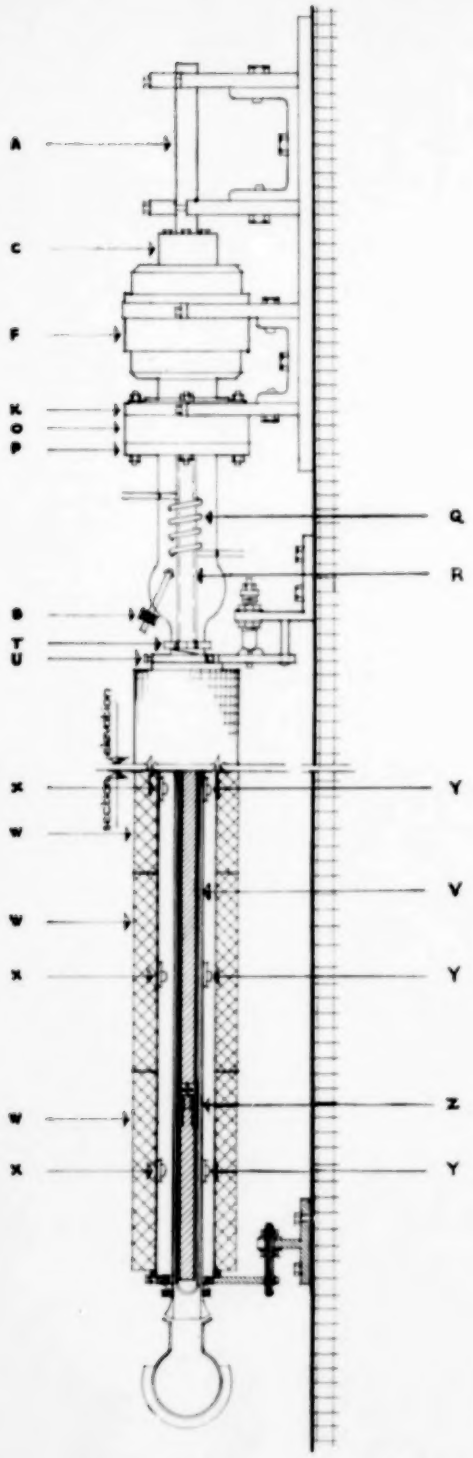

FIG. 2 (a). Column 2. Complete assembly. Approximately to scale.

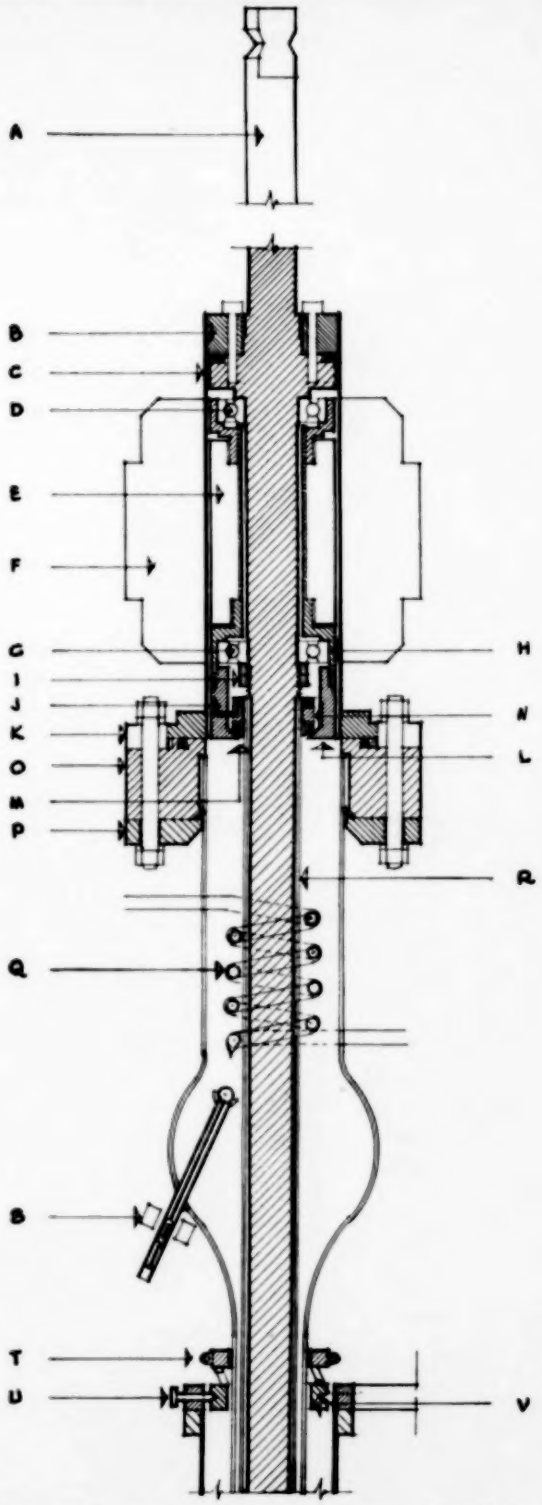

FIG. 2 (b). Column 2. Driving motor and condenser section.

thin stainless steel wall of the stationary housing, C, by the field of an external stator, F, supplied from the a.c. mains. The stainless steel housing is connected to the column proper by means of a vacuum tight system of flanges and O-rings, so that the column may be operated at reduced pressure.

The glass rotor and squirrel cage turn about a central fixed shaft, A, which extends downwards into the hollow closed rotor and is rigidly secured at its upper end in a massive wall clamp. The ball races of the squirrel cage serve as the upper bearings of the rotor; as these are located above the spiral water condenser they are relatively inaccessible to the column vapours.

The lower bearing, Z, is a ball race mounted on the stationary inner shaft, A, at a point determined by calculation, about two-thirds the length of the shaft below the wall-clamp. As the lower end of the tubular rotor is closed, this bearing is not exposed to the column vapours.

This arrangement in which the cylindrical rotor turns about an internal bearing on a fixed shaft overhung or cantilevered from the wall clamp above has, of course, a critical speed at which the motion becomes unstable. Fairly extensive preliminary work was carried out to determine the dynamical characteristics of this arrangement of rotor and cantilevered shaft; using data obtained in these investigations the apparatus was designed so that the normal operating speed of the motor, 1470 rev/min, is far above the critical, and the rotor runs without perceptible vibration.

The annular clearance between the rotor and the fixed precision-bore outer tube is about 0·1 cm and the annular rectifying section is 61 cm long. Since there are no bearings in the annular space to maintain this relatively small clearance between rotor and outer tube, or stator, these parts must be exactly located in their proper relation by the wall mountings. These demountable fixtures were made in accordance with Kinematic Design principles [8], and have the property that, once aligned, they allow of the ready dismantling and reassembly of the column without significant change of rotor-stator clearance. The mountings are also designed to allow of longitudinal thermal expansion of the column jacket without distortion or change of alignment.

Near adiabatic operation, important for high performance wetted wall columns in general, is ensured by the following automatic system. The rectifying section is enclosed by a tubular copper jacket, surrounding which are three sets of electrical heaters, W. The electrical input to these is controlled by relays operated by the out of balance current in a Wheatstone network, of which the ratio arms are connected in sequence by a motor-driven rotary switch with each of three pairs of matched thermistors mounted on the outer glass tube of the column and its copper jacket. When one of the thermistor pairs is unbalanced the current in the appropriate jacket heater is increased. Using this system the temperature difference across the air space between the column and jacket is found not to exceed 0·2°C, as measured by thermocouples located at the mid-points of the three heated sections.

The column is designed for intermittent take-off, and has a magnetically operated condensate valve, S, immediately below the condenser. In ordinary use the valve solenoid is energized periodically by a process timer. In the experiments to be described, however, the column was operated at total reflux and the valve was kept closed except when a condensate sample was required for analysis.

Still pot samples were withdrawn through a syphon of fine-bore glass tubing fitted by means of a ground glass joint to a side arm of the still pot flask.

The boil up rate was controlled manually by means of a variable transformer in the circuit of the still pot heating mantle. A boil-up rate meter [9] was interposed between the still pot and the column base, with which the flow rate of returning reflux could be measured to approximately $\pm$ 2·5 per cent.

The arrangements in the experiments with the smaller apparatus, Column 1, were substantially the same. The column dimensions were: rotor diameter 1·6 cm, annular clearance 0·1 cm, length of rectifying section, 60 cm*. This column was so designed that the rotor speed could be varied readily; the rotor was driven by a $\frac{1}{4}$ h.p. induction motor through a variable gear. The cantilevered shaft for this early column was designed before the mechanical data used in the construction of Column 2 were obtained, and it was found in operation that the desired range of working speeds lay close to the critical for the rotor-cantilever system. An additional constraint or guard bearing was therefore provided below the rotor at the base of the working section of the column. This took the form of a Teflon bush supported and centered in the outer tube by a glass spider ground to fit the bore; in a concentric hole drilled in the bush ran a short pivot of glass rod about 0·3 cm diameter, fused to the lower end of the rotor and ground concentric with the external surface. The annular clearance between pivot and bush was of the order 0·01–0·02 cm. This guard bearing or cheek ring, used in conjunction with the internal cantilevered bearing, gave little trouble at speeds up to 3000 rev/min, though exposed to the hot vapours and reflux in the rectifying section.

In experiments with Column 1 the rotor speed was measured by means of a stroboscopic lamp and checked by means of a mechanical tachometer having a friction

*A 45 cm rectifying section was used in some of the work at higher rotor speeds.

wheel which could be applied directly to the surface of the upper part of the rotor. For Column 2 the stroboscopic lamp alone was used.

In all experiments the test mixture contained approximately 20 mole per cent *n*-heptane, 80 mole per cent methyl cyclohexane. The component hydrocarbons, of the purest commercial grade, had the refractive index values given in [10]. Head and still pot samples from the column were analysed refractometrically at 20°C. with an Abbé refractometer having an accuracy of 2-3 units in the fourth decimal place. This allowed plate values to be determined with an error not exceeding 4 per cent under the operating conditions used.

The columns usually reached thermal equilibrium, as indicated by the column and jacket thermocouples, 4–5 hr after start up; after this, material equilibrium was assumed to have been reached when two consecutive head samples, one taken not less than ½ hr after the other, had the same refractive index. The plate values of the columns were obtained from these equilibrium refractive index readings by construction from a large-scale diagram prepared from the data of Bromiley and Quiggle [10].

Results and Discussion

Column 1 gave some trouble, particularly at the higher speeds, due to bowing of the rotor, and its performance was sometimes erratic. Results obtained with it are recorded in Table 1.

Column 2, the later of the two machines to be built, proved to be remarkably reliable and trouble free in operation. No source of variable frequency a.c. was available, and it was therefore operated in all experiments at the fixed design speed, 1470 rev/min (or at zero rev/min). Curve A of Fig. 3 gives its performance under atmospheric pressure at various throughputs at total reflux. It can be seen that at the lowest boil up rate used, viz. 130 ml/hr, the column gives about 57 plates in its 61 cm working length. This

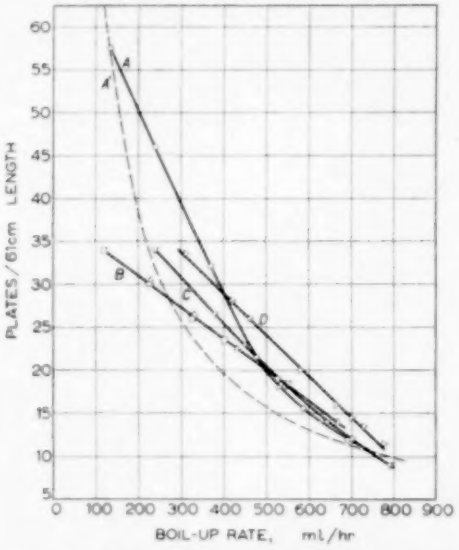

Fig. 3. A′ Westhaver theory for glass rotor
A (○) Glass rotor (0·12 cm annulus)
B (□) Copper rotor (0·33 cm annulus)
B (△) Copper rotor with sweeping wires
C (▽) Copper rotor with nichrome spirals
D (▷) Copper rotor with wire fins (16 S.W.G.)
Rotor speed = 1470 rev/min.

Table 1. *No. of theoretical plates for column* 1.

Boil-up rate (ml/hr)	*Rotor speed* (rev/min)							
	0	410	560	780	1,500	2,500	2,900	3,350
350	9·0	16·0	16·5	16·0	10·0	15·0	—	14·5
335	12·5	—	—	—	14·0	18·0	—	17·0
325	15·7	—	—	—	17·5	24·0	—	18·0
300	18·0	—	—	—	20·0	24·0	27·0	—
250	20·5	—	—	—	23·0	27·5	—	—
225	23·5	—	—	—	36·0	42·0	—	25·0

Length of rectifying section 45 cm. Diameter of inner cylinder 1·6 cm. Diameter of outer cylinder 1·8 cm.

separating power is greatly superior to that to be expected from, e.g., a spinning band column of the same length and overall diameter working under the same conditions. The hold-up, measured by allowing the apparatus to come to equilibrium, removing the still pot and allowing the column to drain into a graduated vessel, is not greater than 1·5 ml over the whole boil-up range investigated. At 130 ml/hr therefore, the efficiency factor [1] referred to above, becomes:—

$$\frac{57}{61} \times 130 \times \frac{61}{1{\cdot}5} \approx 5000 \text{ plates/hr}$$

This value compares very favourably with that for columns of other types, but is only half the best value obtained by WILLINGHAM *et al.* [1] for their rotary concentric cylinder machine, probably (as will be shown below) because the rotor speed here is not great enough to excite turbulence in the vapour.

As the working section of the apparatus is entirely of glass, the very favourable characteristics of this column should recommend it for general laboratory purposes.

Liquid and vapour phase resistances

Experiments were undertaken with modified versions of Column 2 to determine the relative significance of the liquid and vapour phase mass transfer resistances. In these, the glass rotor was first replaced by a copper one of smaller diameter, (annular clearance 0·33 cm), and the separating power of the new system was measured for various boil-up rates at the normal rotor speed. These measurements are recorded on curve B of Fig. 3.

Next the copper rotor was furnished with two "wipers," straight lengths of fine piano wire, (0·035 cm diameter), parallel to the axis, attached to the rotor at either end by spring strips so arranged as to cause the wires to bear against the inner surface of the fixed outer tube of the column. It was found that when the rotor revolved this simple arrangement quickly dislodged a fine layer of tale dusted on to the inside surface of the outer tube, and it was therefore concluded that the wires would disturb a film of reflux there. The separating power of the column fitted with this rotor was now measured at various boil-up rates, as before. The results recorded in Fig. 3 fall almost exactly on curve B, the curve obtained with the bare copper rotor. Apparently the stirring of the reflux film does not significantly improve the column efficiency. It thus appears that the liquid phase resistance in this system is negligible.

Finally, the copper rotor was provided with two longitudinal fins of 16 gauge copper wire soldered to the surface along their length. These did not touch the surface of the film of reflux at the outer wall but did presumably stir the vapour stream when the rotor revolved. From the results recorded on curve D it is evident that their presence considerably enhances the separating power of the column. Taken together with the previous result, this confirms that the mass transfer resistance here resides in the vapour phase.

Further confirmation of this conclusion is provided by the following result. Two long finely wound nichrome helices were attached to the rotor in such a way that when the latter revolved the wire coils touched the interior surface of the outer glass tube. Such an arrangement has been recommended [11] as constituting an exceptionally effective form of "spinning band." In the present experiments, the wire helices are found to improve the performance of the bare rotor but to give poorer results than the solid fins of 16 gauge wire, as appears from curve C of Fig. 3. This would be expected on the basis of the previous conclusion, since, though they disturb the liquid film as the solid fins do not, the fine wire coils are probably less effective in the important function of agitating the vapour stream.

These results offer direct evidence that resistance to radial diffusion within the liquid film has no significant effect on column performance in the present circumstances*. This conclusion

*It is possible that the sweeping wires cause some longitudinal mixing in the reflux film, such as might mask an improvement in column performance brought about by the improved radial mixing in the liquid; but since the net effect remains undetectable over a wide range of experimental conditions it may be concluded that both liquid mixing effects are of very small importance.

VOL. 10 1959

bears on a matter of controversy. Thus NATRADZE [12] concludes from observations on annular and open tube distilling columns that the liquid phase resistance makes a considerable contribution to the total resistance to mass transfer between the phases. PECK and WAGNER [13], on the other hand, conclude that the liquid phase diffusion resistance is in general negligible in wetted wall columns, a view which is supported by the work of ZUIDERWEG [15], MALYUSOV *et al.* [16] and others.

However in view of the fact that the work of CHARI and STORROW [14] suggests that the relative importance of liquid and vapour resistances in rectification is a function of the nature and composition of the test mixture, the general question cannot be decided on the result of a single experiment. But it appears that the experimental technique described is of general application in the study of liquid and vapour mass transfer resistances, and it is hoped to extend these enquiries to other systems.

Significance of Taylor vortices

In the present case it is now clear that the observed performance of the Columns 1 and 2 can be related to the conditions in the vapour stream alone. Thus, the improvement in separating power obtained by increasing the rotor speed, shown for Column 1 in Table 1, is attributable to the increase in radial mixing in the vapour stream, and is not (for example) to any significant extent due to the disturbance of the film of reflux by the whirling vapour. It would therefore be expected that observed changes in the overall performance of these columns would reflect changes in the radial diffusion coefficient in the vapour stream; and consequently, that particularly marked changes in column performance would accompany changes in the vapour flow regime.

In view of this it is somewhat surprising that the performance of such columns is apparently little improved at rotor speeds at which Taylor vortices would be expected to appear in the vapour current. Such vortices [6], occupying toroidal regions coaxial with the annulus, cause circulation of the fluid between the inner and outer cylinders in the plane of their common axis; this motion has been shown [7], [20] greatly to enhance the transfer of heat from a cylindrical wall into an annular gas stream, and it would be expected to promote radial mass transfer also. However, it appears from the results given in Table 1 that the column performance is relatively little improved at the critical speed for vortex formation in a stagnant fluid. Using TAYLOR's approximate equations 5.43 and 7.11 of [6], and assuming the value for the kinematic viscosity of the column vapour given in [15], it would be expected that vortices would appear in the annulus of Column 1 at about 350 rev/min; Table 1 shows that although there is a rise in the separating power of the column (from 9 to 15 plates) between rotor speeds of 0 and 410 rev/min, there is no further significant change in performance as the rotor speed is increased.* Even the small improvement observed might be accounted for, not by the effect of vortices, but by the improved distribution of reflux obtained when the rotor is driven fast enough to throw liquid from its surface onto the outer wall of the annulus.

Similarly, according to TAYLOR's equations, vortices would be expected to appear at a rotor speed of approximately 130 rev/min in the column of WILLINGHAM *et al.* [1]. These authors made no measurements near this speed; but between 0 and 1750 rev/min their results show an increase of separating power of a few plates only. In view of the results given in Table 1 it seems possible that this increase does not occur progressively (as is assumed in [1]), but abruptly, near the Taylor critical speed. But in any case this is an insignificant change compared with that observed at higher rotor speeds, attributable to the onset of general turbulence. Again, for Column 2 furnished with the copper rotor the appearance of the vortices would be expected at about 50 rev/min. The fact that the attachment of fins to the rotor materially improves the performance at 1470 rev/min indicates that the radial mixing induced by the fins is a substantial improvement on that

*It is interesting to note from Fig. 4 that the breakdown of Couette streamline flow in this system at a rotor speed of 410 rev/min would be in accordance with the results of FAGE [17], but not with those of CORNISH [18] or KAYE and ELGAR [7].

which obtains when the smooth rotor operates well above the Taylor critical speed.

These facts suggest, either (a) that Taylor vortices are not formed at or near the Taylor critical speed in these columns; or (b) that they are not effective in promoting mass transfer from the outer wall of the annulus to the vapour stream; or (c) that they do enhance such radial mass transfer but at the same time give rise to other effects which counter the expected improvement in column performance.

There is no direct evidence for the presence of vortices in these experiments; and TAYLOR's criterion for their formation, quoted above, applies to systems in which there is no axial flow, not strictly to the present case. However, the occurrence of Taylor vortices in annuli in which there is axial flow is apparently established by the work of KAYE and ELGAR [7]. It is known that the critical rotor speed for the change of regime from purely laminar flow is higher when there is axial flow than when the fluid is stagnant. The precise criterion for this transition in the case of simultaneous axial and circumferential flow is still in doubt, no successful theoretical treatment of the problem having yet appeared and some of the experimental investigations having given somewhat conflicting results [17], [18]; but on the basis of what is known at present it appears that at the axial vapour velocities used in the distillation experiments the critical speed for the development of vortices should differ very little from that calculated from TAYLOR's equations in all the cases considered. Thus, unless some feature peculiar to fractionating column operation inhibits vortex formation, it is reasonable to suppose that vortices are present at the low rotor speeds given above. It then appears from the results quoted that they may have an effect on column performance manifested at or near the critical speed for their formation, but which does not then increase significantly as the rotor speed is raised; and that this effect is in any case small compared with that of the change (presumably the development of turbulence) found to occur [1] in the vapour at relatively high rotor speeds.

It is thought that these conclusions, which must remain tentative until the existence of Taylor-type vortices under column conditions is definitely established, might be reconciled with the observation [7] that the vortices are effective in promoting radial heat transfer in the following way. KRAMERS *et al.* [19] have shown that the Taylor vortices are strikingly effective in promoting longitudinal, as well as radial, mixing. In the heat transfer experiments described in [7] only radial mixing effects were involved; the overall performance of wetted-wall fractionating columns, however, is sensitive to both radial and longitudinal diffusion effects. If both increase together, the improvement in column performance to be expected from improved radial mixing will be to some extent offset by increased back-mixing, which impairs the counter-current character of the vapour-liquid contacting process. Studies of these radial and longitudinal diffusion effects in annuli, designed to throw light on this matter, are at present in progress.

Conditions for turbulence

The significance of the high critical rotor speed observed by WILLINGHAM *et al.* [1] may now be considered. It appears from the experimental work of KAYE and ELGAR [7] that the annular vapour stream in these columns could be in any one of four flow regimes under different conditions of axial and circumferential motion. The stability limits for these regimes are represented by the curves bounding the lettered areas in Fig. 4, which relates to the flow of air in an annulus, and is reproduced (with additions) from [7]. Of these four, it seems that three regimes are of account under ordinary conditions of column operation, viz. laminar, (l), laminar + vortex, ($l + v$), and turbulent + vortex, ($t + v$). The fourth possible flow regime described by KAYE and ELGAR, in which the fluid is purely turbulent with no regular vortices present, is apparently not stable in the range of axial flow rates used in the columns described here. It thus appears probable that the critical rotor speed observed by WILLINGHAM *et al.* at about 2300 rev/min corresponds to the transition between the vapour flow regimes indicated in Fig. 4 as "laminar + vortex" and "turbulent + vortex."

Unfortunately the criterion for this transition

VOL. 10 1959

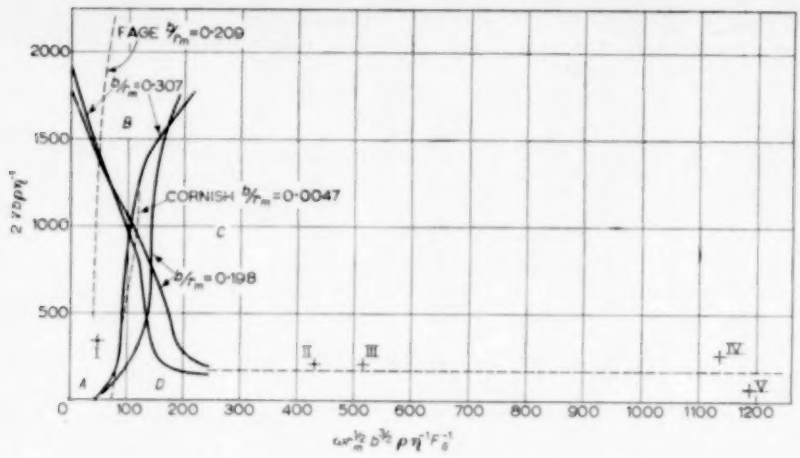

FIG. 4. Flow regimes in an annulus. Inner cylinder rotating: axial fluid stream. Curves of KAYE and ELGAR, [7].

A. Laminar flow. C. Turbulent flow + vortices.
B. Turbulent flow. D. Laminar flow + vortices.
I. Column I. 410 rev/min, 450 ml. hr^{-1} reflux, $b/r_m = 0{\cdot}11$. Vortices.
II and III. Column of WILLINGHAM *et al.* 1500 ml. hr^{-1} reflux, $b/r_m = 0{\cdot}027$
II. 2,000 rev/min: no turbulence. III. 2,400 rev/min: turbulence.
IV and V. Column 2. (copper rotor). 1470 rev/min.
IV. 430 ml. hr^{-1} reflux, $b/r_m = 0{\cdot}26$. V. 120 ml. hr^{-1} reflux, $b/r_m = 0{\cdot}27$.

for the column of WILLINGHAM *et al.* cannot be obtained from the results of KAYE and ELGAR. The latter workers used two annuli in their experiments, having b/r_m values very much larger than that for the column of WILLINGHAM *et al.* (0·198 and 0·307 as compared with 0·03 in WILLINGHAM's work). Although the diagrams given in [7] might be supposed to include the effect of b/r_m changes, and the authors do in fact use them in attempts to correlate results obtained at other b/r_m values, it seems probable that the curve representing the $(l + v)/(t + v)$ boundary should be plotted with b/r_m as a parameter, as indicated in Fig. 4. This appears likely from the following argument. Six variables are here involved in specifying the flow regime, viz. V, ω, r_m, b, ρ and η. The largest number of these that will not form a dimensionless product is three; hence, by the Π theorem, three dimensionless groups are required to characterize the flow, not two only as used by KAYE and ELGAR. Otherwise expressed, the dimensionless groups used by these authors are (1) a Reynolds number relating to axial flow, (2) the dimensionless product of three groups, viz. a Reynolds number relating to the circumferential flow, the group $(b/r_m)^{1/2}$, and a geometrical factor, $1/F_G$. The value of this product (referred to in [7] as the Modified Taylor number) can be shown from TAYLOR's work to characterize the transition from laminar to vortex motion, independently of b/r_m, in systems where there is no axial flow; but there is no justification for supposing that it has a like significance in characterizing the transition to turbulence, in determining which the quantity b/r_m is probably involved in some functionally different way. It seems therefore that KAYE and ELGAR's curves can be used only to correlate results obtained in experiments at the b/r_m values for which the curves are plotted. The differences between their published curves obtained at two different values of this ratio bear this out.

It is not therefore surprising that Fig. 4 does not fit the data of WILLINGHAM *et al.*, indicating for their column a strong dependence of critical rotor speed on axial vapour velocity which the experimental results [1] do not support. Points on Fig. 4,

representing conditions in the column of WILLINGHAM *et al.* at rotor speeds of 2,000 and 2,400 rev/min and a boil-up rate of 1,500 ml/hr. lie close to the (extrapolated) nearly horizontal right hand branch of the curve marking the $(l + v)/(t + v)$ transition in KAYE and ELGAR's system. This implies a critical dependence of vapour regime on axial vapour rate, and indicates that the rotor speed at which the vapour becomes turbulent should depend very markedly on the axial velocity. But Fig. 7 of [1] shows that conditions in the column are in fact little influenced by boil-up rate; it appears from this figure that the vapour becomes turbulent at a relatively well-defined and constant rotor speed, irrespective of boil-up rate. Evidently for a value of b/r_m as small as that for the column of WILLINGHAM *et al.* the curve representing the boundary of the $t + v$ region is more steeply inclined to the axis at low Reynolds number than those shown. Indeed where the parameter b/r_m becomes very small the following considerations indicate that the curves bounding the $t + v$ region may approximate to elliptical arcs having the major and minor axes on the axes of co-ordinates, and so meeting the horizontal axis at right angles.

This result follows if it is assumed that when b/r_m is very small the criterion for the $(l + v)/(t + v)$ transition (*i.e.* the critical Reynolds number based on mean vapour velocity) is nearly the same as that for the laminar-turbulent transition for pressure flow between stationary flat parallel planes. Since the motion due to rotation is in fact a shearing flow (for which the turbulence criterion is not known) this is clearly a questionable assumption; but for zero axial velocity it does lead to the turbulence criterion used in [1], for whose validity there seems to be experimental evidence from at least one other source [3]. Where there is both axial and circumferential flow, the transition from one regime to the other would on this basis be expected to occur at some critical value of a Reynolds number based on the Pythagorean sum of mean axial and circumferential vapour velocities.

The groups plotted in Fig. 4 may be written :—

$$y = V \cdot 2b\,\rho\eta^{-1} = VY$$

$$x = V_s \cdot r_m\,(r_m - \tfrac{1}{2}\,b)^{-1}\,r_m^{-1/2}\,b^{3/2}\,\rho\eta^{-1}\,F_G^{-1} = VX$$

Then if

$$V' = y'/Y$$

and $$KV'_s = Kx'/X$$

represent a corresponding pair of critical axial and circumferential vapour velocities for the change of regime from $l + v$ to $t + v$, we have :

$$(V'^2 + K^2 V_s'^2)^{1/2}\,b\,\rho\eta^{-1} = Re_c$$

$$\text{Or,}\quad \frac{y'^2}{Y^2} + \frac{x'^2}{X^2}\,K^2 = \left(\frac{\eta\,Re_c}{b\rho}\right)^2 \qquad (1)$$

K depends on the radial velocity gradient, and may be taken as approximately constant in (1), at least where the axial flow rate is not large. In that case, i.e. near the x-axis, X and Y and the quantities on the right-hand side of (1) will be constant for a given fluid and a given pair of cylinders. Under these conditions (1) is the equation of an ellipse having the major and minor axes on the axes of x and y.

From (1), the length of the semi-minor axis is $2Re_c$. The intercept on the x-axis is

$$(b/r_m)^{1/2}\,\frac{Re_c}{K}\cdot\frac{r_m}{F_G\,(r_m - \frac{1}{2}\,b)}$$

which reduces to

$$\left(\frac{b}{r_m}\right)^{1/2}\frac{Re_c}{K} = \left(\frac{b}{r_m}\right)^{1/2} Re_{cs}$$

when b/r_m is very small. Thus for this limiting case, on the assumptions given, the $(l + v)/(t + v)$ boundary curves on Fig. 4 should be a family of elliptical arcs having a common minor axis, and semi-major axes (x-intercepts) proportional to $\sqrt{(b/r_m)}$.

It would be expected from the above treatment that for columns having very small values of b/r_m the simple turbulence criterion proposed in [1] would be, in effect, valid; for under ordinary operating conditions the axial vapour velocity in these columns is small compared with the whirling velocity due to the rotor, and so makes a very small contribution to the vector sum of the two. In this connection it is noteworthy that the observed critical rotor speed corresponds to a value for $V_s\,b\,\rho/\eta$ of approximately 3,000, not only for the column described in [1], but for the larger columns of [3] and [4] also, which similarly have small b/r_m values (0·019 and 0·016 respectively)*.

Column 2 fitted with the copper rotor, however, has a b/r_m value (0·27) intermediate between

*The authors of [4] conclude that rotor surface speed alone is the criterion governing the abrupt change of column performance. This appears unlikely on the basis of the present discussion, and the results given do not establish this view.

VOL. 10 1959

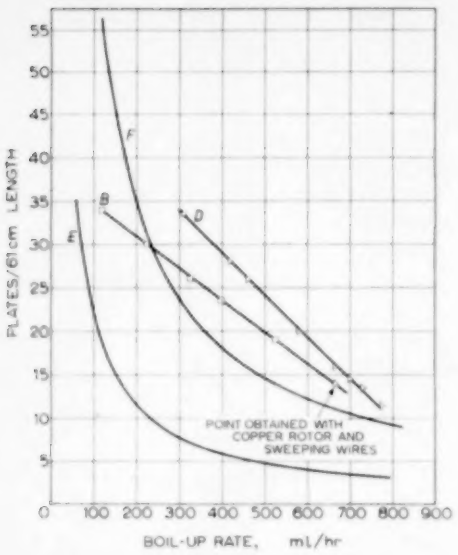

FIG. 5. B (□) Smooth copper rotor
D (▷) Copper rotor with wire fins
E Westhaver theory for laminar vapour
F Westhaver theory for turbulent vapour
Rotor speed = 1470 rev/min.

the two values to which the curves in Fig. 4 relate; this diagram should therefore furnish a turbulence criterion for the system. The fixed operating speed (1470 rev/min) for the copper rotor corresponds to a modified Taylor number of 1100—1200*; as shown in Fig. 4 this implies a very sensitive dependence of flow regime on vapour rate. Thus at low boil-up rates the vapour stream would be expected to be laminar, but at high boil-up rates the flow would be expected to become turbulent according to Fig. 4, although the rotor speed is here not high enough to satisfy the simple criterion for turbulence proposed in [1]. This effect would tend to flatten, or make more horizontal, the curve of separating power versus throughput for this column operating at 1470 rev/min in comparison with that for the same column fitted with the glass rotor, for which the b/r_m value is much smaller and the dependence of vapour regime on axial flow rate correspondingly less marked. For, as the boil-up rate is increased the separating power in any case tends to fall as the radial vapour–liquid equilibrium is progressively less able to establish itself; but in the case of the copper rotor system it might be expected that this fall would be to some extent offset by the improved radial mixing at higher vapour rates due to the development of turbulence. This introduces the interesting possibility of designing rotary concentric cylinder columns giving good separation at high vapour rates (i.e. large throughputs for a compact unit) at conveniently low rotor speeds; and showing a much smaller dependence of separating power on throughput than is customary with film type columns.

Figure 3 shows that the experimental separating power-throughput curve for the copper rotor is indeed flat compared with that for the glass rotor, and in Fig. 5 this curve is compared with the theoretical curve calculated from WESTHAVER's equation [1] on the assumption of laminar vapour flow. At low vapour rates the performance of the column is evidently not very different from that to be expected on the latter assumption; but at higher vapour rates the plate values are very much greater than those predicted, and the experimental curve agrees much more closely with the Westhaver curve calculated on the assumption of vapour turbulence*. Two points corresponding respectively to the lowest vapour rate used and to a vapour rate at which the experimental curve of Fig. 5 lies closer to the

*The value of b used is in all cases that for the annular vapour stream; i.e. difference of column cylinder radii less reflux film thickness. Hence the Taylor number is a function of boil-up rate as well as rotor speed.

*The theoretical curves used here are based on modified forms of WESTHAVER's equations, in which the liquid phase resistance is assumed negligible, in accordance with the experimental findings reviewed above. However, it must be pointed out that in view of the possible presence of vortices in the vapour stream, of which WESTHAVER's treatment takes no account, their applicability here is questionable. A comparison of the curves A and A' of Fig. 3 for the glass rotor system indicates the extent to which the WESTHAVER laminar theory fails in a case for which the above criteria indicate a laminar + vortex regime. On this basis the discrepancy between the experimental and laminar theory curves (B and E of Fig. 5) for the copper rotor is apparently greater than would be accounted for by the presence of the vortices alone.

upper (turbulent) Westhaver curve, are plotted on Fig. 4. Though the curves of that figure do not extend to high enough Taylor numbers to establish the conclusion, it seems that these points might well lie above and below the boundary between the turbulent + vortex and laminar + vortex flow regimes. It thus appears that the overall performance of this column can be related to the general fluid mechanical observations of KAYE and ELGAR.

CONCLUSIONS

The form of rotary concentric cylinder fractionating column described (column 2) is of practical use as a laboratory column, having no exposed bearings, lending itself to all-glass construction and having an exceptionally high performance. The principles of operation of such columns are thus of practical interest; and as the laws governing their performance can be related very directly to hydrodynamic laws, their behaviour throws light on questions of general interest in fluid mechanics.

The results obtained with the columns described are apparently substantially in accordance with the flow regime diagram of KAYE and ELGAR relating to the technically important case of fluid flow in the annulus between a rotor and stator; but consideration of the results of other experiments with rotary concentric fractionating columns suggests an important modification of this diagram.

The apparatus described affords a direct means of investigating the relative importance of liquid and vapour phase mass transfer resistances in rectification. For the mixture of *n*-heptane and methyl cyclohexane studied, the liquid phase resistance at atmospheric pressure is shown to be negligible, and the column performance is governed solely by limitations of radial mass transfer in the vapour. Thus, stirring the reflux film does not affect the column; but the addition of fins to the rotor improves the separating power of the system, as does the development of general turbulence in the vapour in the experiments of WILLINGHAM *et al.* There is, however, little change in column performance at the rotor speeds at which vortices would be expected to appear. Possible causes of this anomaly are under investigation.

Acknowledgements—The British Petroleum Company gave financial support for this work, which is gratefully acknowledged.

Key to Figs. 1, 2 (a) and 2 (b).

A	Fixed central shaft
B	Upper flange of motor housing
C	Thin-walled stainless steel motor housing
D	Upper ball-race of squirrel cage rotor
E	Squirrel cage rotor
F	Motor stator
G	Lower ball-race of squirrel cage rotor
H	Hollow shaft of squirrel cage motor
I	Ball race retainer and locking ring
J	Drive pin
K	Lower flange of motor housing
L	Driving member of universal coupling
M	Inner driven member of universal coupling
N	Cork-lined clamping ring
O	Body of glass-metal O-ring union
P	O-ring sealing plate
Q	Spiral water condenser
R	Glass column rotor
S	Take-off valve solenoid
T	Cork lined clamping ring supporting outer column tube
U	Centering screws
V	Glass outer column tube
W	Compensating heaters
X	Thermistors mounted on metal column jacket
Y	Thermistors mounted on outer column tube
Z	Lower bearing assembly

NOTATION

b = annular width
r_m = mean radius of annulus
x = abscissa } in Fig. 4
y = ordinate }
F_G = geometrical factor in Taylor's equations

$$= \frac{\Pi^2}{41{\cdot}2\left(1-\frac{b}{2r_m}\right)\sqrt{\left\{0{\cdot}0571\left[1-0{\cdot}632\left(\frac{b/r_m}{1-b2/r_m}\right)\right]+\frac{0{\cdot}00056}{1-0{\cdot}632\,[(b/r_m)/(1-b/2r_m)]}\right\}}}$$

K = mean circumferential vapour velocity/V_s
Re_c = critical Reynolds number for turbulence for fluid flow between flat parallel planes, based on mean velocity of fluid
Re_{cs} = critical Reynolds number for turbulence for circumferential shearing flow between concentric cylindrical surfaces, based on velocity V_s of moving convex surface
V = mean linear axial velocity of fluid
V_s = surface speed of rotor
$X = r_m (r_m - \frac{1}{2} b)^{-1} r_m^{-1/2} b^{3/2} \rho\eta^{-1} F_G^{-1}$
$Y = 2b \rho\eta^{-1}$
η = fluid viscosity
ρ = fluid density
ω = angular velocity of rotor

References

[1] Willingham C. B., Sedlak V. A., Westhaver J. W. and Rossini F. D. *Industr. Engng. Chem.* 1947 **39** 706.

[2] Irlin A. L. and Brunce B. P. *Zh. Anal. Khim.* 1950 **1** 44.

[3] Mair B. J., Krouskop N. C. and Rossini, F. D. *Testing of a Rotary Concentric-Tube Distilling Column.* Report of Investigation of the American Petroleum Institute Research Project 6. Petroleum Research Laboratory, Carnegie Institute of Technology. 29 Feb. 1956.

[4] Hawkins J. E. and Burris W. A. *Analyt. Chem.* 1956 **28** 1715.

[5] Golubyev I. F., Meshcheryakov I. V. and Olevsky V. M. *Jrnl. Gos. Inst. Azot. Prom.* 1956 **5** 316.

[6] Taylor G. I. *Phil. Trans.* 1923 A**223** 289.

[7] Kaye J. and Elgar E. C. *Trans. Amer. Soc. Mech. Engrs.* 1958 **80** 753.

[8] Pollard A. C. F. *The Kinematic Design of Couplings in Instrument Mechanisms.* Hilger, London 1929.

[9] Matterson K. J. M.Sc. Thesis, London, 1957.

[10] Bromiley E. G. and Quiggle D. *Industr. Engng. Chem.* 1933 **25** 1136.

[11] Challis J. Private Communication I.C.I. Billingham, July 1955.

[12] Natradze A. G. *Zh. prikl. Khim.* 1954 **27** 600.

[13] Peck R. E. and Wagner E. F. *Trans. Amer. Inst. Chem. Engrs.* 1945 **41** 737.

[14] Chari K. S. and Storrow J. A. *J. Appl. Chem.* 1951 **1** 45.

[15] Zuiderweg F. J. *Chem. Engng. Sci.* 1952 **1** 174.

[16] Malyusov V. A., Umnik N. N. and Javoronkov M. N. *Dokl. Akad. Nauk SSSR* 1956 **106** 199.

[17] Fage A. *Proc. Roy. Soc.* 1938 A**165** 501.

[18] Cornish R. J. *Proc. Roy. Soc.* 1933 A**140** 227.

[19] Croockewit P., Honig C. C. and Kramers H. *Chem. Engng. Sci.* 1955 **4** 111.

[20] Clark L. G. and Hagerty W. W. *J. Amer. Inst. Chem. Engrs.* 1957 **3** 523.

Chemical Engineering Science, 1959, Vol. 10, pp. 268 to 273. Pergamon Press Ltd. London. Printed in Great Britain

The deposition of airborne droplets on wire gauzes

R. T. JARMAN

Colonial Insecticides Research Unit, Porton Down, Salisbury, Wilts.

(*Received* 12 *January* 1959)

Abstract—The droplet collection efficiency of wire gauzes exposed normal to an airstream has been measured and also computed using a rather crude theoretical model of the processes occurring. A spinning-top sprayer was used to produce a uniform cloud of dyed oil droplets in a wind tunnel; the cloud concentration was found by exposing a cascade impactor and measuring the deposit colorimetrically. The theory predicted the variations of collection efficiency with droplet size and closeness of wires, but afforded no explanation of the anomalous low experimental values found with 30 μ diameter droplets.

Résumé—Les toiles métalliques en fer exposées normalement à un courant d'air ont une capacité pour rassembler les particules qui a été non seulement mesurée, mais calculée à l'aide d'une théorie quelque peu grossière des processus réels. Un pulvérisateur a tête tournante a servi à former un nuage uniforme de gouttelettes d'huile colorées dans un tunnel. La concentration en gouttelettes a été trouvée par mesure colorimétrique du dépot sur un séparateur à impacts successifs. La théorie prévoit les variations de l'efficacité de rassemblement en fonction de la dimension des particules et des dimensions des mailles, mais n'explique pas les valeurs expérimentales anormalement basses trouvées avec des particules de 30μ de diamétre.

Zusammenfassung—Die Wirksamkeit des Tropfenfanges von Drahtsieben, die senkrecht zu einem Luftstrom stehen, wurde gemessen und unter Benutzung einer rohen Modellvorstellung berechnet. Ein rotierender Zerstäuber erzeugte eine gleichförmige Wolke von angefärbten Öltropfen in einem Windkanal; die Konzentration in der Wolke wurde mit Hilfe eines Kaskaden-Auffängers kolorimetrisch bestimmt. Die Theorie konnte die Wirksamkeit des Tropfenfanges als Funktion der Tropfengrösse und Maschenweite voraussagen, nicht aber die anomal niedrigen Versuchsergebnisse im Bereich von 30μ Tropfendurchmesser.

INTRODUCTION

WIRE gauzes are very useful for sampling small droplets drifting with the wind, as, unlike the cascade impactor [10], no elaborate subsidiary equipment such as pumps and batteries are needed. They have been used to sample insecticide sprays [1, 2] etc. and natural clouds and fog [3, 4].

When a piece of gauze is placed in the atmosphere some of the air originally flowing towards it flows around it and some through the holes. Particles in the atmosphere tend to follow the airflow, but because of their greater inertia they do not deflect as readily as the air.

Therefore the air reaching the gauze contains less particles than are found in the same cross section upstream, because some of the particles are deflected around the whole gauze network. The concentration of particles in the air-stream which eventually passes through the gauze is increased as the smaller number of particles are mixed with an even smaller proportion of the air. As this aerosol comes very close to the gauze, the air flows around the cylinders (through the holes) and again some particles take a straighter path and hit the cylinders. While particles of some kinds may bounce off, oil droplets deposit on metal surfaces. The relation between the deposit on a plane gauze normal to the airstream and the upstream aerosol concentration has been

*Present Address: 164 Tremona Road, Southampton

measured experimentally in a wind tunnel, and also calculated using a simple, approximate theory.

The results are discussed in terms of the collection efficiency (E) which is the deposit on the gauze as a percentage of the liquid which would have deposited if the droplets had not been deflected by the air currents. It is expressed mathematically by the equation

$$E = \frac{100\,Q}{A'\,c\,Ut} = \frac{100\,Q}{A\,(1-\beta)\,c\,Ut} \qquad (1)$$

where Q = the volume of droplets deposited
A = the cross-sectional area of the gauze in the plane normal to the airstream
A' = actual (projected) frontal area of material
β = area of holes per unit area of gauze
c = the concentration of droplets, in volume of droplets per unit volume of air
U = the free stream velocity
t = the time the object is exposed to the droplet cloud

Experimental Method

The collection efficiency was measured by comparing the deposit on wire gauzes with the deposit on the first stage slide of a cascade impactor when each were exposed in turn to a fairly uniform cloud of droplets in a horizontal wind tunnel. Using equation (1) for each object we have,

$$E = \frac{E}{E_c}E_c = \frac{Q}{Q_c}\cdot\frac{A_c}{A\,(1-\beta)}\cdot\frac{t_c}{t}\cdot E_c \qquad (2)$$

where the subscript c refers to the cascade impactor. All the ratios on the R.H.S. were measured. The collection efficiency of the cascade impactor (E_c) was obtained from some recent measurements by May [9] assuming the results obtained when sampling at $17\frac{1}{2}$ l/min in a 3 miles/hr wind would apply when sampling at 10 l/min in a 1 m/sec wind.

A perspex wind tunnel with a 1 ft diameter working section was used. The spinning top sprayer [11] situated 3 ft upwind of the working section produced a cloud of uniformly sized droplets, but disturbed the airflow somewhat. To minimize this a coarse wire gauze was placed immediately downwind of the sprayer. The characteristics of the airflow in the working section are shown by the profiles in Table 1, which were obtained using a shielded hot wire anemometer [12].

Table 1. *Wind speed (cm/sec) — viewed from upwind*

Left	2 in.	1 in.	*Centre*	1 in.	2 in.	*Right*
2 in. up	101	105	115	105	102	
Centre	105	97	91	107	107	
2 in. down	111	111	105	102	97	

The variation of the droplet cloud concentration in space, was found by exposing the cascade impactor at various positions across the working section, and measuring the dyed spray deposit colorimetrically using a Unicam Absorptiometer. The results of one of these tests using droplets of 35 μ dia. is shown in Table 2. The deposit "shadow" is associated with the wind "shadow," partially because less air carried less droplets. The concentration also varied in time, ranging $\pm$ 11 per cent about the mean value.

Table 2. *Concentration variations (arbitrary units)*

	1 in. *Left*	*Centre*	1 in. *Right*
$\frac{1}{2}$ in. above centre	18	14	20
$\frac{1}{2}$ in. below centre	20	17	19

The liquids, kerosene and Kerosene Extract Bottoms [K.E.B.] dyed with 1 per cent and 8 per cent grasol blue respectively, were fed to the spinning top at 1-2 cm^3/min. Three wire samples (2 × 2 cm, 3 × 3 cm and 4 × 4 cm) were exposed to the spray alternately with the cascade impactor for intervals of 1-9 min. The deposits were washed off with petroleum ether and the quantity estimated colorimetrically using the Unicam Absorptiometer. This was only roughly linear, so the exposures were arranged to

produce similar pointer deflections. The size of the droplets being used was found by exposing an MgO coated slide [10, 13] in the cascade impactor and measuring the diameters of the pits produced under a low powered microscope.

RESULTS OF THE EXPERIMENTS

The wind speed was restricted to 1 m/s and the variation of the collection efficiency with droplet size and the closeness of the wire mesh was studied. The results are shown as plotted points on Figs. 1, 2 and 3 and are tabled in the appendix. We see that the collection efficiency increased with droplet size and decreased with the closeness of the wire mesh.

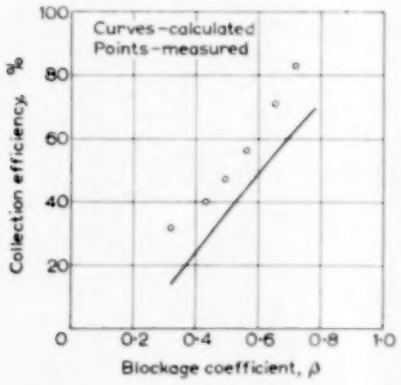

FIG. 1. The variation of collection efficiency with β. (18 μ dia. K.E.B. droplets).

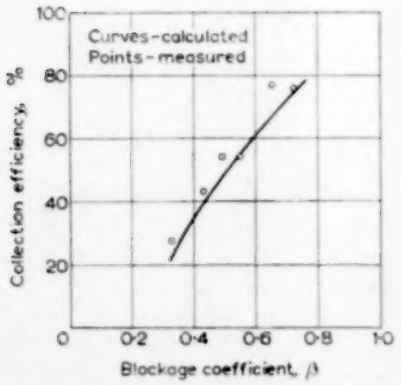

FIG. 2. The variation of collection efficiency with β. (30 μ dia. kerosene droplets).

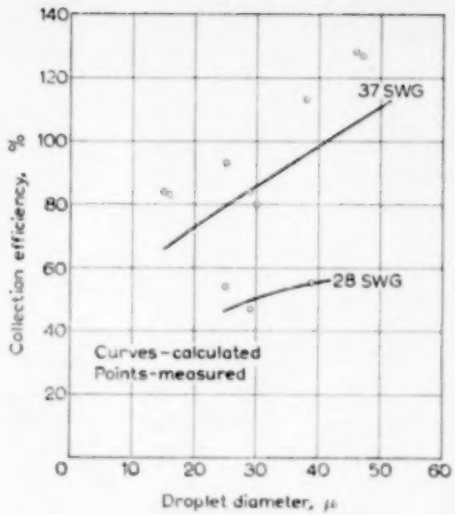

FIG. 3. The variation of collection efficiency with droplet size.

THEORETICAL STUDY

To summarize these results and to make interpolations from them easier, a brief study of the theory of deposition of windborne droplets onto objects was made. Analytical methods of calculating the percentage of droplets depositing, using first principles, did not seem promising; some of the difficulties have been described by RANZ and WONG [7]. However numerical methods have been used successfully to calculate the trajectories of droplets in an airstream flowing around isolated, infinite cylinders by DAVIES and PEETZ [8] and others, and the fraction of the airflow that goes through a gauze has been established empirically [6]. Therefore it was possible to postulate possible models of the processes occurring, and to calculate how the collection efficiency varied with droplet size, wire size and spacing, and wind speed in these theoretical cases. In each case it would be necessary to make a number of assumptions that could not be justified *a priori*. In the model described here the simplest and most obvious assumptions were made and the collection efficiencies calculated from it simulate the variation with closeness of wire, and with a notable exception the variation with droplet size. This simple

VOL. 10 1959

and unsophisticated analysis of the problem may throw some light on the physical processes occurring. It also shows the accuracy obtained when such calculations are used to assess the deposition occuring on complex objects; this is often necessary in practice.

It has been found that the fraction of the air that flows through the gauze (u/U) is given by the equation

$$u/U = (1 + \tfrac{1}{4}k)^{-1} \qquad (3)$$

where k is the resistance coefficient of the gauze [5]. Simmons and Cowdrey [6] measured k and found that with a square mesh of cylinders, and $u/U < 10$ m/sec to a first approximation,

$$k = (1 - \beta)/\beta^2 \qquad (4)$$

In the computation, the complex airflow and particle trajectories near the square mesh gauzes were assumed to approximate to an aerosol of concentration (c) flowing at the reduced velocity (u) towards isolated infinite cylinders of the same diameter as the wire. In this case,

$$E = E' \frac{u}{U} = E' \left(1 + \frac{1 - \beta}{4\beta^2}\right)^{-1} \qquad (5)$$

where E' is the collection efficiency of an isolated, infinite cylinder in a wind of speed (u).

For comparison with the experimental results E' was computed using the results of Davies and Peetz [8], who expressed the collection efficiency of an isolated, infinite cylinder in terms of the dimensionless parameter P, the Reynolds number (Re) and the ratio of the particle radius ($\frac{1}{2}Dp$) to the cylinder radius ($\frac{1}{2}Dc$). P for spherical particles, is defined by the equation

$$P = \frac{\rho u D_p^2}{9 \eta D_c} \qquad (6)$$

where ρ is particle density and η the coefficient of viscosity of air. The Reynolds number of the flow around an infinite cylinder is given by the equation

$$Re = \frac{u D_c \rho_a}{\eta} \qquad (7)$$

where ρ_a is the density of the air, and u its velocity. Sedimentation of droplets onto horizontal cylinder was not considered by Davies and Peetz [8] but using the methods of Ranz and Wong [7] it was shown that negligible sedimentation onto the horizontal cylinders of the mesh occurred. Values of P and Re in the various experiments were computed, taking the coefficient of viscosity of air to be $1{\cdot}79 \times 10^{-3}$ poise, and the density of air, kerosene droplets and Kerosene Extract Bottoms droplets to be $1{\cdot}3 \times 10^{-3}$, 0·82 and 0·92 g/cm^3 respectively. It was found that Re varied from 6 to 18, so the results of Davies and Peetz [8] for $Re = 10$ were used in the computations. The collection efficiencies computed in this way are compared with the experimental results in Fig. 1, 2 and 3, and are tabulated in the appendix.

Discussion of Results

Figures 1, 2 and 3 show that the simple theory tends to underestimate the collection efficiency, and the mean square deviation between calculated and measured collection efficiencies is 13 per cent. The underestimate probably arises because the droplet inertia and concentration are underestimated; the droplets decelerate in the slower airstream near the gauze, but probably not to as low a speed as the airflow (u) and so more droplets deposit than in the quasi-equilibrium case used in the calculations. The variations with closeness of wire and droplet size are well simulated by the theory, apart from the unexpected anomalous experimental results with approximately 30 μ diameter droplets which may be due merely to an extreme undetected experimental error; a possible, but unlikely, cause is that for some unexplained reason the 30 μ diameter droplets adhere less firmly to the wires than other oil droplets.

When applying these results to droplets of other liquids it should be remembered that they may not adhere in the same way as oils [14]. Also in winds exceeding 10 m/sec the airflow through the gauze is different [6], and this fast turbulent airflow might increase the collection efficiency [3] so strictly speaking, these results do not apply to those conditions; though they may be the best guide available to the field worker! In the non-turbulent conditions (wind < 10 m/sec) the collection efficiency is independent of the size

of the sheet of gauze exposed normal to the wind, and so these results can be applied to large sheets of wire gauze. In the open, atmospheric turbulence might effect the collection efficiency, but no information is to hand on that, and these results have been useful for interpreting aerial spraying trials of insecticides and other liquids [15, 16].

The correspondence between the results obtained by computation from a very unsophisticated theoretical model and the measurements shows that simple calculations using results obtained for the flow around simple smooth objects, may be quite useful, though not highly accurate, when used to predict the deposition of droplets onto various complex objects in the field.

Acknowledgements—The writer would like to thank Mr. P. T. KING for assistance with the measurements, and Drs. D. J. THOMAS and R. C. PANKHURST for calling his attention to References 5 and 6, which were so useful in the theoretical study. He is grateful to Begg, Cousland & Co. Ltd. and N. Greening & Sons Ltd. for kindly providing the variety of wire gauzes used.

NOTATION

A = cross-sectional area of gauze
Ac = intake area of cascade impactor
A' = frontal area of actual gauze wires
C = concentration of droplet cloud
Dc = wire diameter
Dp = droplet diameter
E = collection efficiency of gauze (defined in equation 1)
Ec = collection efficiency of cascade impactor
E' = collection efficiency of isolated infinite cylinder
k = resistance coefficient of gauze (defined in equation 3)
P = inertia parameter (defined in equation 6)
Q = volume of droplets deposited on gauze
Qc = volume of droplets collected by cascade impactor
Re = the Reynolds Number of airflow around an isolated cylinder (equation 7)
t = period of exposure of gauze
t_c = period of exposure of gauze cascade impactor
U = free stream velocity
u = average wind speed through gauze
β = area of holes per unit area of gauze
ρ = particle density
ρ_a = air density
η = coefficient of viscosity of air

APPENDIX

Table of the measured and calculated collection efficiences

Wire size (SWG)	*No. of wires /in.*	*Liquid used*	*Droplet dia. (μ)*	*Collection efficiency (%)*	
				Measured	*Calculated*
37	18	kerosene	15	84	66
			16	83	67
			25	93	80
			29	84	84
			30	80	85
			38	113	96
			46	128	106
			47	127	107
28	20	kerosene	25	54	46
			29	47	50
			39	55	56
32	14	kerosene	30	76	74
	18			77	66
	24			54	55
	28			54	47
	32			43	40
	40			28	22
32	14	K.E.B.	18	83	62
	18			71	55
	24			56	43
	28			47	35
	32			41	29
	40			32	14

REFERENCES

[1] BROWN A. W. A. and MULHERN T. D. *Mosquito News* 1954 **14** 175.
[2] BURNETT G. F. and THOMPSON B. W. *Bull. Ent. Res.* 1956 **47** 495.
[3] NAGEL J. F. *Quart. J. R. Met. Soc.* 1956 **82** 452.
[4] TWOMEY S. *Weather* 1957 **12** 120.
[5] TAYLOR G. I. and DAVIES R. M. Rep. Memo No. 2237, Aero. Res. Council, H.M.S.O., London 1944.
[6] SIMMONS L. F. G. and COWDREY C. F. Rep. Memo. No. 2276, Aero. Res. Council, H.M.S.O., London 1945.

[7] Ranz W. E. and Wong J. B. *Industr. Engng. Chem.* 1952 **44** 1371.

[8] Davies C. N. and Peetz C. V. *Proc. Roy. Soc.* 1956 **A234** 269.

[9] May K. R. *Amer. Med. Assoc. Arch. Industr. Health* 1956 **13** 481.

[10] May K. R. *J. Sci. Instrum.* 1945 **22** 187.

[11] May K. R. *J. Appl. Phys.* 1949 **20** 932.

[12] Simmons L. F. G. *J. Sci. Instrum.* 1949 **26** 407.

[13] May K. R. *J. Sci. Instrum.* 1950 **27** 128.

[14] Brunskill R. T. *Proc. Brit. Weed Contr. Conf.* 1956 593.

[15] Hill R. F. and Jarman R. T. *J. Agric. Engng. Res.* 1957 **2** 243.

[16] Hill R. F. and Jarman R. T. *J. Agric. Engng. Res.* 1958 **3** 205.

Chemical Engineering Science, 1959, Vol. 10, pp. 274 to 280. Pergamon Press Ltd. London. Printed in Great Britain

The absorption of carbon dioxide by a quiescent liquid

E. A. HARVEY* and W. SMITH

Dept. of Chemical Engineering, Imperial College of Science and Technology, Prince Consort Road, London, S.W.7.

(*Received* 16 *February*, 1959)

Abstract—An interferometric technique is described by which the absorption of carbon dioxide into quiescent water has been examined. There is no measurable resistance at the interface to solution of the gas into pure water, the rate of absorption into the liquid being governed by molecular diffusion. A measurable interfacial resistance is found when carbon dioxide is absorbed by solutions of surface-active agents.

Résume—Les auteurs décrivent une méthode interférométrique qui permet d'étudier l'adsorption du CO_2 dans l'eau au repos. La résistance à l'interface de la solution du gaz et de l'eau pure est trop faible pour être mesurable, la vitesse d'adsorption dans le liquide étant déterminée par la diffusion moléculaire. Les auteurs trouvent une résistance interfaciale mesurable quand le CO_2 est absorbé par des solutions d'agents tensio-actifs.

Zusammenfassung—Zur Bestimmung der Absorption von Kohlendioxyd durch ruhendes Wasser wird eine interferometrische Versuchstechnik beschrieben. Da bei der Lösung des Gases in reinem Wasser kein messbarer Grenzflächenwiderstand vorhanden ist, wird die Geschwindigkeit der Absorption in die Flüssigkeit durch die molekulare Diffusion bestimmt. Ein messbarer Grenzflächenwiderstand wird bei der Absorption von Kohlendioxyd durch Lösungen von oberflächenaktiven Stoffen gefunden.

INTRODUCTION

A VARIETY of techniques have been devized for the purpose of detecting and measuring interfacial resistance to the absorption of a gas by a liquid [1, 2, 3, 5, 6, 8, 11, 13]. In all cases the experimental arrangements have been such that liquid and gas have been moved relative to each other. At the time when the present work was commenced, in no case was the exact nature of the motion of the liquid known and its effect upon conditions at the interface could not, therefore, be reliably assessed. Also the rate of absorption was determined from the total quantity of gas dissolved over a relatively long exposure time and the size of any interfacial resistance could not be calculated from such data with accuracy. For these reasons it seemed desirable to obtain some data on the absorption of a pure gas by a stationary liquid; for by using a pure gas it is ensured that there is no resistance to transfer in the gas phase, and by using a stationary liquid the unknown influence of the motion of this phase is thereby eliminated. In the work to be described the pressure of carbon dioxide over the surface of pure water and over solutions of surface-active agents was suddenly altered. The non-steady absorption of the gas into the liquid, resulting from this change of conditions, was followed by an interferometric method. It will be shown that even a small interfacial resistance (0·25 sec/cm) can be measured with accuracy from data obtained in this way.

Several of the earlier workers [3, 5, 8] found an apparent interfacial resistance to the absorption of gas by water. More recent work [1, 2, 6, 11, 13], however, has shown that the resistance must be very small. In particular LYNN *et al.* [11] and also CULLEN and DAVIDSON [1] measured the quantity of gas absorbed by a liquid flowing over the surface of a sphere: by assuming that the liquid was inviscid, the form of the motion

* Present address: Division of Applied Chemistry, National Research Council, Ottawa 2, Canada.

was deduced. Diffusion coefficients of carbon dioxide into water, calculated from data obtained by CULLEN and DAVIDSON on the assumption that there is no interfacial resistance, have the same value as diffusion coefficients measured by other means. When absorbing carbon dioxide into solutions of surface-active agents CULLEN and DAVIDSON did measure a resistance at the interface at low concentrations, but at high concentrations of surface-active agents they found no resistance. Measurements on similar systems have been included in this work.

BASIS OF THE INTERFEROMETRIC METHOD

The method depends upon the measurement of the shift of interference fringes near the surface of a liquid, caused by a change in gas concentration in the liquid. For this purpose a Mach-Zehnder interferometer has been used. This instrument has four optical plates (Fig. 1), of which two (M2 and M3) reflect all the incident light. The other two plates (M1 and M4) are semi-reflecting; that is, about one half of the incident light is reflected and the rest is transmitted. When the instrument has been adjusted correctly the surfaces of all four plates are parallel and their centre points lie at the corners of a parallelogram. Path M1, M3, M4 should equal path M1, M2, M4 to within a few wavelengths of the light to be used.

Light from a high pressure mercury vapour lamp is directed by a lens of short focal length onto a slit, which acts effectively as the light source. The wedge of light formed at the slit is collimated by a second lens to yield a parallel beam of light which is passed into the interferometer, falling on plate M1. The light reflected at this plate is reflected again at plate M2 and transmitted through plate M4. The light transmitted at plate M1 is reflected at plate M3 and again at plate M4, where it recombines with the light from the first path. A pair of compensating plates are introduced into one of the light paths. These provide an optical balance to the cell in which gas absorption is carried out and which is placed in the other path. On the emergent side of the interferometer a lens of long focal length forms an image of the absorption cell. This image is magnified by a microscope objective and thrown onto a screen or photographed. The plates are positioned so that the emergent beams intersect, virtually, in the plane of the absorption cell. Interference fringes, from which all measurements are taken, are formed in this plane, and a magnified image of the absorption cell and the fringes are obtained together. The constructional details of the instrument used in this work and the method by which it was adjusted have been described in full elsewhere [7].

The position of the interference fringes depends directly upon the difference between the optical path lengths of the two light beams, and the optical path length is directly proportional to the refractive index of the medium containing the light. If a gas is absorbed by a liquid placed in one of the two light beams, a non-uniform distribution of gas in the liquid will cause a

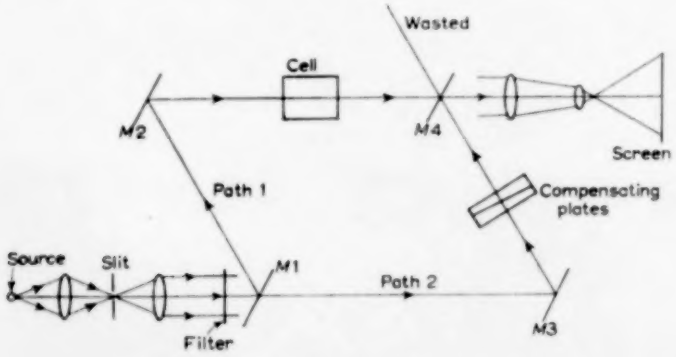

FIG. 1. Optical system and interferometer.

non-uniform distribution of the refractive index in the solution; and this will appear as a distortion of the fringes.

Consider one fringe, initially straight and perpendicular to the liquid surface, indicating that the liquid has a uniform concentration and temperature. At some time after the commencement of absorption of gas through the interface this fringe will be distorted, as shown in Fig. 2. The optical path length through the liquid is the physical path length multiplied by the refractive index, and the physical path length remains constant. With the gases used in this work, at

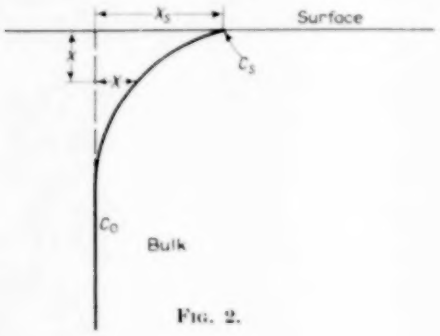

Fig. 2.

the concentrations encountered, the refractive index of the solutions is linearly dependent upon concentration (mass/volume), and therefore for an isothermal absorption process

$$\frac{c - c_0}{c - c_0} = \frac{X}{X_s} \qquad (1)$$

where c is concentration and

X is fringe shift in the liquid (Fig. 2).

Subscript s refers to the surface of the liquid and 0 to the bulk of the liquid (where the concentration and temperature remain unchanged from their initial value).

If the solution of gas at the surface of the liquid is in equilibrium with the gas phase, the surface has the saturated concentration c^*, which is known in terms of the gas pressure over the liquid. The fringe shift X^*, given by a concentration change $c^* - c_0$, can be determined from a photograph of fringes taken after a long period of contact, when the surface will be saturated whatever the interfacial resistance. From the measured value of X^* and the known solubility c^*, the relationship between X and $c - c_0$ can be calculated.

Design of the Absorption Cell

The cell in which gas was absorbed into liquid was a horizontal cylinder of stainless steel (Fig. 3). Optical flats formed windows which were placed in recesses at each end of the cell. The windows were sealed against an "O" ring of synthetic

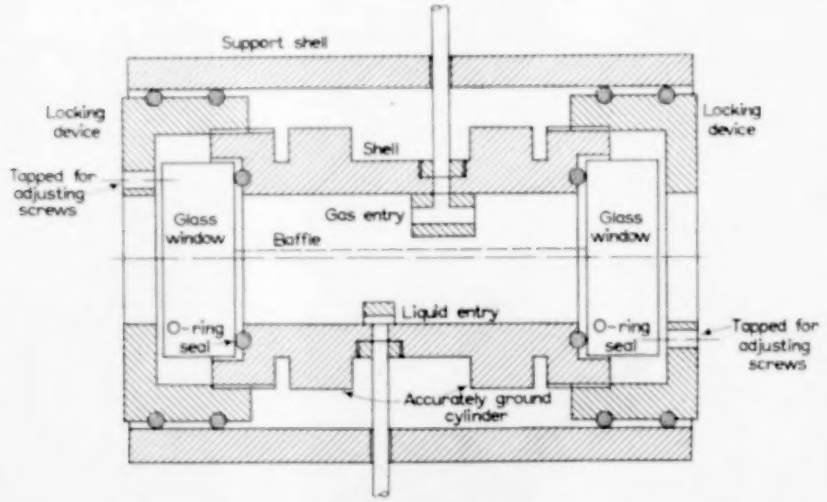

Fig. 3. Section through the absorption cell.

VOL. 10 1959

rubber. Screwed over each end of the cell was a locking device, carrying three screws bearing on the windows opposite the "O" ring. By adjusting these screws the cell windows were aligned parallel, the distance between the windows being measured by a comparator capable of comparing distances to within 1/25,000 in. The cell was supported in the light path by means of a cradle which could be adjusted laterally and vertically and could also be rotated through a small angle. By altering the position of the cell until an image of a small light source reflected by the cell windows coincided with that source, it was ensured that the light path was parallel to the liquid and perpendicular to the cell windows.

A boss diverted the gas, on admission, parallel to the axis of the cell. A stainless steel gauze (200 mesh/in) was placed between the boss and the liquid surface, with the object of smoothing the movement of the gas towards the liquid. The effect on the liquid of a sudden admission of gas into the cell, from a pressure of 5 cm Hg. Abs. to 1 atm, was investigated by observing an image of the surface magnified one hundred times and projected onto a screen. On admission of the gas lycopodium and aluminium powder floating on the surface of the liquid suffered no visible displacement, no swirling of the liquid was observed and the liquid surface remained at the same level. Before the admission of the gas the interference fringes were perpendicular to the liquid surface and stationary, showing that there were no temperature differences or convection currents within the liquid. After admission of the gas the fringes in the bulk of the liquid remained perpendicular to the liquid surface, showing that no convection currents between the surface and the bulk of the liquid had been set up. It was concluded that gas entered the cell without moving the liquid and that distortion of the interference fringes was caused solely by the absorption process. Experiments in which gas was released from the absorption cell also showed no hydrodynamic disturbance.

Photography and Magnification

The interference fringes were photographed with a 16 mm cine-camera which operated at 32 frames/sec. A microscope objective of 16 mm focal length, fitted to the camera, gave a magnification of about ten diameters at the photographic emulsion. The width of emulsion exposed was 1 cm and therefore a fringe spacing of 3/20 mm enabled six fringes to be viewed. The magnification given by the optical system on the emergent side of the interferometer, before the camera, was measured by photographing a slit of known size in the plane of the image of the absorption cell and the fringes. The magnification between this plane and the absorption cell was determined by measuring the size of the image of the end of the absorption cell. In the course of an experiment the camera was operated continuously for 1 sec before admission or release of gas, in order to ensure that the camera had accelerated to working speed, and then for 4 sec afterwards. Thereafter sets of two or three frames were taken at 7, 10, 15 and 20 sec after commencement of the experiment.

Calibration

Apart from distortion of the fringes near the surface of the liquid, caused by a change in the concentration of dissolved gas, a sudden alteration of the pressure of gas in the cell moves all the fringes in the bulk of the liquid rapidly sideways. This is due to a change in the refractive index of water with pressure. The fringes, however, remain parallel to each other and in the same relative position, and the movement of the fringes is completed in less than the interval between two frames of the camera (0·03 sec).

At the beginning of absorption, just after gas has been admitted to the cell, a movement of the fringes commences near the surface of the liquid, rises to a maximum value in about $\frac{1}{2}$ sec and then dies away within 5 sec, leaving a fringe shift evidently caused by change in the concentration of gas in the liquid. This preliminary movement of the fringes is due to the conduction of heat through the liquid. An alteration of the total pressure in the cell alters the partial pressure of the water vapour above the liquid and brings about condensation or evaporation at the liquid surface with the liberation or absorption of latent heat.

Heat conduction is a more rapid process than diffusion in a liquid, and the temperature in the liquid becomes uniform much more rapidly than does the concentration. However, for the same initial pressure change, the same amount of heat will be transferred whatever gas is being used, because the amount of water vapour condensing or evaporating at the surface will be the same. The resultant temperature distribution will also be the same, since the thermal conductivity of water is changed very little by low concentrations of gas. Air is only slightly soluble in water and has no observable effect on the refractive index of water when left in contact for periods which are long compared with the duration of the experiments. Thus, by subtracting the fringe shift caused by heat effects after admission of air from that observed during the absorption of carbon dioxide, each measured at the same time after the commencement of an experiment, the fringe shift due solely to the change in the concentration of carbon dioxide in the water is obtained.

Interfacial Resistance During Absorption of Carbon Dioxide

An interfacial resistance ($1/k_s$) is usually defined by the relationsihp

$$(\partial Q/\partial \theta)_{x=0} = k_s (c^* - c_s) \qquad (2)$$

where k_s is the interfacial mass transfer coefficient,

Q is the mass of gas absorbed through unit area of interface in a time θ and

x is distance normal to the interface.

For uni-directional diffusion in the non-steady state

$$\partial c/\partial \theta = D\, \partial^2 c/\partial x^2 \qquad (3)$$

where D is the diffusion coefficient.

The solution of equation (3) for diffusion into a "semi-infinite" liquid with initially uniform concentration c_0, using equation (2) as a boundary condition, is

$$\frac{c - c_0}{c^* - c_0} = \operatorname{erfc} \frac{x}{2\sqrt{(D\theta)}} - \exp\left(\frac{k_s}{D} x + \frac{k_s^2}{D}\theta\right) \operatorname{erfc}\left(\frac{x}{2\sqrt{D\theta}} + k_s \sqrt{\frac{\theta}{D}}\right) \qquad (4)$$

Values of k_s are most easily computed from a knowledge of the change with time of the concentration of the gas at the surface of the liquid; and this is determined from the variation of fringe shift with time at the surface of the liquid (X_s) recorded on the interferograms. A theoretical relationship for the surface concentration in terms of time is found by putting $x = 0$ in equation (4).

$$\frac{c_s - c_0}{c^* - c_0} = 1 - \exp\left(\frac{k_s^2}{D}\theta\right) \operatorname{erfc}\left(k_s \sqrt{\frac{\theta}{D}}\right) \qquad (5)$$

This cannot be converted to an explicit equation for k_s, but provided that $k_s\sqrt{\theta/D}$ is greater than about 3, equation (5) can be written

$$\frac{c_s - c_0}{c^* - c_0} = 1 - (1/k_s)\sqrt{\frac{D}{\pi\theta}} \qquad (6)$$

In terms of fringe shifts

$$X_s = X^* - X^* (1/k_s)\sqrt{(D/\pi)}\,(1/\sqrt{\theta}) \qquad (7)$$

A plot of X_s versus $1/\sqrt{\theta}$ should therefore be a straight line, for sufficiently small values of $1/\sqrt{\theta}$; this line will cross the X_s axis at X^*. From the slope of this line and equation (7), k_s can be approximately determined. Using this value of k_s, X_s can be plotted against $1/\sqrt{\theta}$ according to equation (5), and it can be checked whether or not the measured values fall about this curve for high values of θ. When there is no interfacial resistance, that is, k_s is infinite, X_s will be constant at the value X^*.

For the absorption of carbon dioxide into water X_s was found to have a substantially constant value, corresponding to the saturated concentration, X^* (Fig. 4 and Table 1). Within the time interval of one frame of the cine-camera (about 1/50 sec) the interference lines assumed that form which would be caused by molecular diffusion of the gas through the liquid with the surface of the liquid saturated. This means that k_s must be at least about 4 cm/sec, the highest value which could be detected with certainty. (There must always be some "resistance" at the interface, for the highest rate at which gas can arrive there is fixed by the value of the kinetic collision number. This limiting value of k_s for carbon dioxide at 1 atm. and 0°C is 5240 cm/sec).

VOL. 10 1959

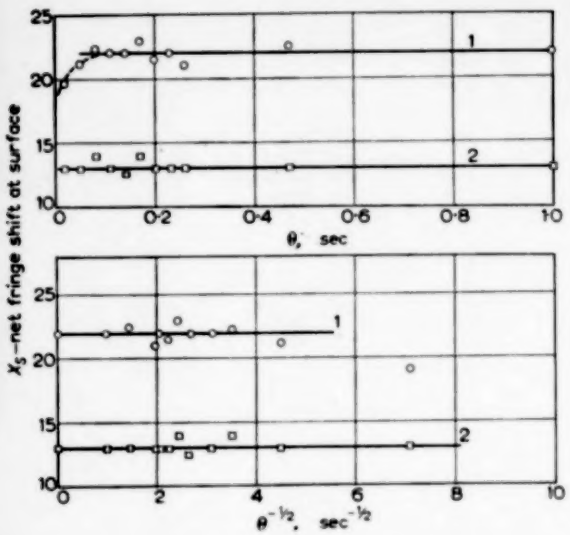

FIG. 4. Carbon dioxide absorbing into distilled water.
Initial pressure 75·1 cm Hg Abs.
Final pressure (i) 34·1 cm Hg Abs.
(ii) 4·4 cm Hg Abs.

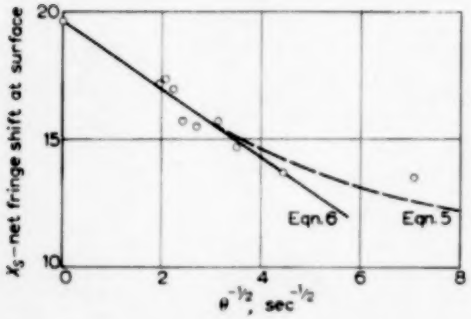

FIG. 5. Carbon dioxide absorbing into 0·41% lissapol-N, $k_s = 0{\cdot}028$ cm/sec.

Table 1. Transfer of carbon dioxide into distilled water.

The following experiments were carried out. In no case was a resistance detected.

Initial pressure (cm Hg Abs)	*Final pressure* (cm Hg Abs)	*Pressure change* (cm Hg)	*Temperature* (°C)
1·7	32·3	30·5	14·7
1·9	74·1	72·2	14·7
2·1	55·4	53·3	14·7
76·9	53·7	− 23·2	10·8
75·1	34·1	− 41·0	10·8
75·1	4·4	− 70·7	10·8
46·9	74·4	27·5	10·0
47·3	28·2	− 19·1	10·0
47·3	10·4	− 36·9	10·0
28·8	74·3	45·5	7·6
29·0	54·9	25·9	7·6
29·0	9·4	− 19·6	7·6

For carbon dioxide dissolving into aqueous solutions of surface-active agents X_s was not independent of $1/\sqrt{\theta}$ and the analysis described above was used to calculate k_s (Fig. 5 and Table 2). The interfacial resistance was measured at a low and at a high concentration of two surface-active agents. It was found that the resistance was substantially the same in all four cases.

In order to be able to compare this work with the work of CULLEN and DAVIDSON [1], about the same concentrations of the same surface-active agents were used. At the low concentration CULLEN and DAVIDSON found an interfacial resistance of the same magnitude as that found here, but at the high concentration they found no resistance. In this work the resistance was the

Table 2. Transfer of carbon dioxide into solutions of surface-active agents

Surface-active agent	*Temp.* (°C)	*Conc.* (% by wt.)	*Initial pressure* (cm Hg Abs)	*Final pressure* (cm Hg Abs)	k_s (cm/sec)
Lissapol − N	5·1	0·41	14·1	32·1	0·028
,,	5·6	0·083	13·7	30·4	0·023
Teepol	8·6	0·286	14·0	30·3	0·028
,,	6·2	1·00	14·0	30·3	0·033

same at both concentrations. The difference between the two sets of results may be due to the fact that the liquid was motionless in our experiments, whereas in the experiments of Cullen and Davidson the liquid was moving over the surface of a sphere. The same kind of result has been noted for solvent extraction. Thus, for example, Lindland and Terjesen [10] and Melhus and Terjesen [12] extracted iodine from water by carbon tetrachloride in the presence of oleyl-*p*-anisidinesulphonate in a drop extractor and measured an interfacial resistance which rose rapidly with concentration of the surface-active agent to a constant value. Holm and Terjesen [9] who carried out the same experiments in a stirred vessel, where the phases are in a disturbed condition, found that the rate of transfer of iodine passed through a maximum value with concentration of surface-active agent.[14]

Acknowledgments—The authors would like to thank Prof. D. M. Newitt and Prof. P. V. Danckwerts for their kind help during the course of this work. We are indebted to Dr. P. Eisenklam for the loan of the interferometer, and one of us (E. A. H.) acknowledges a maintenance grant awarded by the Department of Scientific and Industrial Research.

Notation

c = concentration of gas in liquid (mass/volume)

X = distance moved by fringe from its initial position

Q = mass of gas absorbed in unit time/area of interface

θ = time after admission of gas

x = distance perpendicular to the interface

k_s = interfacial mass transfer coefficient (distance/time)

D = diffusion coefficient

Subscript s = surface of liquid, subscript $_0$ = initial condition of liquid, superscript * = equilibrium value corresponding to gas pressure.

References

[1] Cullen E. J. and Davidson J. F. *Chem. Engng. Sci.* 1956 **6** 49.

[2] Cullen E. J. and Davidson J. F. *Trans. Faraday Soc.* 1957 **53** 113.

[3] Danckwerts P. V. and Kennedy A. M. *Trans. Inst. Chem. Engrs.* 1954.

[4] Danckwerts P. V. and Kennedy A. M. *Chem. Engng. Sci.* **32** S53. 1958 **8** 201.

[5] Emmert R. E. and Pigford R. L. *Chem. Engng. Progr.* 1954 **50** 87.

[6] Goodgame T. H. and Sherwood T. K. *Chem. Engng. Sci.* 1954 **3** 37.

[7] Harvey E. A. Ph.D. Thesis, University of London 1958.

[8] Higbie R. *Trans. Amer. Inst. Chem. Engrs.* 1935 **31** 365.

[9] Holm A. and Terjesen S. G. *Chem. Engng. Sci.* 1955 **4** 265.

[10] Lindland K. P. and Terjesen S. G. *Chem. Engng. Sci.* 1956 **5** 1.

[11] Lynn S., Straatemeier J. R. and Kramers H. *Chem. Engng. Sci.* 1955 **4** 63.

[12] Melhus B. J. and Terjesen S. G. *Chem. Engng. Sci.* 1957 **7** 83.

[13] Vielstich W. *Chem. Ing. Tech.* 1956 **28** 543.

[14] Boye-Christensen G. and Terjesen S. G. *Chem. Engng. Sci.* 1959 **9** 225.

Chemical Engineering Science, 1959, Vol. 10, pp. 281 to 284. Pergamon Press Ltd. London. Printed in Great Britain

A note on the "Danckwerts" boundary conditions for continuous flow reactors

J. R. A. Pearson

Imperial Chemical Industries Ltd., Akers Research Laboratories, The Frythe, Welwyn, Herts.

(*Received* 24 *October* 1958)

Abstract—A mathematical justification is given for the use of the "Danckwerts" boundary conditions for continuous flow reactors. It is shown that the apparent indeterminacy, which Danckwerts resolves intuitively, is caused by the use of a discontinuous coefficient of diffusion. By treating this as the limit of a continuous function and imposing continuity of the reactant concentration as the physically relevant boundary condition, the Danckwerts solution is obtained in the limit.

Résumé—L'auteur donne une justification mathématiques des conditions aux limites utilisées par Danckwerts dans le cas d'un réacteur à écoulement continu. Il montre que l'indétermination apparente résolue intuitivement par Danckwerts est inhérente à un coefficient de diffusion discontinu. Il considère ce coefficient comme la limite d'une fonction continue et il impose une continuité à la concentration du réactant comme étant la condition limite physiquement correcte : la solution de Danckwerts est alors obtenue à la limite.

Zusammenfassung—Die Grenzbedingungen nach Danckwerts für den kontinuierlich durchströmten Reaktor werden mathematisch gerechtfertigt. Die anscheinende Unbestimmtheit, die Danckwerts intuitiv auflöst, ist durch die Verwendung eines diskontinuierlichen Diffusionskoeffizienten verursacht. Behandelt man diesen als Grenzfall einer kontinuierlichen Funktion und setzt die Stetigkeit der Konzentration des Reaktanten als die physikalisch entscheidende Grenzbedingung fest, so erhält man die Danckwerts-Lösung im Grenzfall.

1. Introduction

In an oft-quoted paper (*Chem. Engng. Sci.* 1953 **2** 1), Danckwerts has considered the steady state flow of reactant through a packed tubular reaction vessel in terms of a second order ordinary differential equation (equation 30 in *loc. cit.*). This equation for the steady state concentration, c, of reactant in a first order reaction supposes that c is a function of one space variable only, y, the distance down the tube. The streaming velocity, u, the rate constant, k, and the (constant) coefficient of diffusion, D, enter as parameters into the diffusion equation, which may thus be written

$$D \cdot \frac{d^2c}{dy^2} - u \cdot \frac{dc}{dy} - kc = 0 \dagger. \qquad (1)$$

The boundary condition at the entry to the tube, $y = 0$, where the diffusion coefficient discontinuously changes from zero, is obtained by a consideration of mass balance, and is

$$uc^* = uc - D \cdot \frac{dc}{dy}, \quad y = 0, \qquad (2)$$

where c^* is the concentration in the entering stream.

A similar relation is obtained for c at the exit from the tube, $y = L$, where D again changes discontinuously, but is replaced by Danckwerts, on intuitive grounds, by the stronger condition

$$\frac{dc}{dy} = 0, \quad y = L. \qquad (3)$$

Conditions (2) and (3) lead to a unique solution for c; however this solution, as presented in

† Danckwerts' notation is retained for ease of comparison.

DANCKWERTS' paper, appears to rely for its uniqueness on the acceptance of an intuitive boundary condition. If only because this boundary condition has not been universally accepted, it seems desirable to investigate a little more closely the formal mathematical implications of the idealization represented by equation (1) and the boundary conditions (2) and (3).

First of all, we observe that in the general solution to (1), using boundary condition (2) at $y = 0$ and a similar condition at $y = L$, *a discontinuity in* c, *at either* $y = 0$ *or* $y = L$, *or both, is necessarily consequent upon the imposed discontinuities in* D. Within the reactor, i.e. where $0 < y < L$, we naturally consider only continuous solutions for c. This we do for sound physical reasons, but not for mathematical ones, for it may easily be verified that solutions exist for c that are discontinuous within the region $0 < y < L$. This suggests, as a next step, that we should eliminate, if possible, the discontinuity in D, *and seek solutions for* c *that are continuous everywhere*, and are therefore physically acceptable. We may do this in a variety of ways. In the following section, we shall deliberately choose a form for D, the diffusion coefficient, which is continuous everywhere and which, by means of an obvious limiting process, may be made to approach as closely as we please to the " top hat " distribution of DANCKWERTS. It will be shown that a unique solution for c is in fact obtained without resort to intuition, and that this solution tends, in the limit, to the solution obtained by DANCKWERTS. In other words the apparently intuitive boundary condition (3) becomes the inevitable result of the limiting process applied to the continuous solution.

2. MATHEMATICAL TREATMENT

We replace the constant coefficient of diffusion used by DANCKWERTS by the continuous form

$$\text{(i)}\quad D = AD_0 y \qquad \text{when } 0 \leqslant y < 1/A \quad \text{(4.i)}$$

$$\text{(ii)}\quad D = D_0 \qquad \text{when } 1/A \leqslant y \leqslant L - (1/A) \quad \text{(4.ii)}$$

$$\text{(iii)}\quad D = AD_0(L - y) \qquad \text{when } L - (1/A) < y \leqslant L \quad \text{(4.iii)}$$

where D_0 and $A > 1$ are constants. This is shown diagrammatically in Fig. 1. The diffusion

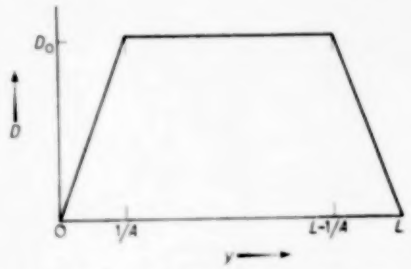

FIG. 1. Coefficient of diffusion, D, as a function of y.

equation which, for a non-constant coefficient of diffusion, must be written

$$\frac{d}{dy}\left(D \cdot \frac{dc}{dy}\right) - u \cdot \frac{dc}{dy} - kc = 0, \qquad (5)$$

becomes, in the three regions (i), (ii) and (iii),

$$\text{(i)}\quad y \cdot \frac{d^2 c_1}{dy^2} + \left(1 - \frac{u}{AD_0}\right)\frac{dc_1}{dy} - \frac{k}{AD_0} c_1 = 0, \quad \text{(6.i)}$$

$$\text{(ii)}\quad \frac{d^2 c_2}{dy^2} - \frac{u}{D_0} \cdot \frac{dc_2}{dy} - \frac{k}{D_0} c_2 = 0, \quad \text{(6.ii)}$$

$$\text{(iii)}\quad z \cdot \frac{d^2 c_3}{dz^2} + \left(1 + \frac{u}{AD_0}\right)\frac{dc_3}{dz} - \frac{k}{AD_0} c_3 = 0, \quad \text{(6.iii)}$$

where we have written $z = L - y$, (7)

and c_1, c_2 and c_3 refer to the solution for c within the three regions. The boundary conditions that we must apply to this set of three equations are

$$\left.\begin{aligned} &c_1 = c^* && \text{at } y = 0, \\ &c_2 = c_1, \quad \frac{dc_2}{dy} = \frac{dc_1}{dy} && \text{at } y = 1/A, \\ &c_3 = c_2, \quad \frac{dc_2}{dy} = -\frac{dc_3}{dz} && \text{at } y = L \\ & && \quad -(1/A), (z = 1/A), \end{aligned}\right\} \quad (8)$$

since mass balance at $y = 1/A$ and at $y = L - 1/A$ requires that dc/dy as well as c be continuous there. We have specified two boundary conditions for c_3 and c_2, but only one for c_1. Thus, at first sight, the system is apparently indeterminate.

VOL. 10 1959

We now consider the general solution for each of the three equations (6). That for (6.ii) can be written directly as

$$c_2 = c_{21} \exp\left[\frac{uy}{2D_0}\left\{1 + \sqrt{\frac{1 + 4kD_0}{u^2}}\right\}\right] + c_{22} \exp\left[\frac{uy}{2D_0}\left\{1 - \sqrt{\frac{1 + 4kD_0}{u^2}}\right\}\right], \quad (9)$$

c_{21} and c_{22} being arbitrary constants. This involves two linearly independent solutions which are finite in the region (ii). Those for (6i) and (6iii) are best considered in terms of ascending power series expansions about the points $y = 0$ and $z = 0$. (It will be sufficient to do this because we will later apply the limiting process $A \to \infty$). Thus, if we write

$$c_1 = y^r (a_0 + a_1 y + \ldots\ldots + a_n y^n + \ldots\ldots \quad (10)$$

and substitute into equation [6(i)] we find that

$$r = 0 \text{ or } \frac{u}{AD_0},$$

giving the two linearly independent solutions

$$c_1^{(1)} = a_0 [1 + (k/AD_0 - u)\, y + 0\,(y^2) \ldots\ldots] \quad (11)$$

and $$c_1^{(2)} = b_0\, y^{(u/AD_0)} [1 + (k/AD_0 + u)\, y + 0\,(y^2) \ldots .] \quad (12)$$

that are bounded within the region (i).

At $y = 0$, $c_1^{(1)} = a_0$, $c_1^{(2)} = 0$.

At $y = 1/A$, $c_1^{(1)} = a_0 + 0\,(1/A^2)$,

$$c_1^{(2)} = b_0\,(1/A)^{(u/AD_0)} + 0\,(1/A),$$

$$\frac{dc_1^{(1)}}{dy} = \frac{ka_0}{AD_0 - u} + 0\,(1/A^2),$$

$$\frac{dc_1^{(2)}}{dy} = b_0 \cdot \frac{u}{D_0}\,(1/A)^{(u/AD_0)} + 0\,(1/A),$$

since $1/A$ is small.

Similarly if we write

$$c_3 = z^s (d_0 + d_1 z + \ldots\ldots d_n z^n + \ldots), \quad (13)$$

and substitute into equation (6iii) we find that

$$s = 0 \text{ or } -\frac{u}{AD_0},$$

giving *only one* solution

$$c_3^{(1)} = d_0\,(1 + (k/AD_0 + u)\, z + 0\,(z^2) \ldots .) \quad (14)$$

that is bounded in the region (iii).

At $z = 0$, $c_3^{(1)} = d_0$.

At $z = 1/A$, $c_3^{(1)} = d_0 + 0\,(1/A^2)$,

$$\frac{dc_3^{(1)}}{dz} = (kd_0/AD_0 + u) + 0\,(1/A^2).$$

We now see that the five boundary conditions (8) are in fact sufficient to define a unique solution for c, in terms of c^*, since there are only five constants, c_{21}, c_{22} [from (9)], a_0 [from (11)], b_0 [from (12)] and d_0 [from (14)] to be determined.

We need not evaluate explicitly these constants in terms of c^*, but proceed at once to the limit $A \to \infty$. This corresponds, in the limit, to the discontinuous form for D chosen by Danckwerts. As $1/A \to 0$, we see that

$$c_1^{(1)}\,(1/A) \to c_1^{(1)}\,(0),$$

but that $c_1^{(2)}\,(1/A) \to b_0$ while $c_1^{(2)}\,(0) = 0$. In other words the solution $c_1^{(2)}$ represents, in the limit, a discontinuity in c. Thus (2) is the correct limiting boundary condition. Similarly, as $1/A \to 0$,

$$c_3^{(1)}\,(1/A) \to c_3^{(1)}\,(0)$$

while $\dfrac{dc_3^{(1)}}{dz}\,(1/A) \to 0$. Thus the strong boundary condition (3), implying continuity of c at $y = L$. is recovered.

3. Discussion

It might be argued that the choice (4i), (4ii) and (4iii) for D is in some sense particular, and that a different limiting solution would be obtained by using a different continuous distribution for D within the regions (i) and (iii). This is not so, and the same limiting solution can in fact be demonstrated for a very wide class of functions D. What we have done in section 2 is to give but an illustrative example of the effect of the sign of u on solutions for c in equation (5) in the neighbourhood of points where D becomes equal to zero. This purely mathematical dependence on the sign of u can be interpreted physically, as

Danckwerts has done, in terms of different boundary conditions to be applied at the entry to or at the exit from a packed tubular reactor, where the diffusion coefficient changes rapidly from zero.

The same procedure can be adopted to obtain relevant boundary conditions in more complicated situations involving diffusion where there are several reactants, and where temperature varies. It can readily be shown that the boundary condition (3), which implies continuity of the variables at the exit, is recovered in every case. It need hardly be pointed out that the use of a discontinuous diffusion coefficient so simplifies the solution of the diffusion equation that it enables analytical results to be obtained in many cases where a more physically acceptable form for D would make exact solution impossible. To this extent, the justification given above becomes of practical value.

VOL. 10 1959

SELECTION OF CURRENT PAPERS OF INTEREST TO CHEMICAL ENGINEERS

E. M. Sparrow and R. Siegel: Transient film condensation. *J. Appl. Mech.* (*Trans. Amer. Soc. Mech. Engrs.* Series E.) 1959 120-121.

A. Slibar and P. R. Paslay: Retarded flow of Bingham materials. *J. Appl. Mech.* (*Trans. Amer. Soc. Mech. Engrs.* Series E.) 1959 107-113.

R. P. Benedict: The calibration of thermocouples by freezing point baths and empirical equations. *J. Engng. for Power* (*Trans. Amer. Soc. Mech. Engrs.* Series A.) 1959 177-188.

D. J. Ryley: Analysis of a polydisperse aqueous spray from a high-speed spinning-disk atomizer. *Brit. J. Appl. Phys.* 1959 **10** 180-186.

P. F. Whelan: Froth flotation. *Research* 1959 **12** 133-140

H. J. Merk: Rapid calculations for boundary-layer transfer using wedge solutions and asymptotic expansions. *J. Fluid Mech.* 1959 **5** 460-480.

G. A. Gilbert: Sedimentation and electrophoresis of inter-acting substances. I. Idealized boundary shape for single substance aggregating reversibly. *Proc. Roy. Soc.* 1959 A **250** 377-388.

D. K. C. Macdonald, E. Mooser, W. B. Pearson, I. M. Templeton and S. B. Woods: On the possibility of thermoelectric refrigeration at very low temperatures. *Phil. Mag.* 1959 **4** 433-446.

SELECTION OF CURRENT SOVIET PAPERS OF INTEREST TO CHEMICAL ENGINEERS*

D. V. Bezugliy: Production of sodium carbonate and bicarbonate by ion-exchange processes. (*Zh. prikl. Khim.* 1959 **32** 262-268).

V. T. Vdovichenko, N. P. Galenko and A. V. Lapionov: Conversion of methane to carbon disulphide by sulphur anhydride. (*Zh. prikl. Khim.* 1959 **32** 347-350).

P. I. Petrovich: Study of the process of nitration of benzene to 2, 4-dinitrophenol. (*Zh. prikl. Khim.* 1959 **32** 353-357).

A. V. Trofimov, H. G Markova and E. I. Dobkina: Synthesis of acetylene from calcium carbonate. (*Zh. prikl. Khim.* 1959 **32** 399-404).

V. S. Etlis, K. S. Minsker, A. I. Kirillov and M. M. Kichirenko: Production and properties of polypropylene. (*Zh. prikl. Khim.* 1959 **32** 418-423).

A. I. Teterevkov and Ya. E. Bilnyanski: On the effects of mass transfer between gas and liquid in the process of chlorination of a suspension of magnesium oxide in molten chloride. (*Zh. prikl. Khim.* 1959 **32** 438-440).

L. A. Mokhov, Yu. F. Udalov and V. C. Khalturin: Special indicator tubes for rapid determination of oxides of nitrogen in air in industrial premises. (*Zh. prikl. Khim.* 1959 **32** 452-453).

A. G. Morachevski and R. Sh. Rabinovich: Liquid–vapour equilibrium in the system chloroform–ethanol. (*Zh. prikl. Khim.* 1959 **32** 458-459).

L. Ya Margolis: Principal regularities in catalytic oxidation of hydrocarbons. 2. Oxygen adsorption on oxidizing catalysts. (*Izv. Akad. Nauk. SSSR, Otd. khim. Nauk.* 1959 225-231).

O. K. Bogdanova, A. P. Schheglova and A. A. Balandin: Catalytic dehydrogenation of *iso*pentane–*iso*pentene mixtures. (*Izv. Akad. Nauk SSSR, Otd. khim. Nauk* 1959 350-352).

V. B. Kogan and T. S. Tolstova: Properties of ternary azeotropic mixtures of components with limited mutual solubility. II. (*Zh. fiz. Khim.* 1959 **33** 276-278).

A. V. Storonkin and N. P. Markuzin: The shape of the isotherm for the separation of the ternary solution triethylamine–phenol–water into layers at 15 and 35°C. (*Zh. fiz. Khim.* 1959 **33** 279-287).

V. A. Zagoruchenko: The vapour pressure of liquid methane. (*Zh. fiz. Khim.* 1959 **33** 326-327).

A. G. Antonova, F. P. Ivanovski, T. G. Filchenkova and A. I. Krasilshchikov: Adsorption phenomena in the system hydrogen–carbon dioxide–carbon monoxide–water vapour. (*Zh. fiz. Khim.* 1959 **33** 416-421).

D. F. Sokolova, N. M. Morozov and N. I. Temkin: Kinetics of ammonia synthesis under conditions of low pressure and diffusion retardation. (*Zh. fiz. Khim.* 1959 **33** 471-479).

N. P. Keier: An investigation into the nature of the deviation of chemical adsorption from the Langmuir type with the aid of isotopic methods. (*Zh. fiz. Khim.* 1959 **33** 492-499). Study of the adsorption of ethanol on ZnO.

Yu S. Zaslavski: Application of radioactive isotopes to problems in petroleum processing (*Khim. Tekhnol. Topl. Masel* 1959 **4** No. 1 5-13).

G. I. Blinov, I. A. Makarov and R. L. Pinkusovich: Application of radioactive control equipment in hydrogenation practice. (*Khim. Tekhnol. Topl. Masel* 1959 **4** No. 1 15-19).

N. P. Melnikova, P. G. Igonin and I. A. Shakhzadova: Investigation of adsorption properties of various types of coke by means of radioactive indicators. (*Khim. Tekhnol. Topl. Masel* 1959 **4** No. 1 28-31).

***To assist readers, translations of any article appearing in the above list can be obtained at a reasonable charge. All orders should be addressed to the Administrative Secretary of the Pergamon Institute at either 4 Fitzroy Square, London W.1, or 122 East 55th Street, New York 22, whichever is more convenient.**

M. A. KALIKO and N. M. PERVUSHCHINA : Study of the nature of surface of cracking catalyst by adsorption of cations of cesium labelled with radioactive cesium. (*Khim. Tekhnol. Topl. Masel* 1959 **4** No. 1 35-40).

K. A. ALEKSEEVA and B. L. MOLDAVSKI : Transformation of phenols during vapour-phase hydrogenation. (*Khim. Tekhnol. Topl. Masel* 1959 **4** No. 1 43-48).

P. I. LUKYANOV, I. V. GUSEV and N. I. NIKITINA : On the forces exerted by a moving compact bed of granular material on the walls of a vertical tube. (*Khim. Tekhnol. Topl. Masel* 1959 **4** No. 1 63-68).

A. A. PETROV and N. P. BORISOVA : Investigation of de-emulsifying properties of oxyethylated alkyl phenols. (*Khim. Tekhnol. Topl. Masel* 1959 **4** No. 2 66-71).

V. Z. VOTLOKHIN : Automatic continuous colorimeter. (*Khim. Tekhnol. Topl. Masel* 1959 **4** No. 3 10-12).

Z. I. GELLER, P. E. SUDAKOV and Yu. L. RASTORGUEV : Measurement and control of viscosity of oil products in flow. (*Khim. Tekhnol. Topl. Masel* 1959 **4** No. 3 13-16).

V. P. ANDERS, P. A. FROLOVSKI, V. F. REMNEV and M. S. SLOBODKIN : Automatic chromatograph for recording the composition of hydrocarbon gases in flow. (*Khim. Tekhnol. Topl. Masel* 1959 **4** No. 3 25-30).

V. M. SHMERKOVICH : Air-cooled condensers. (*Khim. Tekhnol. Topl. Masel* 1959 **4** No. 3 39-42).

M. I. GUREVICH : Instability of some flows with free surfaces. (*Dokl. Akad. Nauk SSSR* 1959 **124** 998-1000).

V. M. DEMENTEV : Problems of aerodynamics of fluidized beds. (*Teploenergetika* 1959 **6** No. 1 50-56).

V. A. KIRILIN and S. A. OULIBIN : Experimental investigation of specific volumes of water and steam at high temperatures. (*Teploenergetika* 1959 **6** No. 1 62-65).

V. G. FASTOVSKI and Yu. V. PETROVSKI : Heat transfer and resistance to air flow in a plate heat exchanger with hemispherical projections. (*Teploenergetika* 1959 **6** No. 1 65-68).

M. E. SHITSMAN : Heat transfer to water, oxygen and carbon dioxide near their critical region. (*Teploenergetika* 1959 **6** No. 1 68-72).

B. S. PETUKHOV and L. D. NOLDE : Heat transfer in viscous gravitational flow of liquid in pipes. (*Teploenergetika* 1959 **6** No. 1 72-80).

A. P. ORNATSKI and V. K. SHCHERBAKOV : Intensification of heat transfer in the critical region with the aid of ultrasonics. (*Teploenergetika* 1959 **6** No. 1 84-85). Effect of ultrasonic vibrations on heat transfer to boiling liquids in the nucleate boiling regime.

N. A. MOZHAROV : Investigation into critical velocity of stripping the liquid film off the wall of a pipeline. (*Teploenergetika* 1959 **6** No. 2 50-53). Stripping of condensate film during flow of saturated steam.

Errata

RIUS A., OTERO J. L. and MACARRÓN A. Equilibres liquide – vapeur de mélanges binaire donnant une réaction chimique : systèmes méthanol – acide acétique ; éthanol – acide acétique ; *n*-propanol – acide acétique ; *n*-butanol – acide acétique. *Chem. Engng. Sci.* 1959 **10** 105.

On p. 110 " Les Tableaux numériques 3 à 7 " should read " Les Tableaux numériques 3 à 6."

On p. 111 in the Notation " α = volatilité relative = $Y_1 . X_2/X_1 . T_2$ " should read " α = volatilité relative = $Y_1 . X_2/X_1 . Y_2$."

Tables 1 – 6 were omitted from the text and are given below.

Tableau **1.** *Constantes physiques des produits utilisés*

	Méthanol	Éthanol	*n*-Propanol	*n*-Butanol	Acide acétique
Index de réfraction					
Observé	(20°C) 1,3286	(20,5°C) 1,3612	(20°C) 1,3856	(20°C) 1,3990	(22,9°C) 1,3714
Bibliographie	(20°C) 1,3288 [5]	(20,5°C) 1,3610 [5]	(20°C) 1,3854 [5]	(20°C) 1,3991 [5]	(22,9°C) 1,3715 [5]
Densité (g/ml)					
Observé	(15°C) 0,7958	(20°C) 0,7899	(18,8°C) 0,8044	(22,2°C) 0,8077	
Bibliographie	(15°C) 0,79577 [9]	(20°C) 0,7895 [3]	(18,8°C) 0,8047 [9]	(22,2°C) 0,8082 [3]	
Température d'ébullition					
Observé	(703,3mm) 62,9°C	(710,6mm) 76,8°C	(710,6mm) 95,3°C	(708,4mm) 115,8°C	(697,6mm) 115,1°C
Bibliographie	(703,3mm) 62,85 [9]	(710,6mm) 76,78 [9]	(710,6mm) 95,32 [9]	(708,4mm) 115,65 [9]	(697,6mm) 115,11 [10]
Température de congélation					
Observé					16,58 – 16,64°C
Bibliographie					16,7 [9]

Tableau **2.** *Système éthanol–eau* (*Figs.* 3 *et* 4)

No.	P	t	t 760	X_1	Y_1	γ_1	γ_2
1	709,1	95,9	97,7	0,008	0,088	5,35	1,000
2	708,6	93,8	95,5	0,018	0,165	4,82	0,998
3	709,1	91,8	93,6	0,026	0,232	5,02	0,995
4	709,1	91,6	93,4	0,028	0,229	4,63	1,008
5	709,1	86,4	88,2	0,070	0,390	3,82	1,015
6	709,1	85,6	87,4	0,086	0,419	3,68	1,016
7	709,1	84,0	85,8	0,105	0,454	3,26	1,035
8	709,1	83,4	85,2	0,120	0,471	3,01	1,046
9	707,3	79,9	81,7	0,291	0,572	1,717	1,204
10	709,1	79,4	81,2	0,361	0,597	1,473	1,285
11	706,3	78,8	80,7	0,407	0,618	1,378	1,341
12	706,3	77,7	79,6	0,561	0,682	1,154	1,573

Tableau 3. *Système méthanol–acide acétique* (*Figs.* 5, 6, 10 *et* 14)

No.	P	t	X_1	Y_1	γ_1	γ_2	α
1	710,5	115,8	0,000	0,000	—	—	—
2	709,3	112,0	0,037	0,109	0,555	1,060	3,18
3	709,3	109,9	0,058	0,165	0,570	1,082	3,21
4	709,3	105,0	0,107	0,303	0,654	1,113	3,62
5	711,1	102,8	0,137	0,353	0,640	1,163	3,44
6	709,3	97,4	0,208	0,491	0,691	1,195	3,67
7	709,3	94,8	0,250	0,556	0,705	1,205	3,75
8	705,9	92,7	0,280	0,603	0,720	1,200	3,91
9	705,9	91,7	0,306	0,630	0,726	1,210	3,86
10	711,1	86,8	0,387	0,735	0,798	1,180	4,39
11	709,3	84,7	0,427	0,776	0,817	1,150	4,65
12	711,1	81,7	0,492	0,831	0,843	1,100	5,08
13	705,9	79,9	0,517	0,853	0,875	1,075	5,42
14	705,9	76,0	0,601	0,911	0,920	0,910	6,79
15	703,3	73,7	0,657	0,934	0,940	0,858	7,39
16	703,3	71,6	0,713	0,951	0,955	0,828	7,81
17	703,3	69,1	0,785	0,971	0,960	0,725	9,17
18	704,7	67,3	0,839	0,983	0,985	0,627	11,09
19	704,7	65,9	0,882	0,989	0,996	0,571	12,02
20	703,3	63,8	0,959	0,996	1,000	0,660	10,64
21	703,3	63,0	0,995	0,999	1,000	0,703	5,02
22	703,3	62,9	1,000	1,000	—	—	—

Tableau 4. *Système éthanol–acide acétique* (*Figs.* 5, 7, 11 *et* 15)

No.	P	t	X_1	Y_1	γ_1	γ_2	α
1	710,5	115,8	0,000	0,000	—	—	—
2	708,1	112,8	0,055	0,107	0,537	1,052	2,06
3	707,5	111,9	0,073	0,144	0,560	1,057	2,14
4	706,0	110,0	0,103	0,197	0,576	1,089	2,14
(5)	700,8	107,7	0,133	0,274	0,664	1,090	2,46
6	707,5	107,2	0,166	0,312	0,622	1,097	2,28
7	708,1	104,7	0,207	0,393	0,686	1,106	2,48
8	710,0	103,5	0,233	0,437	0,710	1,108	2,55
(9)	689,7	99,9	0,282	0,526	0,764	1,100	2,82
10	705,5	98,8	0,347	0,597	0,749	1,094	2,79
11	706,0	93,0	0,460	0,750	0,870	1,000	3,53
(12)	690,6	91,1	0,516	0,793	0,860	0,970	3,59
13	707,2	88,9	0,587	0,854	0,903	0,886	4,11
(14)	705,4	86,5	0,659	0,900	0,924	0,804	4,66
(15)	697,9	83,8	0,728	0,934	0,947	0,730	5,29
(16)	700,8	81,3	0,816	0,966	0,966	0,610	6,41
17	706,0	78,3	0,924	0,990	0,996	0,492	8,14
18	710,6	76,8	1,000	1,000	—	—	—

Remarque. Les points entre parenthèse ( ) correspondent à des mesures realisées avec un autre appareil d'équilibre quelque peu différent, mais fonctionnant aussi selon le même principe. Il n'avait qu'un seul réservoir, chargé avec un mélange binaire de produits à 99,5 pour cent.

Tableau 5. Système n-*propanol–acide acétique* (*Figs.* 5, 8, 12 *et* 16)

No.	P	t	X_1	Y_1	γ_1	γ_2	α
1	710,5	115,8	0,000	0,000	—	—	—
2	704,2	114,1	0,126	0,159	0,641	1,023	1,31
3	706,8	114,1	0,132	0,154	0,599	1,040	1,20
4	708,2	113,3	0,205	0,256	0,660	1,023	1,32
5	706,8	111,3	0,312	0,397	0,712	1,025	1,45
6	706,8	109,9	0,377	0,493	0,765	0,990	1,61
7	701,8	108,5	0,437	0,578	0,812	0,950	1,76
8	706,8	107,8	0,488	0,638	0,825	0,920	1,85
9	701,8	107,2	0,500	0,651	0,841	0,920	1,86
10	704,2	105,5	0,586	0,745	0,864	0,861	2,06
11	701,8	103,1	0,669	0,831	0,935	0,775	2,43
12	702,9	101,0	0,757	0,900	0,950	0,675	2,89
13	702,9	99,2	0,823	0,940	0,975	0,590	3,37
14	704,2	98,4	0,868	0,960	0,973	0,543	3,65
15	703,7	97,3	0,908	0,976	0,995	0,484	4,12
16	710,6	95,3	1,000	1,000	—	—	—

Tableau 6. Système n-*butanol–acide acétique* (*Figs.* 5, 9, 13 *et* 17)

No.	P	t	X_1	Y_1	γ_1	γ_2	α
1	710,5	115,8	0,000	0,000	—	—	—
2	702,2	115,7	0,018	0,009	0,497	1,008	0,495
3	702,2	116,3	0,060	0,039	0,625	1,000	0,636
4	700,7	116,9	0,105	0,078	0,706	0,989	0,721
5	706,9	117,0	0,117	0,085	0,690	0,998	0,701
6	706,8	117,7	0,161	0,124	0,713	0,984	0,737
7	707,0	118,6	0,234	0,188	0,720	0,973	0,758
8	706,7	118,8	0,254	0,209	0,734	0,968	0,776
9	707,0	119,5	0,304	0,259	0,741	0,960	0,800
10	707,0	119,8	0,355	0,311	0,755	0,945	0,820
11	706,8	120,3	0,459	0,439	0,813	0,907	0,922
12	707,3	120,3	0,485	0,475	0,831	0,890	0,961
13	707,3	120,3	0,545	0,555	0,865	0,856	1,041
14	707,9	120,1	0,590	0,614	0,889	0,828	1,105
15	707,9	119,8	0,657	0,702	0,922	0,769	1,229
16	707,9	119,4	0,731	0,790	0,946	0,700	1,384
17	705,6	118,2	0,824	0,889	0,980	0,584	1,710
18	706,4	117,2	0,920	0,960	0,984	0,475	2,086
19	706,4	116,6	0,954	0,980	0,990	0,413	2,362
20	708,4	115,8	1,000	1,000	—	—	—

Remarque. Pour construire la Fig. 9 et pour calculer les coordonnées du point azéotropique, nous avons corrigé le. températures à 706 mm Hg (pression moyenne des déterminations), en employant le coéfficient $\Delta t/\Delta P = 0{,}042$°C/mm Hgs Les coordonnées du point azéotropique, calculées selon la méthode de KAISER [13], sont : $P = 706$ mm Hg, $t = 120{,}3$°C, $X_1 = Y_1 = 0{,}518$.

VOL. 10 1959

HEERTJES P. M., VAN MENS M. H. and BUTAYE M. The absorption and chemisorption of ammonia in a jelly. *Chem. Engng. Sci.* 1959 **10** 47.

The right hand side of equation (4) on page 48 should read :

$$\frac{C_B^* (\mathfrak{D}_B)^{\frac{1}{2}} \exp(-\alpha/\mathfrak{D}_B)}{\operatorname{erfc}(\alpha/\mathfrak{D}_B)^{\frac{1}{2}}}$$